Thèse de Doctorat
de l'Université Pierre et Marie Curie

Spécialité : Cerveau, Cognition, Comportement

École doctorale ED3C

Présentée par
Jérémie PINOTEAU

Pour obtenir le grade de
Docteur
de l'Université Pierre et Marie Curie

Traitement d'informations tactiles dans une architecture neuronale en boucle fermée

---

Soutenue le 19 novembre 2013 devant le jury composé de :

Rapporteurs :	Jeffrey Krichmar	-	Université de Californie
	Calogero Oddo	-	École Supérieure Sainte-Anne de Pise
Examinateurs :	Didier Bazalgette	-	Direction Générale de l'Armement
	Moustapha Hafez	-	Commissariat à l'Énergie Atomique et aux Énergies Alternatives
	Vincent Hayward	-	Université Pierre et Marie Curie
	Eduardo Ros	-	Université de Grenade
Directeur :	Angelo Arleo	-	Centre National de la Recherche Scientifique Université Pierre et Marie Curie

Processing of fine touch information in a closed loop neural architecture

Abstract

In recent years, roboticians have taken biology as a source of inspiration and have tried with increasing effort to reproduce biological functions and structures in artificial systems. In particular, robotics and neuro-engineering have been merging more and more often into a unitary discipline that tries to reproduce basic principles of the nervous system with a double goal: *(i)* make robots interact with the world in a human-like fashion and *(ii)* exploit artificial models as benchmarks for testing novel scientific hypotheses. Following these two objectives, the work presented in this thesis places itself in the field of neuro-robotics and has been carried out to develop a closed loop neural architecture for active sensing and fine touch discrimination.

The system consists of several modules. To reproduce the same neural coding principles as those observed at the periphery of the somatosensory pathway, two computational models emulating the spiking dynamics of primary afferents and cuneate neurons were implemented. The information transmitted through these first two stages of processing was quantified via information theory analysis tools. In a real-world application, the mechanoreceptor model was coupled to an artificial fingertip. Second order neuron responses to primary afferent signals were supplied to a classifier, which computed the probability estimates of the stimulus being delivered. Such probabilities were not only used to recognize the stimulus but also to devise a movement policy for the fingertip in a dynamic recognition task scenario. The closed loop system was completed with a neuro-mimetic model of the cerebellum implementing a low-level controller for the fingertip movements.

Testing the closed loop architecture on a Braille reading task showed that both primary afferent and cuneate neuron populations efficiently and reliably transmitted enough information to perform a perfect discrimination. Stimulus spatial patterns were mapped by primary afferent activity during the scanning of Braille characters. Perceptual ambiguities were resolved by the processing operated at the cuneate nucleus level. Relying on second order neuron activity, the classifier was capable of performing a complete discrimination of stimulus patterns. The control loop was closed by modulating the fingertip scanning velocity in order to speed up reading according to contextual information.

The presented neural architecture can be extended to further study both the neural bases of fine touch in humans, and neuro-mimetic solutions for processing

tactile signals in humanoid robots. Eventually, the neural system could help investigate biologically plausible sensory feedbacks in neuroprosthetic applications.

Résumé

L'observation des êtres vivants interagissant avec leur environnement a permis de constater l'importance du rôle joué par la perception tactile. Ceci a amené à doter un nombre croissant de systèmes robotiques modernes, destinés à opérer dans des environnements réels non contrôlés, de capacités tactiles avancées. Etant donné les performances observées dans les systèmes biologiques, les solutions robotiques développées sont souvent inspirées et comparées aux mécanismes physiologiques permettant la perception tactile. Cette approche a pour double avantage *(i)* d'améliorer les capacités de robots en imitant les principes sous-tendant la précision et l'efficacité des systèmes biologiques, et *(ii)* d'utiliser les systèmes artificiels pour étudier de manière théorique de nouvelles hypothèses scientifiques. S'inscrivant dans ce cadre, les travaux réalisés pour cette thèse ont porté sur la reproduction des mécanismes d'encodage de l'information tactile au sein d'une nouvelle architecture neuro-computationnelle. Ce système modélise la boucle de contrôle sensorimotrice lors de tâches de toucher actif et de discrimination fine.

L'architecture conçue comprend des modèles bio-mimétiques reproduisant les mécanismes d'encodage de l'information tactile par les neurones du premier et second ordre du système somatosensoriel périphérique. Les signaux neuronaux à la sortie de ces modèles sont interprétés par des processus de discrimination et de décision de mouvement qui simulent les traitements s'opérant au niveau cortical. Finalement, la boucle de contrôle est fermée par un modèle bio-inspiré du cervelet corrigeant les erreurs de trajectoire lors du déplacement du système. Une implémentation neuro-robotique du système a été testée dans le contexte d'une tâche de lecture de caractères Braille.

Des études reposant sur la théorie de l'information ont permis d'établir que les modèles de neurones du premier et du second ordre encodent et transmettent de manière fiable et efficace une quantité d'information suffisante pour permettre une discrimination parfaite de l'ensemble des stimuli. Ceci résulte d'un encodage des caractéristiques spatiales des stimuli dans l'activité des afférents primaires similaire à celui observé dans le système biologique. Ces signaux sont ensuite traités par les neurones du noyau cunéiforme de manière à réduire les ambiguïtés apparaissant dans l'encodage de différents stimuli. Une interprétation probabiliste des signaux neuronaux à la sortie du noyau cunéiforme suffit alors

au processus de discrimination pour reconnaître l'ensemble des motifs des lettres Braille. En fonction des informations délivrées par ce processus, la vitesse de lecture est modulée afin d'accélérer l'identification des stimuli.

Le développement de ce système pourra contribuer à la compréhension des bases neuronales du traitement de l'information tactile au niveau périphérique, ainsi qu'au développement de solutions neuro-mimétiques pour améliorer les capacités tactiles en robotique humanoïde. En émulant, dans un système artificiel, les mécanismes de codage neuronal sous-tendant la perception tactile, cette architecture vise également à participer à la conception de retours sensoriels biologiquement plausibles dans des systèmes de neuro-prothèses.

Acknowledgements

I would like to thank the members of the jury: Prof. Jeffrey Krichmar, Prof. Calogero Oddo, M. Didier Bazalgette, Dr. Moustapha Hafez, Prof. Vincent Hayward and Prof. Eduardo Ros for agreeing to review the work carried out for this PhD study. They have kindly offered important feedback for improving the quality of this manuscript and have contributed to an interesting discussion regarding the foundations, results and significance of my work.

I would also like to express my gratitude to the partners with whom I collaborated during my PhD and who were essential for completing this research project: Roland Johansson, Andrew Pruszynski and the entire team of the Laboratory of Dexterous Manipulation who welcomed me in their lab, provided me with experimental data for analysis and modeling, and shared their knowledge and enthusiasm for the subject of human touch. Eduardo Ros, Jesús Garrido and Niceto Luque for developing and providing support for the EDLUT simulation environment, the robotic arm model and, of course, for a very enjoyable Oktoberfest evening. Jean-Baptiste Passot, for his work on the cerebellar model and, what are for me, its black boxes. Patrick van der Smagt and Jörn Vogel for their essential help in the robotic implementation and testing phases. Marco Maggiali for suggesting and providing the artificial touch sensor upon which a significant part of this work relied. Henrik Jörntell for providing data and inputs on the infamous cuneate nucleus. More generally, I thank all the partners of the SENSOPAC European project through which this research started and I would like to acknowledge the contribution of the Direction Générale de l'Armement, represented by Didier Bazalgette, whose funding allowed me to carry out my research project.

I would like to warmly thank Angelo for welcoming me into his team and giving me the opportunity to explore this subject. He has put great effort into building an enjoyable work environment in which scientific curiosity and rigor were always encouraged. During these past years, he has always been available and eager to share his experience and provide good advice on both scientific and other life matters. It has been a pleasure and a privilege to work with him.

I am also grateful to all the ANC team members who have worked with me over the past years and who were essential for building the friendly atmosphere of our team. Felix and Julien who I hope enjoyed their all too brief stay in the

team. Romain who introduced me to this field; Elsa and Beryl who challenged my knowledge of it during our many meetings. Tim for his easy laugh and his Chilli Con Carne. Laureline for her knowledge of statistics and, more importantly, for showing me the snowy mountains outside Lyon. Denis for sharing his wisdom on all things and much more. Manu and JB for the cheerful spirit they gave to the team. Eleonore for her amazing energy and her (unhealthy) obsession with ping-pong. And Luca without whom much of the research presented here would not have been possible, a man of great kindness whom I am now lucky enough to consider a dear friend.

I would like to thank all my friends who have unfailingly stood by me during these past few years and who have always shared their laughs and their smiles. And finally I would like to thank my entire family for always supporting me in my decisions and encouraging me to be curious and work towards doing something that I enjoy with my life. To all of you, for being who you are, thank you.

Contents

List of Figures

List of Tables

Part I

Introduction

Chapter 1

Introduction

1.1 Context

Since their origins as industrial tools, robots have evolved to now play important roles in a wide range of fields. Applications as rehabilitation and assistive robots, social robots, bio-robots, medical robots and humanoids are growing more and more common with technological advancements. Initially the subject of science fiction (Gates, 2007), robots are becoming a constant presence in everyday life, assisting humans or replacing them in complex tasks. This has led to an important paradigm shift in the field of robotics. Contrary to manufacturing robots which only interacted with specialized staff, the new types of robots must prove capable of advanced (and safe) interaction with humans and adaptable to changing environments in an autonomous way. Hence, the importance of investigating human interaction with the world as to provide both a starting point and a goal for designing new generation humanoids robots.

In general, controlled interaction with the environment requires sensory information from several different modalities such as vision, hearing, touch or smell. Although the study of these modalities has been unequally divided, all were shown to be important. In particular, the sense of touch has been found to be essential when physical interactions with the environment are required. The loss of cutaneous sensation (Westling and Johansson, 1984), or kinesthetic (Cole, 1995), induced subjects, which still had access to other sensory modalities, to no longer maintain a stable grasp of objects or control their posture, respectively. In effect, the sense of touch is an essential modality for retrieving object properties such as shape, surface texture, stiffness or temperature, which provide feedback information during contact interactions. It also contributes to be aware of the distinctions between one's body and his or her environment.

The sense of touch is the result of the somatosensory system. Contrary to other sensory modalities, the system underlying cutaneous touch is spread across

the entire body skin. Receptors responding to specific stimuli (*eg.* vibrations, pressure, light touch, temperature etc. . . , see Purves et al., 2008) are located in the dermis and epidermis to detect and transmit sensory information to central areas of the nervous system. Though extracting different features of the stimuli, all receptor types function in a similar way. When contact is made with an object, the skin's properties are altered as it conforms to the object's surface. Heat transfers to the skin induce responses from thermoceptors, while the skin deformation is recorded by a large number of mechanoreceptors. Stimulus features (*eg.* amplitude, local curvature, roughness, etc. . .) are transformed by mechanoreceptors into trains of action potentials (Adrian, 1926b), somewhat akin to a digital signal. Overall spatial properties of the stimulus are processed in parallel by a population of receptors. Signals are mediated by a multistage processing before reaching central areas (Hsiao and Yau, 2008).

At the first stages of the somatosensory pathway, mechanoreceptor responses are transmitted to second order neurons, located in the dorsal column nuclei of the brainstem, according to a somatotopic organization (Whitsel et al., 1969; Leiras et al., 2010). Cuneate neurons decode and re-encode primary signals prior to their transmission to thalamic and subsequently to cortical areas that mediate downstream experience-dependent haptic percepts (Fyffe et al., 1986b; Marino et al., 2001). In the case of active sensing tasks, an adaptive control closes the perception-action loop (Johansson and Flanagan, 2009). For this, motor control processes and sensory systems tightly interact to optimize information acquisition. Sensory signals are used to modulate movement policies and generate exploratory behaviors, notably by anticipating future sensory inputs (Lederman and Klatzky, 1993; Grant et al., 2009). Conversely, motor signals are used through mechanisms such as efference copy (Blakemore et al., 2000) or more broadly corollary discharge (Crapse and Sommer, 2008) to compensate for unwanted sensory signals resulting from the movement.

1.2 Objectives

The principles of efficiency and robustness that underly the behavior of biological systems have often been a source of inspiration for the work of engineers (Brooks, 1991; Bekey, 2005; Pfeifer et al., 2007). Following these principles, an increasing amount of attention is being brought to imitating the

biological mechanisms behind the sense of touch (Lederman and Pawluk, 1992; Pfeifer et al., 2007; Maheshwari and Saraf, 2008; Dahiya et al., 2010; Loeb et al., 2011a; Dahiya and Valle, 2013). However, if most of these studies show an interest on how the somatosensory system processes information about touch, they especially stress the relevance of functional bio-mimetism for the development of new touch sensors. Although there exists an extensive body of experimental, theoretical and neuro-computational studies on the neural coding mechanisms behind tactile sensation (Hsiao and Yau, 2008; Johansson and Flanagan, 2009; Mackevicius et al., 2012; Lederman and Klatzky, 2009), most applications, though not all (Spigler et al., 2012; Ratnasingam and McGinnity, 2011b), remain only distantly related to their biological sources. To the best of our knowledge, no unified architecture mirroring the multistage neural coding mechanisms underlying the peripheral to central transmission of fine touch percepts and their use for active exploration has yet been proposed.

This manuscript addresses this by presenting a closed loop, neuro-robotic architecture capable of performing fine touch discrimination. A computational model of mechanoreceptive afferents and of the cuneate network was established on the basis of the neural coding principles observed at these stages of the somatosensory system. The output signals of these models were analyzed using theoretical tools in order to assess the quality of the encoding. Second order output signals were also fed to a probabilistic classifier tasked with decoding the tactile information. A closed loop system was built by associating the mechanoreceptor model with an artificial fingertip, whose position was modulated according to the classification results. In addition, a neuro-mimetic model of the cerebellum was used for the low-level control of the fingertip position. This architecture was tested using a real robotic implementation for which the capacitive sensors were fixed to a robotic hand-arm system to act as the artificial skin of the fingertip. The architecture was tested using a Braille reading protocol.

The main goal of this work was to develop a novel neural architecture relying on the coding and processing principles observed in the human peripheral somatosensory system to allow the discrimination of coarse textures and embossed surfaces by tactile robotic devices.

Other than contributing to the development of haptic robotics for real world applications, this study has two objectives. On the neural engineering side, accounting for the neural coding principles of the tactile information

transmission might contribute to providing neuroprosthetic devices (Nicolelis and Lebedev, 2009; Hochberg et al., 2012) with biologically plausible sensory feedbacks (Raspopovic et al., 2012). On the neurobiology side, and on the mid-term, the proposed neuro-engineering approach might be useful to test hypotheses on how primary contact features are encoded/decoded along the ascending somatosensory pathway and used for further processing.

1.3 Road map of the dissertation

This thesis consists of two main parts. The first of these parts (chapters 2 to 4) reviews the anatomo-functional properties of the somatosensory system and presents some neural coding mechanisms underlying fine touch discrimination. The second (chapters 5 to 7) presents the neuro-robotic architecture inspired by the anatomo-functional and neural coding properties described in the first part.

The topics considered in each chapter are:

Chapter 1 introduces the context, nature and objectives of this work.

Chapter 2 reviews the anatomo-functional properties of the human somatosensory system. With the neuro-robotic architecture in mind, the emphasis has been placed on the peripheral ascending pathways conveying fine touch information.

Chapter 3 describes neural coding mechanisms and their role in fine touch sensory coding.

Chapter 4 illustrates the coding in primary afferents through a theoretical analysis performed on microneurography recordings.

Chapter 5 reviews how different stages of the architecture have been addressed in other neural engineering and modeling studies.

Chapter 6 presents the closed loop system along with its different components.

Chapter 7 describes the performance of the neuro-robotic system in a Braille reading task.

Chapter 8 discusses the system's results and limitations, and addresses possible future improvements.

1.4 Terminology

The *sense of touch* in humans is composed of two main sub-modalities: kinesthetic and cutaneous. They are characterized by the origin of their sensory inputs. Cutaneous sense receives inputs from the skin whereas kinesthetic receptors are located in muscles, tendons and joints (Loomis and Lederman, 1986). The cutaneous information provides contact information about the environment, while the kinesthetic systems informs on static and dynamic body postures. For what is known as *haptic perception*, both sub-modalities are combined (Loomis and Lederman, 1986). *Tactile perception* refers to the perception originating solely from cutaneous stimulation.

The sense of touch can be described as either *active* or *passive* depending on the context. Active touch is defined by the addition of motor control inputs to the afferent information (Loomis and Lederman, 1986).

Fine touch, also known as discriminative touch, is a sensory modality which allows the subject to localize the touch source. Conversely, when localization is not possible it is called *crude touch* (or non-discriminative touch). The posterior column-medial lemniscus pathway is the pathway responsible for sending fine touch information to the cerebral cortex of the brain (see chapter 2), while crude touch is carried in the spinothalamic tract.

The neuro-robotic architecture developed in this study was designed to perform discrimination of tactile percepts inspired by the neural coding mechanisms underlying fine touch. The system is *closed loop*, meaning that it uses sensory information to modulate its movement behavior. An active sensing policy has been implemented for it to quickly recognize different stimuli; however, motor signals were not directly used to help the discrimination.

Part II

Neural Bases of Fine Touch

Chapter 2

The somatosensory system

In the human nervous system, information underlying fine touch is conveyed from the periphery to central areas through the somatosensory system, which is also responsible for supporting the other sensory modalities of touch, temperature, proprioception and nociception. Information pertaining to all these modalities is effectively combined in the central nervous system in order to create a complete body image.

This chapter will provide an overview of the different stages relaying sensory information through the somatosensory system. Though the different modalities of the sense of touch are evoked, the focus has been placed on the sub-systems underlying fine touch functions. In particular, given the subject of the present study, this chapter will concentrate on the pathway of sensory information emanating from the fingertips –which play an important role in fine touch– and focus particularly on the early stages of processing.

2.1 Overview of the human somatosensory system

The ascending sensory system consists of three distinct pathways: the *anterolateral system*, the *dorsal column-medial lemniscal pathway*, and the *somatosensory system to the cerebellum*. All three pathways share a similar organization comprising three stages of neurons relaying the sensory information before it reaches the cerebral cortex. In the case of bodily sensation (with the exception of the head and neck) first order neurons extend from the sensitive zone (*eg.* skin, muscles, joints) to the *dorsal root ganglia* (DRG) of the spinal cord where their cell body is located. Second order neurons are found in either the spinal cord or the brainstem and project towards central areas such as the thalamus, the reticular system, or the cerebellum. Although a partial functional

Pathway	Anatomical tracts	Function
Anterolateral (ALS)	Spinothalamic Spinothalamic Spinomescencephalic Spinotectal Spinohypothalamic	Pain, temperature, crude touch, pressure and proprioception
Dorsal column-medial lemniscal (DCML)	Fasciculus gracilis Fasciculus cuneatus	Fine touch, vibratory sense, position sense
Somatosensory to the cerebellum	Anterior spinocerebellar Posterior spinocerebellar Rostral spinocerebellar Cuneocerebellar	Proprioception, pain and pressure

Table 2.1: General description of the ascending sensory pathways. (adapted from Gartner and Patestas, 2009)

overlap exists, each pathway primarily relays a unique set of information (see table 2.1).

Fine or discriminative touch is mediated by the DCML pathway (cf. table 2.1). Peripherally, it finds its origin with mechanoreceptors (also referred to as primary afferents, mechanoreceptive afferents or first order neurons) which extend from the epidermis to the DRG and later project onto the cuneate and gracile nuclei (which are composed of second order neurons) in the case of upper and lower body sensation respectively. The axons of these second order neurons synapse contralerally with thalamical neurons (third order neurons). Figure 2.1 provides a schematic overview of the DCML pathway.

Functionally, the ascending somatosensory pathway can be divided into the *general somatic afferent system* (GSA) which collects and transmits sensory information originating from somatic structures, and the *general visceral afferent system* (GVA) which plays a similar role for visceral structures.

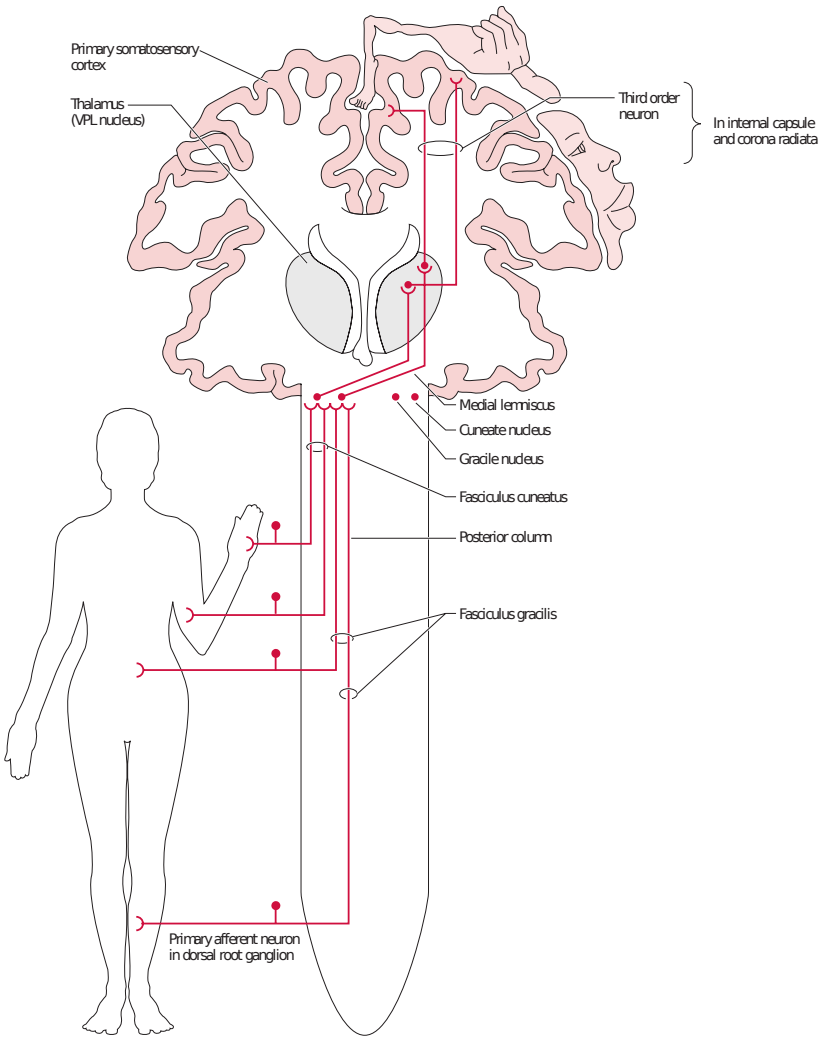

Figure 2.1: The dorsal column–medial lemniscal pathway relaying discriminative touch and vibratory sense from the body to the somatosensory cortex (VPL: ventral posterior lateral). (adapted from Gartner and Patestas, 2009)

2.2 Cutaneous receptors

Cutaneous sensation originates from thousands of cells, that can be described as unipolar neurons, which innervate the skin's epidermis and dermis. The human skin contains three types of such somatosensors: thermoceptors, nociceptors and mechano-receptors respectively relaying information about temperature, pain and mechanical forces (Lumpkin and Caterina, 2007). They vary according to their morphology and modality of response but share a basic organization and function in a similar way. A stimulus containing specific features to which a given cell responds will elicit a mechanism of sensory transduction by which the stimulation alters the ionic permeability of that cell's nerve ending and eventually leads to the generation of action potentials (Lumpkin et al., 2010). The neural signals thereby generated are propagated along the cell's axon towards the spinal cord and the DRG nested in each vertebra.

The sensory afferents are often classified according to the speed of action potential propagation, which itself is influenced by the myelin thickness around the axon. $A\alpha$ and $A\beta$ fibers are thickly myelinated cells having a low response threshold and are believed to correspond to sensors relevant for light-touch. Conversely, slower-conducting, small diameter myelinated $A\delta$ fibers, and unmyelinated C fibers belong to nociceptive and thermoceptive units (Gartner and Patestas, 2009). The cutaneous mechanoreceptors associated with fine touch are believed to rely on $A\beta$ fibers, $A\alpha$ fibers being essentially used by proprioceptive mechanoreceptors (Gartner and Patestas, 2009; Maricich et al., 2009). However, some studies link either the highly conductive $A\alpha$ (Johansson and Vallbo, 1983) or both $A\alpha$ and $A\beta$ fiber types to fine touch (Kandel et al., 2000). It is also unclear whether or not conduction velocities vary depending on the mechanoreceptor type and location, as most seem to remain between 35 and 80 mm/s, with a majority of afferents over 50 mm/s (Johansson and Vallbo, 1983; Kakuda, 1992).

The specificity of the different mechanosensory signals originates in the specialized cellular ending morphologies. However, tissue mechanics and surrounding non-sensory cells also contribute to shape the response to mechanical stimuli. Recent studies suggest that human tactile acuity is influenced by the skin's macro-structure such as, for example, the fingertip size, surface curvature, and gross epidermal stiffness, as well as its micro-structure involving different skin layers or the shape of fingertip ridges (Cauna, 1954;

Van Doren, 1989; Scheibert et al., 2009). Nontheless, mechanoreceptors seem to be affected by these factors differently, depending on their type and properties (Gerling and Thomas, 2008).

2.2.1 Primary afferent endings

Up to seven different types of cutaneous and subcutaneous receptors are recognized in humans (Kandel et al., 2000), however, only four are found in the glabrous skin of the fingertip. Fingertips possess one of the highest densities of cutaneous receptors of the entire human body, each one being innervated by up to 2000 mechanoreceptive units (Johansson and Vallbo, 1979). Consequently, fingers have been found to be particularly relevant in tasks of fine touch and precise manipulation (Johansson and Flanagan, 2009). The four receptors types present in the fingertips correspond to four different encapsulations of the nerve endings in the skin (fig 2.2):

Meissner's corpuscule. Meissner corpuscles are found 0.3 mm deep in the epidermis at a density of 130 units/cm^2 (on the fingertip). Their receptive field usually remains small and well defined (around 10 mm^2), and they are known to be most sensitive (measured in terms of output firing rate) to stimulation frequencies around 50 Hz. These corpuscles are the endings of *fast adapting type I afferents* (FAI).

Merkel cell. Merkel complexes are found in the basal epidermal layer of touch-sensitive areas of the skin, at the tip of epidermal ridges. They are located approximately 0.5 mm deep at a density of about 70 units/cm^2 in the case of fingertips. Their receptive fields usually span between 4 and 10 mm^2. Studies suggest that Merkel cells are activated by neurotransmitters that might be released from either other sensory neurons, or from neighboring keratinocyte cells (which predominantly compose the epidermis). It has also been suggested that Merkel cell signaling might even be autocrine (Maricich et al., 2009), meaning that the activation signal would be both generated and read by the cell itself. The early loss of Merkel cells have been shown to prevent mechanosensitivity in the linked afferent, however, it remains unclear if these cells retain their importance in later stages of development, as these symptoms could not be reproduced in the case of a later loss (Lumpkin et al., 2010). Merkel cells are associated to *slow adapting type I afferents* (SAI), which provide information about pressures and textures or more generally low frequency (5 Hz

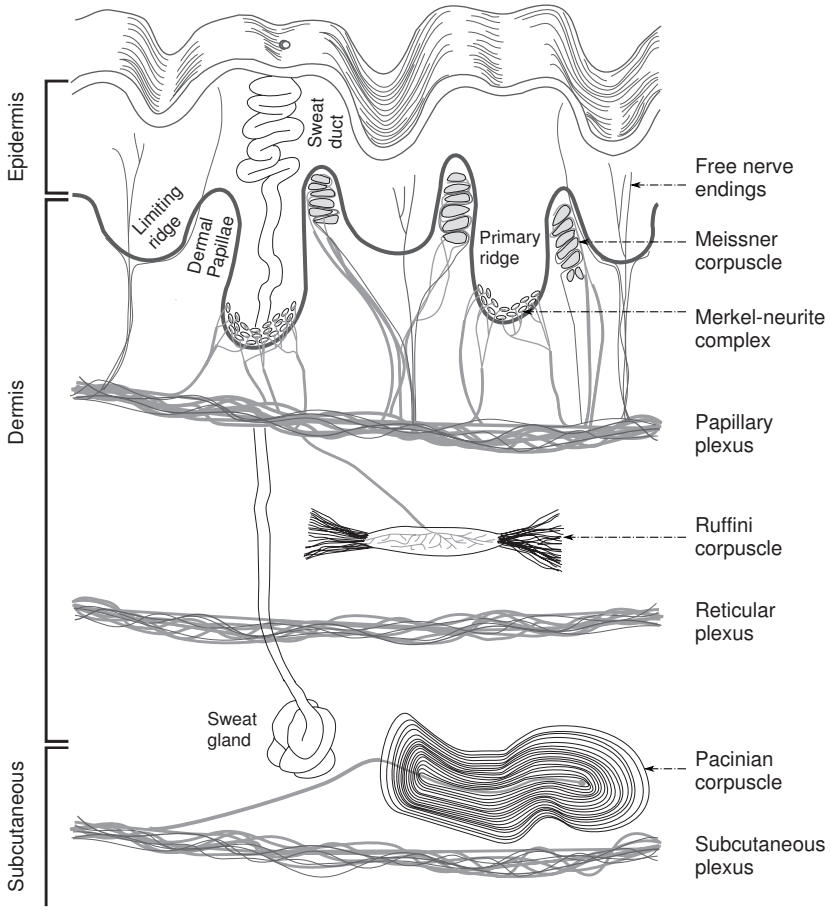

Figure 2.2: A schematic view of the fingertip glabrous skin illustrating the endings of the four different types of mechanoreceptive afferents, as well as the free nerve endings of nociceptors. Meissner's corpuscles are located in the tips of the dermal papillae, which are as close to the surface of the skin within the dermis as is possible. A single axon can innervate multiple Meissner's corpuscles. The terminals of Merkel afferents are located next to Merkel cells, which are specialized epidermal cells in the tips of the primary epidermal ridges. A single afferent axon innervates many Merkel cells on several primary ridges. Ruffini corpuscles are thought to be encapsulated strands of connective tissue and nerve endings. The Pacinian corpuscles are located in the deeper parts of the dermis and in the subcutaneous tissues. A single axon innervates a single Pacinian corpuscle and, likewise, a single Pacinian corpuscle is innervated by a single afferent axon. (adapted from Johnson, 2004; Mountcastle, 1974)

Encapsulation	Meissner's corpuscle	Merkel cell	Pacinian corpuscle	Ruffini ending
Depth (mm)	0.3	0.5	2	1
Density (unit/cm^2)	130	70	15	10
Receptive field (mm^2)	10	10	100	60
Stimulation frequency	High ($f_{opt} \sim 50$Hz)	Low	High ($f_{opt} \sim 250$Hz)	Low
Mechanoreceptor type	FAI	SAI	FAII	SAII

Table 2.2: Overview of fingertip mechanoreceptor characteristics. (adapted from Debrégeas et al., 2009)

or lower) skin deformations.

Pacinian corpuscle. Pacinian corpuscles are found in the deeper layers of the skin as well as in the sub-cutaneous tissues. The nerve terminal is surrounded by layers of concentric lamellae which filter mechanical deformations so that only high-frequency components reach the nerve terminal. Smaller and simpler lamellated endings (Golgi-Mazzoni bodies) have also been observed and probably belong to the same type of unit. They are located about 2 mm deep into the skin at a density of approximately 15 units/cm^2 on the fingertip. They have a large receptive field (approximately 100 mm^2) and respond optimally to high frequency vibrations usually between 200 and 300 Hz (Johansson et al., 1982; Bell et al., 1994). Despite their large receptive field, they are useful for detecting fine textures (whose spatial oscillation period is lower than 200 μm), perhaps thanks to the help of fingerprint patterns (Debrégeas et al., 2009). Pacinian corpuscles are associated to *fast adapting type II afferents* (FAII).

Ruffini corpuscle. Ruffini corpuscles are receptors that are located in the dermis and have a thin and spindle-shaped capsule. The nerve terminals are intermingled with collagen fibrils longitudinally passing through the corpuscle and anchoring it in the dermal collagen at its poles, thereby providing the mechanical linkage to the fibrous tissues of the dermis. They are situated 1 mm deep at a density of 30 units/cm^2 in the glabrous skin of the fingertip, and have large receptive fields of 60 mm^2 of area. These receptors are the sensors of *slow adapting type II afferents* (SAII).

2.2.2 Functional classification of primary afferents

Table 2.2 provides an overview of the known characteristics of the different mechanoreceptor types. Apart from the morphological differences in their encapsulation, mechanoreceptors can also be classified according to their functional properties (Johnson et al., 2000; Johnson, 2001). FA mechanoreceptors are essentially phasic cells, meaning that they respond to changes in the stimulus and are therefore particularly sensitive to dynamic or transient deformations of the skin. Conversely, SA neurons are tonic in nature and will respond continuously as long as a stimulation is applied. SA mechanoreceptors are therefore more useful than FA neurons to recognize static (or slowly varying) forces applied to the skin.

Both SA and FA neurons can be sub-categorized in a type I and type II. Type I mechanoreceptors have smaller receptive fields with sharper, well defined borders which allows them to generate a high quality representation of local spatial discontinuities. This property combined with their very high density on the fingertips allows for a high spatial acuity in fine touch operations. On the contrary, type II mechanoreceptors have large receptive fields with smooth, poorly defined borders. As a result, they can be stimulated by skin deformations occurring far away from the center of their receptive fields. They are less numerous –they constitute only about 30% of the total number of afferents in the glabrous skin– and have a relatively low density which remains broadly uniform across the entire hand (Vallbo and Johansson, 1984). Despite these shortcomings, it is believed that they still provide important information concerning high frequency vibrations –for FAII– or direction sensitivity to skin stretch –for SAII (Knibestöl, 1975). Furthermore, although all four mechanoreceptor types have been shown to respond on occasion to hand movements, it is suggested that type II neurons in particular provide proprioceptive information in addition to the exteroceptive information (Johansson and Vallbo, 1983). Indeed, joint positions and movements seem to elicit responses from type II afferents (Hulliger et al., 1979). Psychophysical studies also suggest that type II afferents are useful for kinesthesia in the human hand (Burgess et al., 1982).

A significant difference between type I and type II mechanoreceptors concerns the shape of their receptive fields on the skin. Whereas type II receptive fields have only one point of maximal sensitivity –generally located

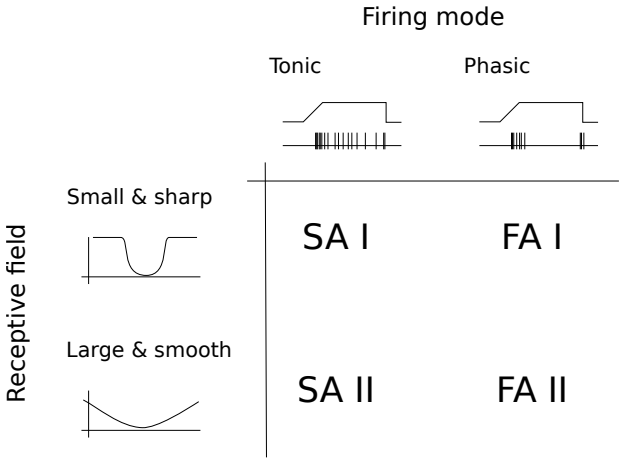

Figure 2.3: Distinguishing properties of tactile afferent types in the glabrous skin of the human hand. Columns show the firing mode (or equivalently the rate of adaptation). Graphs represent schematically the spiking response (lower trace) to perpendicular indentations of the skin (force of indentation is shown on the upper trace) for each unit type. Rows indicate receptive field properties. Plots illustrate the spiking threshold as a function of position of the indented probe on the skin. The minimal points of the curve are the most sensitive areas (likely the center of the receptive field).

near the center of the sensitive zone– (Darian-Smith, 1984), type I receptive fields have a complex structure with multiple high-sensitivity points (Darian-Smith, 1984; Phillips et al., 1992) called hotspots. Though no direct evidence has been found, it can be supposed that hotspots are linked to the structure of the afferent endings (Johansson, 1978; Vallbo and Johansson, 1984). As hotspots number between 12 and 17 and between 4 and 7 for FAI and SAI afferents respectively, it has been suggested that there may be as many corresponding Meissner corpuscles and Merkel cells terminating each afferent.

Figure 2.3 illustrates the functional classification of the four different types of fingertip cutaneous mechanoreceptors. Of the 17000 units innervating the human hand, 43% are FAI afferents, 13% are FAII, 25% are SAI and 19% are SAII. This count however hides the fact that the highest densities of mechanoreceptors are found on the fingertips which collect up to 2000 afferent endings each (Johansson and Vallbo, 1979). In the fingertips, type I mechanoreceptors are present at considerably larger densities than their type II equivalents (see table 2.2), suggesting a particularly important role of type I afferents in conveying fine touch to the central areas of the nervous system.

2.3 Dorsal column nuclei

Mechanoreceptive afferents supporting fine touch project to second order neurons in the dorsal column nuclei. These are the cuneate nucleus and the gracile nucleus which receive projections exclusively from afferents of the upper body (arms and trunk) and lower body (mainly the legs) respectively. Consequently, sensory information originating from the fingertips is relayed first through cuneate neurons before reaching higher order areas.

2.3.1 Anatomy of the cuneate nucleus

Anatomically, the cuneate nucleus is composed of roughly three distinguishable areas: the caudal, the middle and the rostral cuneate nucleus (Berkley et al., 1986). The middle area can be further decomposed into the core (central sub-area) and the shell (peripheral sub-area) (Fyffe et al., 1986a). The core is essentially composed of a cluster of cuneothalamic neurons projecting into the contralateral ventral posterior lateral thalamic (VPL) nucleus, surrounded by local interneurons. The shell is basically made up of interneurons. The caudal and rostral areas of the cuneate nucleus contain interneurons and neurons projecting to other structures such as the cerebellum, the spinal cord and other parts of the diencephalon (Berkley et al., 1986).

The cuneate nucleus mainly receives inputs from primary afferents and corticocuneate fibers originating from the contralateral sensorimotor cortex. Within the middle area, primary afferents establish connections with both interneurons and projection neurons (Fyffe et al., 1986a), while the cortico-cuneate make synaptic contact essentially with inhibitory interneurons in the shell (Cheema et al., 1984). The cuneate nucleus also receives some inputs from other sub-cortical nuclei (Hsiao and Yau, 2008).

2.3.2 Functional role of the cuneate nucleus

The cuneate nucleus has not been the subject of as many neurophysiological studies as the peripheral afferents or the primary somatosensory cortex have. Given the evidence that has been acquired, the cuneate nucleus is usually believed to be little more than a relay for afferent signals emanating from

cutaneous and proprioceptive structures. Indeed, there appears to be a quasi equivalence between the firing of cuneate neurons and that of their cutaneous and proprioceptive afferent inputs. In other terms, there is a high synaptic efficacy by which most pre-synaptic spikes appear to directly induce a post-synaptic one (Amassian and Giblin, 1974; Hsiao and Yau, 2008). This suggests that afferent information is almost identically reproduced at the cuneate level. This would also explain how cutaneous receptive fields of neurons located higher up in the somatosensory pathway manage to remain relatively small –and even sometimes of comparable size to primary afferent receptive fields– in the thalamus (Wang et al., 1995) . It is also noteworthy that segregation between submodalities seems to exist already at the cuneate level (Dykes et al., 1982; Kandel et al., 2000). All in all, very few modifications to the informative signal seem to occur in this dorsal column nuclei.

Consequently, little convergence and divergence of sensory input is supposed to take place at this stage. However, after observing the structure and dimensions of cat cuneate neurons, it has been estimated that each mechanoreceptive afferent projects to approximately 1700 cuneate neurons and that each cuneate neuron connects with some 300 afferents (Jones, 2000). A more recent study on decerebrated cats has pointed out that of these numerous putative connections, less than 10 are actually functionally active –meaning that they can actually elicit a post-synaptic potential (Bengtsson et al., 2013). Somewhat coherently, the same study has recorded cutaneous receptive fields of cuneate neurons approximately twice as large as their peripheral afferent counterparts (at 20 ± 17 mm^2 and 12 ± 10 mm^2 respectively).

Evidently, this does not mean that no processing takes place in the cuneate nucleus. Indeed, a computational approach has allowed to suggest that a small number of high efficacy synapses might be well suited for an efficient transmission of information allowing an optimal discrimination of signals downstream of the cuneate nucleus (Brasselet et al., 2009; Bengtsson et al., 2013).

Furthermore, the case for a cuneate processing of tactile signals is further supported by experimental evidence on the existence of more complex center-surround receptive fields in the cuneate nucleus (Canedo and Aguilar, 2000). Center-surround receptive fields possess an excitatory center surrounded by an inhibitory neighborhood and are particularly well known for their role in the processing of visual signals (Kuffler, 1953; Wiesel and Hubel, 1966). The surround inhibition is at least in part generated by fast afferent connections and

may serve to effectively reduce the size of cuneate receptive fields. Feedback signals from the sensorimotor cortex (both excitatory and inhibitory) have been observed (Gordon and Jukes, 1964; Canedo and Aguilar, 2000). Though the exact role of these feedback signals remains unknown, it is hypothesized that they may facilitate the information flow notably by enhancing the temporal precision of spikes (Canedo and Aguilar, 2000).

The cuneate nucleus' complex structure suggests that its role, as previously pointed out, is more than that of a synaptic relay for tactile information. However, its precise dynamics and function remain largely unknown for the time being.

2.4 Thalamus

Second order neurons from the cuneate nucleus (and more generally from the dorsal column nuclei) send projections through the medial lemniscus tract to synapse with type I cells in the contralateral *ventral posterior lateral* (VPL) nucleus of the thalamus. The thalamus also receives inputs from primary afferents through the dorsal horn of the spinal cord. The output of the VPL network is sent, with varying strength, to the primary somatosensory cortex (SI) –areas 3a, 3b, 1 and 2– and, to a lesser extent, to the secondary somatosensory cortex (SII).

The VPL is organized as an ensemble of rod-like structures which can be functionally segregated into a core and two successive surrounding regions. The core is composed of cells which have observed properties similar to SAI peripheral afferents. Neurons in the first surrounding regions have larger receptive fields and can be either slow or fast adaptive-like neurons. The outermost shell contains cells that respond to deep or proprioceptive inputs. The core region sends projections to areas 3b and 1 of SI, suggesting that these are the areas responsible for processing fine touch signals. On the contrary, the shell projects towards areas 3a and 2 of SI, which are consequently thought to process proprioceptive information (fig. 2.4).

Thalamic pathways relaying information to the cortex are well segregated, usually responsible for a specific sub-modality, such as whisker motion (in rats) and fine touch which are relayed via distinct thalamic neuronal populations (Yu et al., 2006; Diamond et al., 2008).

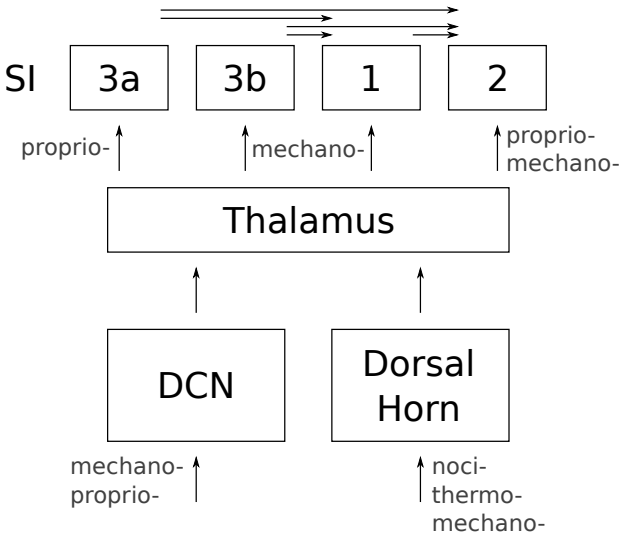

Figure 2.4: A schematic view of the functional connectivity between the dorsal column nuclei (DCN), the ventral posterior lateral of the thalamus (VPL) and the primary somatosensory cortex (SI) regions. (adapted from Hsiao and Yau, 2008)

Similarly to the cuneate nucleus, little functional convergence and divergence is believed to occur in the VPL. However, there are important feedback loops between the cortex and the thalamus which modulate the activity transmission. Studies in rats have allowed to know more about the effects of the thalamocortical loops. Top-down modulation has notably been found to alter the transmission of information based on past experience (Ghazanfar and Nicolelis, 1997; Ego-Stengel et al., 2012), motor activity (Lee et al., 2008) and reward expectation (Pantoja et al., 2007). This modulation was important for explaining activity differences between active and passive touch in the rat vibrissal system (Fanselow et al., 2001; Nicolelis, 2005; Pais-Vieira et al., 2013).

2.5 Somatosensory cortex

Third order neurons in the thalamus primarily send their axons to the primary somatosensory cortex (SI) located in the postcentral gyrus of the parietal lobe. SI contains four different areas: Broadmann's areas 3a, 3b, 1, 2 (Kandel et al., 2000). Most thalamic fibers project to areas 3a and 3b and, to a lesser extent, to areas 1 and 2 of SI. However, extensive connections between different regions of SI have been observed (see fig. 2.4), which suggests that regions 1 and 2 might play more of an integrative role with inputs from the thalamus as well as areas 3a and

3b of SI. The secondary somatosensory cortex (SII) is located in the second bank of the lateral fissure and is innervated from each of the four areas of SI as well as directly, though to a far lesser extent, from the thalamo-cortical neurons. SII projects to the insular cortex, which in turn innervates regions of the temporal lobe that are believed to be important for tactile memory.

An interesting property of SI is that the topographical arrangement of the receptive fields on the skin is preserved (Mountcastle, 1957). SI, like the rest of the cortex, is organized into vertical columns some 300 to 600 μm wide and spreading over six layers of neurons from the cortical surface to the white matter (Powell and Mountcastle, 1959; Mountcastle, 1997). Each cortical column of SI is specific to one location (on the skin or in the body) and one sub-modality (fig. 2.5 B). Neighboring columns in SI will process inputs from afferents whose receptive field centers are close, thus creating a somatotopic arrangement in SI which is known as the *homunculus* (fig. 2.6). The somatotopic maps do not match the spatial topography of the body but rather modulate the representation of body regions depending on their innervation density. The result is that some areas of the body (*eg.* the hands, feet and mouth) are extended whereas other sections are compressed in comparison (*eg.* trunc and legs). For example, there is approximately 100 times more cortical tissue devoted to an area of finger skin than to an equivalent same area of abdomen skin.

Each column also generally only receives inputs from one sub-modality (*ie.* touch, pressure, pain and temperature). This follows quite naturally from the sub-modality segregation already observed in the different pathways and relays (*eg.* DCN and VPL). Furthermore, even within a single sub-modality, inputs may be further segregated. For example, mechanoreceptive signals in area 3b are processed in slow adapting and fast adapting columns (Paul et al., 1972) which receive information from respectively fast adapting and slow adapting receptors (fig. 2.5 B and C).

Each of the four areas of SI receives inputs from the entire body and forms its own somatotopic organization. However, areas tend to be heavily biased towards one type of sub-modality. For example, area 3a is dominated by inputs of proprioceptive signals on muscle stretch whereas area 3b focuses on exteroceptive information from mechanoreceptive afferents. In area 1, fast adapting cutaneous receptors tend to dominate. Contrary to the three other regions, the segregation in area 2 is less marked with inputs from both fast and slow adapting afferents as well as proprioception.

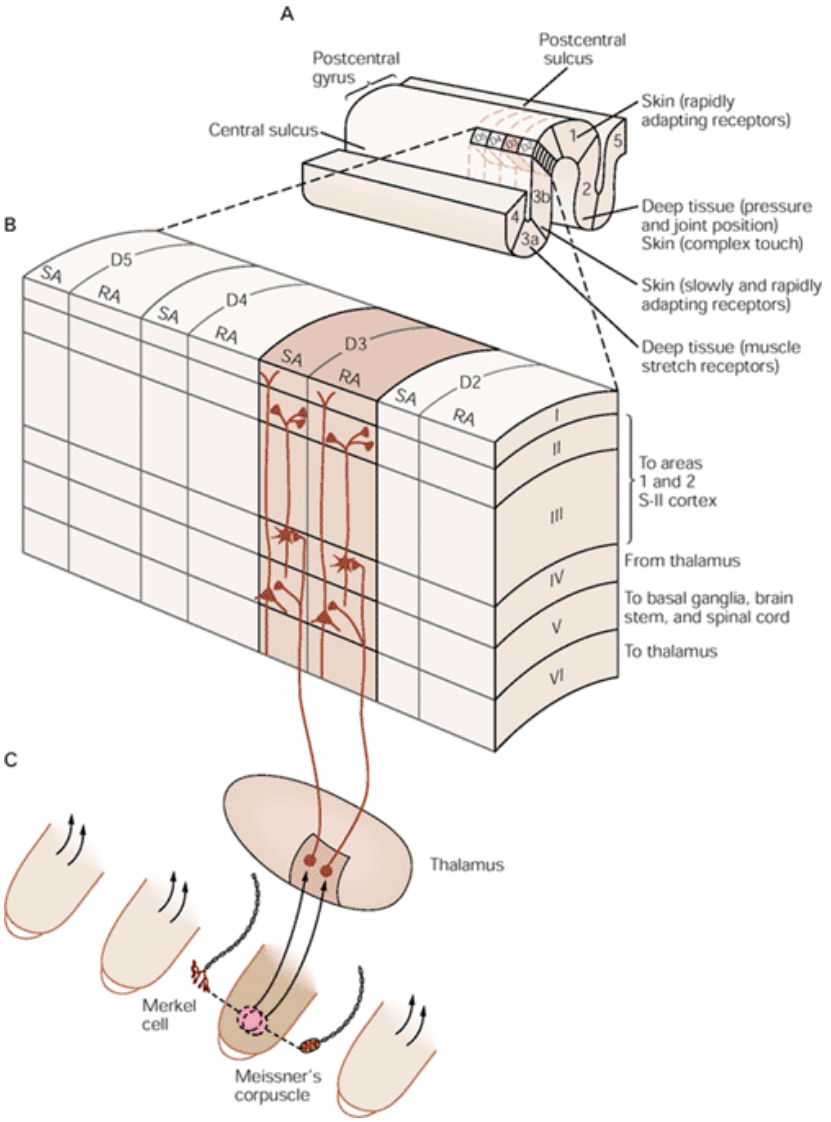

Figure 2.5: Somatotopic and sub-modality organization of the primary somatosensory cortex *A*. In each of the four regions of SI –areas 3a, 3b, 1, and 2– inputs from peripheral receptors in specific parts of the body are organized in columns of neurons. *B*. Detailed view of the columnar organization of inputs from hand digits in area 3b. Alternating columns of neurons receive inputs from fast adapting (FA, also known as rapidly adapting RA) and slow-adapting (SA) receptors in the glabrous skin. *C*. Overlapping receptive fields from FA and SA receptors project to distinct columns of neurons in area 3b. (taken from Kandel et al., 2000, adapted from Sur et al., 1984)

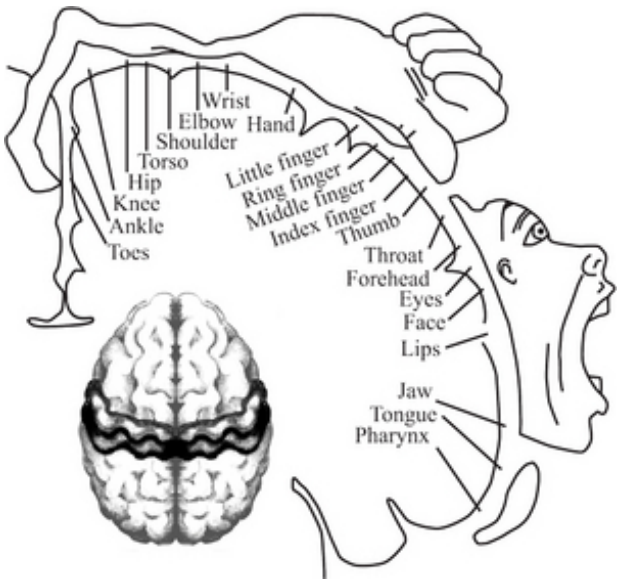

Figure 2.6: Somatotopic arrangement of the SI. Each sensitive area of the body is mapped onto the somatosensory cortex. More sensitive zones of the body (such as hands and lips) are innervated with a higher density of mechanoreceptive afferents and have an extended representation in SI.

Due to the convergence and divergence of the successive relay networks, receptive fields of cortical neurons are larger than those of dorsal root ganglion neurons. However, their size varies significantly depending on the area and layer considered (Sur et al., 1985). Furthermore, receptive field sizes also depend on the peripheral innervation density (or, equivalently, on the magnification in the cortical map). Receptive fields of the fingertips remain fairly local (sometimes covering up to a few fingertips) whereas those from the forearm can cover the entire ulnar surface. Noticeably, area 1 and 2 receptive fields are considerably larger and more complex than those of area 3b, reflecting once more that these two area have functionally different roles. Indeed, area 2 has been shown to contain neurons that act as feature detectors, similarly to neurons from the primary visual cortex (Hubel and Wiesel, 1959). Notably, orientation and direction specific neurons respond selectively to stimulus edges with respectively a particular orientation and a particular movement direction (Hyvärinen and Poranen, 1978; Costanzo and Gardner, 1980). A more recent study by Bensmaia et al. (2008) has established that orientation selective cells can also be found in areas 1 and 3b of SI. Though cells from both areas appear equally capable of discriminating directions, area 1 was found to contain more such orientation selective cells as well as a few direction selective ones. Once again, this

illustrates the fact that areas 1 and 2 act as slightly higher level processing stages, with more powerful feature extraction occurring, than areas 3a and 3b. This is further confirmed by ablation studies performed on animals which showed that lesions of areas 1 and 2 only incurred milder shape and texture (respectively) discrimination deficits (Carlson, 1981), whereas animals without areas 3b were unable to perform a wide range of tactile related tasks (Randolph and Semmes, 1974; Semmes and Turner, 1977).

2.6 Conclusions

- Fine (*ie.* discriminative) touch is mediated by the *dorsal column-medial lemniscal pathway*. This pathway is composed of three synaptic relays before reaching the somatosensory cortex: *primary afferents*, the *cuneate nucleus* and the *ventral posterior lateral nucleus of the thalamus*.
- Four types of primary afferents (also referred to as mechanoreceptors) innervate the glabrous skin of the fingertip. They correspond to four different encapsulations of the afferent endings, which influence their functional properties. Contrary to type II, type I neurons have small well defined receptive fields and capture stimuli with the highest spatial acuity, they outnumber by far type II afferents in the fingertip. Both types of neurons can be either *slow adapting* (providing a tonic response to stimuli) or *fast adapting* (having phasic response).
- The cuneate nucleus is characterized by a low functional connectivity with the primary afferents. Though its role is unclear, complex receptive fields as well as feedback signals from the cortex suggest that the cuneate nucleus constitutes more than a simple synaptic relay for tactile information.
- Important feedback loops between the cortex and thalamus modulate the transmission of tactile signals.
- Tactile information enters the somatosensory cortex through four different Broadmann's areas, each with a specific specialization.
- Signals from different sub-modalities of the sense of touch remain segregated until they reach cortical areas.

Chapter 3

Neural coding of tactile information

Among the nervous system's many functions is that of integrating contextual information from the organism and the environment –obtained through the different sensory systems– and use it to elaborate different types of responses. The study of neural coding aims at understanding under what form the information is processed and transmitted through the nervous system, or, in the words of Perkel and Bullock (1968), elucidating "the representation and transformation of information in the nervous system". A complete understanding of the neural coding principles would allow to both *(i)* predict the neural responses to a given stimulus –*ie.* encoding– and *(ii)* know how the system will read into a specific input signal –*ie.* decoding.

This chapter will briefly present what is known about the neural coding mechanisms and will focus on the two main coding schemes believed to be found in the nervous system (*ie.* temporal coding and rate coding). The second section of this chapter will present the coding of tactile information in the peripheral somatosensory system. In particular, it will address how forms (*ie.* of the spatial structure on surfaces) –perhaps the most important component for fine touch discrimination– are encoded through possible rate and temporal schemes.

3.1 Neural coding

3.1.1 Action potentials

The nature of the informative signal conveyed by neurons is an electrical potential difference between the interior of the cell and its surrounding extracellular environment (Dayan and Abbott, 2001). Under resting conditions,

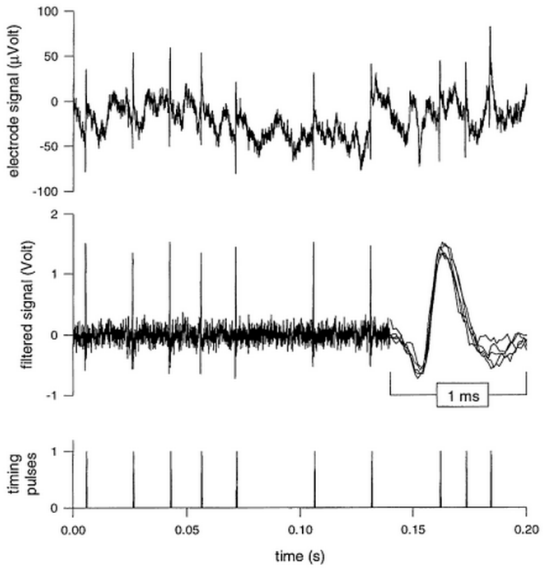

Figure 3.1: Action potentials recoded in the fly's brain. *Top:* recorded voltage difference between an extracellular electrode in a fly's brain and a reference electrode placed in body fluid. *Middle:* same voltage after applying a band-pass filter to remove low frequency noise. The similar shape of action potentials is visible with an expanded time-scale on the right overlay. *Bottom:* isolating voltages higher than a given threshold allows to isolate the timings of action potentials. (taken from Rieke et al., 1999)

the potential inside the cell membrane of a neuron is approximately -70 mV, with the potential of the surrounding environment conventionally set to 0 mV. The difference between these two values is known as the membrane potential. Membrane potential is regulated using ion channels which span all along the membrane to adjust ionic concentrations of, predominantly, sodium (Na^+), potassium (K^+), calcium (Ca^{2+}) and chloride (Cl^-) ions. Depending on the relative concentration levels of these ions, the membrane potential can fall further (hyperpolarization) or on the contrary increase (depolarization). If the depolarization is significant enough to raise the membrane potential beyond a threshold value, a positive feedback process is initiated and an action potential – also known as *spike*– is emitted (Adrian, 1926b,a; Adrian and Zotterman, 1926b,a). Spikes are characterized by a very high potential fluctuation (above 100 mV) over a very short temporal window (approximately 1 ms, see fig. 3.1, center). After the spike, a hyperpolarization occurs making it harder or even impossible for the neuron to emit another spike during a refractory period which can potentially last up to tens of milliseconds.

Contrary to sub-threshold membrane potential fluctuations which are greatly

attenuated over distances of 1 mm, action potentials are continuously regenerated and are supposedly the only form of membrane potential fluctuation which can travel rapidly over large distances without attenuation (Dayan and Abbott, 2001). At the junction between two neurons, known as a synapse, potential fluctuations due to action potentials indirectly lead to the release of neurotransmitters which either stimulate or inhibit the subsequent neuron. From these observed properties, it is assumed that information in the nervous system is essentially conveyed through the medium of action potentials.

As the amplitude, duration and shape of spikes can vary a little (Dayan and Abbott, 2001), the information is contained in the presence and timing of spikes and spike are often represented in a stereotypical manner (see fig. 3.1, bottom). As such, the neural code is all-or-none, somewhat akin to the binary code used in computers, albeit one without central clock. In the rest of this study, spikes will be solely characterized through their timing.

3.1.2 Spike train description

Given the very short duration of spikes compared to that of the entire response and the stereotyped nature associated with them, action potentials are usually represented using Dirac functions (Dirac, 1958):

$$s(t) = \sum_i \delta(t - t_i) \tag{3.1}$$

where $\{t_i\}$ is the set of spike times and δ is the Dirac function which is null everywhere except in the origin, where it is infinite (such that its integral is equal to one). The spike count over a window of time T can then be obtained by integrating the spike train:

$$N = \int_0^T s(\tau) d\tau \tag{3.2}$$

Strictly speaking, the firing rate function is defined as:

$$r(t) = \frac{1}{\Delta t} \int_t^{t+\Delta t} s(\tau) d\tau \tag{3.3}$$

As Δt approaches zero, the firing rate converges towards the original spike train $s(t)$. When dealing with multiple trials, the spike train s can be replaced by its average over the trials $\langle s \rangle$ and Δt should be large enough to contain multiple spikes in order to accurately estimate the firing rate function.

Different methods are used to approximate the firing rate, all of them containing a set of arbitrary parameters. The simplest method is to discretize the timescale into different bins and count the number of spikes within each bin. When adding its results over multiple trials, this method leads to the creation of a peristimulus time histogram (PSTH, also known as poststimulus time histogram). The drawback of this method is that it involves choosing a bin size and placement, which can greatly influence the shape of the estimated firing rate curve. To avoid having to arbitrarily place the bins, another method uses a sliding time window to estimate the firing rate. This method uses the same spike multiple times in order to compute the firing rate at different time points which creates a correlation between firing rates at close times. Both of these methods generate firing rate curves which are piece-wise continuous. For a continuous function, a convolution between the spike train and a kernel (*eg.* Gaussian) is used. In all cases, the temporal resolution has to be chosen arbitrarily depending on the type of coding considered. For a very high temporal resolution, the spatio-temporal structure of the spike train is maintained in what is known as *temporal coding* (Theunissen and Miller, 1995). Conversely, for lower resolutions, the structure of the spike train is mostly lost and the *rate code* is studied.

3.1.3 Spike rate coding

Along with observing the action potentials, E. D. Adrian found that the discharge rate of these spikes was positively correlated with the amplitude of the stimulation (Adrian and Zotterman, 1926b). This has led to an approach of neural coding focused around firing rates in which the number of spikes emitted holds most of the relevant information about the stimulus (notably about its amplitude). Studying the rate code has proven useful in a number of tasks such as (but not restricted to) vision (Dean, 1981), navigation (Burgess and O'Keefe, 1996), motor control (Georgopoulos et al., 1988) and decision making (Sallet et al., 2007).

The assumption behind the concept of rate coding have often led to model neural activity using a Poisson process. A Poisson process is a Markovian point process where the occurrence of a spike event is independent from the timing of the last event. In this context, the probability of observing a number k of spikes

in a temporal window of size Δt follows a Poisson distribution:

$$p_{\Delta t}(k) = e^{-r\Delta t}\frac{(r\Delta t)^k}{k!} \tag{3.4}$$

where r is the firing rate in the temporal window considered. Two distinguishing properties of a Poisson process is that the *Fano factor* (F) and the *coefficient of variation* (C_V) are equal to 1.

$$F = \frac{\sigma_n^2}{\langle n \rangle} \tag{3.5}$$

$$C_V = \frac{\sigma_\tau}{\langle \tau \rangle} \tag{3.6}$$

where σ_n^2 is the variance in spike count, $\langle n \rangle$ the mean spike count, σ_τ and $\langle \tau \rangle$ respectively the standard deviation and the mean interspike interval (ISIs). High values of Fano factor and coefficient of variation reflect a very high variability not only in the temporal structure of spike trains but also in the number of spikes. Consequently, this model suggests that it is necessary to record multiple trials and/or over a long time period in order to accurately estimate the rate signal which is being conveyed. Figure 3.2 provides an illustration of this drawback by showing an estimation of the firing rates for different numbers of trials. It can be observed that for few trials, the estimation is very poor and only for a high number of trials (above 100 in this case) is the firing rate signal adequately reproduced.

This suggests a quite inefficient nervous system, with a high level of redundancy required. Nonetheless, the Poisson process model is supported by some experimental evidence as coefficient of variation values nearing 1 have indeed been observed in cortical neuronal activity (Softky and Koch, 1993). Furthermore, spike counts have been shown to be highly variable, with Fano factors around 1.5 in the visual cortex for example (Tolhurst et al., 1983; Snowden et al., 1992). This slightly higher Fano factor is sometimes explained through the presence of observed bursting activity and it is possible to adapt the Poisson process model to reproduce this behavior (for example by simply replacing the spike event by a burst event).

Further improvements have been brought to the Poisson process model in order to take into account the ISI. Indeed, after a spike is emitted, the refractory period prevents another spike to be generated for a few milliseconds, effectively limiting the range of possible ISIs. This is never taken into account in the Poisson process

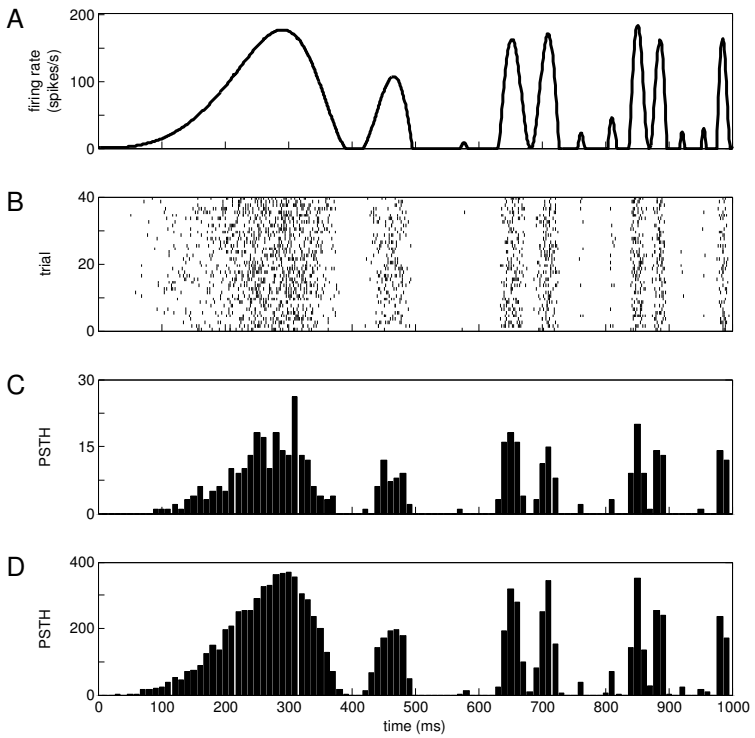

Figure 3.2: Illustration of the Poisson process for generating spike trains following specific firing rates. *A.* Firing rate evolution over time of the desired spike trains. *B.* Raster plot of 40 spike trains generated using a Poisson process for the firing rate curve describe above. Note the high variability in the spike trains. *C.* and *D.* PSTH –computed over 10 and 200 trials respectively– used to estimate the firing rate of the spike trains in the raster plot. Comparing the two plots shows that individual spike trains are poorly informative regarding the firing rate and an important number of trials is therefore necessary to build a correct estimation.

model in which spikes are independent from one another. The *renewal process* corrects this by taking into account the ISI distribution, and is akin to a Poisson process which generates ISIs instead of spikes. Experimental recordings have shown that ISI distributions can be roughly fitted by gamma functions (Bair et al., 1994) and the renewal process can therefore be defined through the probability of having a spike at time t, knowing that the last spike occurred at time $\tilde{t}$:

$$p(\ t \mid \tilde{t}\ ) = \gamma(t-\tilde{t})^{\alpha} e^{-\lambda(t-\tilde{t})} \tag{3.7}$$

with α, γ and λ parameters defining the ISI distribution.

Rate coding limitations

The concept of rate coding has a number of drawbacks which lead many to question its true role in the neural code. They notably include:

Encoding capacity. By its own mathematical definition, rate coding considerably reduces the number of dimensions in the signal space and with it the quantity of potential information being encoded (MacKay and McCulloch, 1952). This is illustrated by the fact that although different spatio-temporal structures of spike trains may have the same rate code, spike trains with different rates will never have the same spike timings. By itself, this observation does not prove that the capacity of a rate code is not sufficient to carry the necessary information, but it does suggest that if it were so, the nervous system would be quite sub-optimal.

Energy cost. As was pointed out by Lennie (2003), the cost of generating a spike is high. In this context, having to generate many spikes to provide a precise estimate of the firing rate –especially for high firing rates– appears inefficient energy-wise.

Signal modulation. Firing rates are modulated at a very high speed, sometimes sorter than the average ISI. Such brief modulations are in effect impossible for the neural system using single spike trains. Their detection would require a high level of redundancy which is not always available at the peripheral level.

Signal estimation. In the cases where only a few (one or two) spikes are received, the rate cannot be reliably estimated. For example, Gautrais and Thorpe (1998) computed that for a Poisson process input whose observed rate was 100 Hz after 10 ms (so 1 spike in the 10 ms window), all that one could say was that there was a 90% chance that the actual frequency was comprised between 5 and 474 Hz. To reduce the estimation error, one has to observe the activity on multiple neurons and/or during a longer temporal window.

Noise origin. Rate coding suggests neurons are highly variable or noisy in their spike timings. This raises the question of the origin of such noise. To this day, the main biophysical model of neuron is the Hodgkin-Huxley model (Hodgkin and Huxley, 1952) which is entirely deterministic. Some explanatory models have been proposed though they often remain disputed (*eg.* Shadlen and Newsome, 1994; Mainen and Sejnowski, 1995; and Softky, 1995).

3.1.4 Spike time coding

Another approach to extracting information from the neural code supposes that individual spike times are relevant to the signal. This stems from the observation that the theoretical capacity of neurons to transmit information is much higher when taking into account the timing of spikes (or of ISIs) as compared to spike counts only (MacKay and McCulloch, 1952; Gautrais and Thorpe, 1998). Furthermore, it is supported by experimental evidence which has shown that *(i)* spike times can in some cases be very reliable (Johansson and Birznieks, 2004), and that *(ii)* spike train processing can be surprisingly fast (Thorpe et al., 1996).

Spike time precision

Although a high level of irregularity has been observed in cortical neuronal activity (as discussed in section 3.1.3), robust spike timings have also been found in neural systems. In particular, sensory systems seem to share a common high temporal precision at least at the peripheral level. Indeed, the temporal precision of spikes has been observed in the case of the auditory (Joris et al., 2004; Furukawa et al., 2000), olfactory (Haddad et al., 2013), visual (Berry et al., 1997), somatosensory –fingertip (Johansson and Birznieks, 2004) as well as whisker (Arabzadeh et al., 2005)–, and electrosensory (Carr et al., 1986) systems.

Attempts to conciliate the high temporal precision sometimes observed with the apparent variability recorded in some systems has led to the view that peripheral systems might be based essentially on spike time codes whereas central systems (in which admittedly more redundancy and longer processing time-windows are available) would rely on rate codes. Consistently with this view, it has been noted that the temporal precision of spikes often seems to decrease as the signal propagates to new areas (Joris et al., 2004), and that some conversion mechanism in the code must therefore occur (Haddad et al., 2013).

However, it is possible that these observations might be the result of a skewed analysis as the presence of rate coding is not necessarily incompatible with an informative spatio-temporal organization of spikes. Indeed, temporal coding has been found relevant in areas (such as the central nervous system) that were previously believed to rely on rate coding mechanisms. For example,

Bair and Koch (1996) found that the response of neurons from the middle temporal (MT) cortex to certain highly dynamic motion stimuli showed a reproducible temporal modulation precise up to a few milliseconds (ranging from 2 to 10 ms). Similarly, Reich et al. (2001) observed that spike times (and notably first spike latencies) in the visual cortex (V1) conveyed information for distinguishing subtle contrast levels. Similar findings have been made in the somatosensory system where a 5 ms temporal precision has been found for spikes (Petersen et al., 2002). The precision of spike timings in cortical neurons has been found to depend on the stimulus transients: constant stimuli induced poor temporal precision, whereas rapid fluctuations produced highly reproducible spike timings (Mainen and Sejnowski, 1995).

Processing speed

Proponents of spike time coding also point towards the very high speed at which sensory information can be processed as further evidence for the importance of spatio-temporal structure of spike trains. Studying the response of primate brains to visual stimuli, Thorpe and Imbert (1989) found that selective neurons reacted as early as 100–150 ms after the stimulus onset. Before reaching these neurons, the informative signal had to cross approximately 10 layers of neurons spread across the cortex. This implied that on average, each of these processing stages had 10 ms to carry out its task. Given that cortical firing rates rarely rise above 100 Hz, and the distances over which the signal travels, it has been argued that processing of the signal is accomplished while only 0 or 1 spikes (or an extreme of 2 spikes in some rare conditions) have been received. Furthermore, this estimation is carried out while neglecting the possible role of recurrence in the processing networks. Another study has demonstrated that unknown visual scenes can be categorized by humans in only 150 ms (Thorpe et al., 1996).

Along the same line, it has been shown that in the somatosensory system only a few spikes (perhaps as few as one spike) from a single mechanoreceptive afferent were sometimes necessary to generate a percept (Vallbo, 1995). And important temporal constraints have also been observed in a number of other sensory systems (Carr, 1993).

Decoding a temporal code

Studying the information contained in the spatio-temporal pattern of spikes is only part of the problem, as it is important to know whether or not neurons have the means to extract this information (let alone if they actually do so). Indeed, information has often been found in the timing of first spikes (*eg.* Johansson and Birznieks, 2004; Gawne et al., 1996; Heil, 2004; Panzeri et al., 2001). However, it is difficult to imagine how the biological organism would have access to the absolute timing of first spikes; or even how first spikes are defined or recognized in the context of a dynamically evolving stimulation.

A number of models have been put forward to explain how such temporal information could be extracted. Yet, all of these are linked in that they seem to rely on the creation of a relative scale to evaluate the spike times.

Relative first spike times. In order to bypass the impossibility to extract the absolute timing of spikes, a relative time scale is created by considering the population activity onset as origin. Using this technique, Gollisch and Meister (2008) managed to recreate, with surprising quality, the stimulus images from the recorded activity of ganglion cells of an isolated salamander retina. Furthermore, while it might be expected that using relative times yields less information than for their absolute counterparts, a study on sound localization performed by Chase and Young (2007) on decerebrated cats showed that relative latencies could actually increased the average amount of information contained in single neuron responses.

Phase coding. Combining the state (and more precisely the phase) of the local field potential oscillations and the timing of spikes has been shown to be highly informative during the analysis of cortical neuron responses to visual and auditory stimuli (Kayser et al., 2009). In this coding scheme, local field potential oscillations act as a reference point to understand the spike times.

Coincidence detector. Perhaps the simplest decoding scheme: the coincidence detector considers the spike times relative to each other (Hopfield, 1995; König et al., 1996). If two spikes elicit post-synaptic potentials that are temporally close, their effects can be combined to either elicit a spike or inhibit the creation of one, in effect modulating the output activity of the post-synaptic neuron. In its most common form, coincidence detector neurons only fire when receiving synchronous inputs.

Rank order coding. Another mechanism found for decoding first spike latencies is the Rank Order coding scheme (Thorpe and Gautrais, 1998). Contrary to the other mechanisms listed above, the rank order system does not rely on the precise timing of spikes but rather on their relative order of arrival. It uses synaptic weights and an inhibitory network (Thorpe et al., 2001) so that only a specific order of incoming spikes generates an outgoing activity.

3.2 Fine touch information coding

The relative contribution of kinesthetic and cutaneous sensation in the identification of surfaces with textures and embossed shapes is still an open question. In the case of fine textures, remote mechanoreceptors are capable of encoding surface roughness suggesting that subcutaneous mechanoreceptors, responsible for kinesthetic sensation, can contribute to the recognition of these textures (Libouton et al., 2012). However, during tactual pattern recognition, no statistically significant difference was found between active and passive touch (Vega-Bermudez et al., 1991); it can therefore be assumed that kinesthetic information plays a minor role compared to fine touch in the characterization of coarser textures. Fine touch, also known as discriminative touch, is a sensory modality which allows the subject to precisely locate the stimulation source. It carries the necessary information about different features of a stimulus in order to locate, characterize and possibly identify it.

Perceptually, textures can almost entirely be defined using two independent dimensions: rough-smooth and hard-soft (Johnson and Hsiao, 1992; Hollins et al., 1993). Perceived roughness has been found to be associated with the spatial modulation of the surface (Connor and Johnson, 1992), although it has been argued that for very fine textures it can also be perceived thanks to a vibrational component (Hollins and Risner, 2000). This section will focus on the coding mechanisms underlying form perception of coarse textures or embossed shapes in the peripheral somatosensory system.

The study of coding mechanisms of tactile information has historically concentrated on the firing rates induced by cutaneous stimulation. More recently, studies have increasingly considered the temporal coding aspects of these responses and it has been proved that spike times carry a high amount of information for discriminating between different stimuli (Johansson and

Birznieks, 2004). Although some of the information can be found through both of these coding mechanisms, it has been argued that they rather complement each other and carry information on different features of the stimulus (Harvey et al., 2013; Saal et al., 2009).

3.2.1 Primary afferent coding of spatial structures

Mechanoreceptor type comparison

Form perception at the finger pads consists in the comprehension of the spatial features of an object or surface through direct contact with the skin. Humans have shown an impressive capability of processing and discriminating spatial features of surfaces, as is illustrated by adult's capability to read grade 2 (contracted) Braille at mean rates of 70-90 words per minute and sometimes even at much higher rates (Nolan and Kederis, 1969). This performance implies that a detailed representation of form must exist at all levels of processing, leading to recognition and perception (Johnson and Hsiao, 1992).

Studying the responses of primary afferents to Braille patterns scanned at 60 mm/s provides an illustration of their spatial acuity (fig. 3.3). Results are showed as spatial event plots, which consist in displaying the recorded spikes onto the stimulus pattern in order to obtain a spatial representation of the outgoing activity. The small and well defined receptive fields of slow adapting (SAI) and fast adapting (FAI) type I afferents (see section 2) lead to a neural representation of stimuli that has roughly the same spatial structure as that of the stimuli. This coding property is sometimes referred to as an isomorphic representation of the stimuli. Responses of individual primary afferents remain relatively homogeneous within the same class, though varying greatly from on class to another. Slow adapting (SAII) and fast adapting (FAII) type II afferents are apparently incapable of resolving spatial details (fig. 3.3) and are likely not involved in coding for form perception. Somewhat coherently, their innervation density is considerably lower that that of type I afferents (see section 2). This is a widely accepted conclusion, which rests on the assumption that the spatial structure is encoded under some form of rate modulation.

The relative contributions of SAI and FAI to encoding the spatial structure of a stimulus have been compared in the context of *static touch* and *dynamic touch* (for a review see Johnson and Hsiao, 1992).

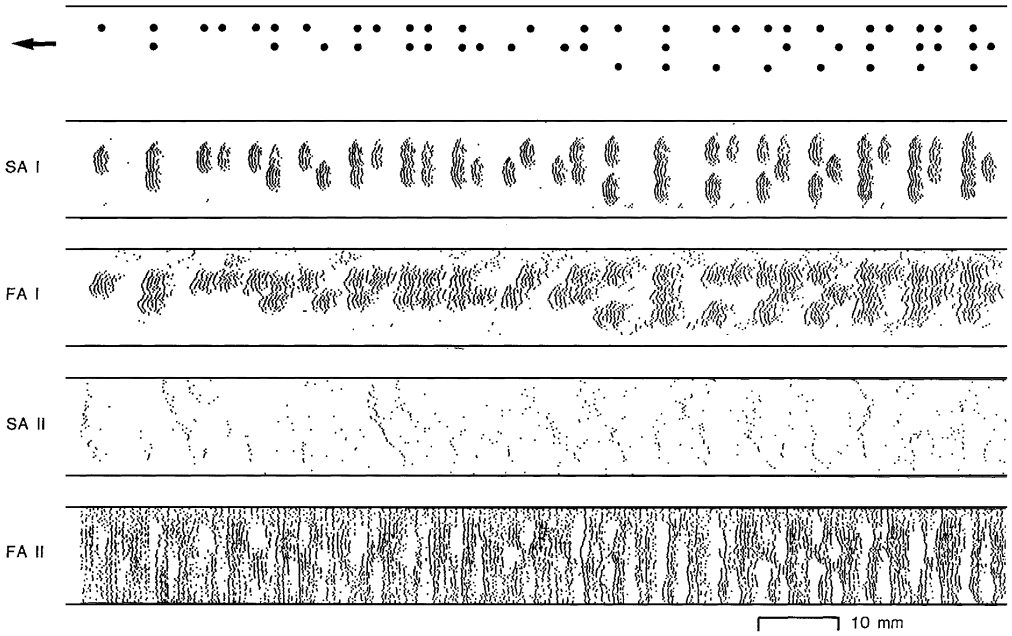

Figure 3.3: Spatial event plots of primary afferent responses to Braille stimuli. The top panel shows the patterns of embossed dots, 0.43 mm high, composing the Braille characters A through R, which were scanned across the receptive fields at 60 mm/sec. Between each scan characters were shifted by 0.2 mm normal to the scanning direction. Each panel shows the responses of a single afferent fiber. The scanning direction was proximal to distal across the skin and the application force 60 g. (adapted from Phillips et al., 1990)

Static touch. In the static touch protocol, mechanical probes do not vary (in intensity or in application position) as the stimulation progresses. Psychophysical studies on the discrimination of orientated gratings, Braille dots and embossed letters (Phillips and Johnson, 1981a; Loomis, 1981; Vega-Bermudez et al., 1991) have shown that humans can perform slightly above chance discrimination of elements separated by 0.5 mm gaps. Performance increased considerably as gaps grew wider and was maximal for gaps larger than 0.9 mm. These results only concern SAI afferents which are able to resolve the spatial structure of all gratings that produced better than chance discrimination behavior. In contrast, FAI afferents begin to resolve the same structures at 1.5 mm gaps. This suggests that in static touch, SAI afferents account for the limits of spatial acuity.

Dynamic touch. During dynamic touch, the fingertip is moved across the surface while the stimulation occurs. Acuity improvements relative to static touch of 10 to 20% have been observed while scanning Braille and embossed

letters (Loomis, 1985; Phillips et al., 1983). This is believed to be linked to the considerable increase in firing rate (more than 10 times higher than in static conditions) observed in SAI afferents, which nonetheless did not show signs of a loss of spatial resolution (Johnson and Lamb, 1981). Similarly to static touch, only SAI mechanoreceptors can account for the observed limits in spatial acuity.

Meanwhile, stimulations using an Optacon, which consists of an array of pins vibrating at 230 Hz, have elicited next to no activity from SAI but excited both FAI and FAII fibers (Gardner and Palmer, 1990). This suggests that FAI may be more responsive than SAI afferents, and despite having a lower spatial resolution, might play a role for detecting small indentations and higher spatial frequency textures. Indeed, the scanning of a textured surface elicits vibrations in the skin, at a frequency determined by the movement velocity and the dimensions of the patterns on the surface (Bensmaia and Hollins, 2003). These vibrations could then be detected and encoded by FAI and FAII afferents.

Although some points are still debated, it is commonly accepted that there is a functional division between the four cutaneous receptive afferents (Johansson and Flanagan, 2009). The SAI system provides a high-quality neural image of the spatial structure of objects and surfaces that is the basis of form and texture perception. The FAI system encodes motion signals of objects contacting the skin which are critical for grip control, as well as higher frequency vibrations. FAII and SAII are not relevant for the perception of form, however, they respectively encode very high frequency vibrations and skin stretch from the entire hand.

Coding of spatial features

It has been argued that SAI and, to a lesser extent, FAI afferents encode isomorphic representations of patterns through the spatial modulation of firing rates (Johnson, 2001). This means that variations in the firing rate matched changes in the surface's shape. Considering this coding scheme, SAI afferents were found to respond to stimulus features such as edges or curvature rather than to the indentation. This behavior might explain the asymmetrical results in the classification task carried out by Vega-Bermudez et al. (1991). In this experiment, some scanned embossed characters were mis-recognized as characters with similar contours. For example, in this test, the letter 'B' was often confused with 'D', but interestingly 'D' was rarely classified as 'B'. The fact that the internal horizontal bar of 'B' is poorly represented in SAI activity explains why the classification of

the two characters was asymmetrical.

The spatial modulation displayed by SAI afferents depends on the spatial period of the stimulus gratings. As illustrated in figure 3.4, low spatial periods elicited little to no modulation in the response. Conversely, spatial modulation of activity increases monotonically with the spatial period (Phillips and Johnson, 1981a). This is believed to result from the mechanics of the skin which make it act as a low pass filter (Phillips and Johnson, 1981b). This coding scheme has been found to be robust to scanning speeds up to 80 mm/s, contact forces up to 1 N and to the type of scanning (passive or active) (DiCarlo and Johnson, 1999; Johnson and Hsiao, 1992; Hsiao and Yau, 2008). As well, by recording SAI and FAI responses to a vibrating grating, Bensmaia et al. (2006) have shown that the spatial modulation of SAI activity is largely insensitive to both the vibrating frequency and amplitude, while FAI activity is only insensitive to the former.

SAI coding properties

The spatial modulation of SAI firing rate encodes the spatial structure of a surface, and can account for the perception of roughness in coarse textures. The SAI system is also known for responding linearly (from a firing rate perspective) to skin deformations. This notably includes skin indentations of at least 1,5 mm (Blake et al., 1997; Johnson et al., 2000) and object curvature (Goodwin and Wheat, 1999; Bisley et al., 2000). However, SAI activity shows a much greater sensitivity to curvature and surface features than to indentation levels in itself. This is the consequence of both the mechanical properties of the skin and the positioning of the Merkel cells encapsulating the afferent endings. These make SAI receptive fields properties resemble those of center-surround receptive fields from the central nervous system (Vega-Bermudez and Johnson, 1999). For the same reason, SAI receptive fields and spatial acuity do not increase and decrease, respectively, considerably higher levels of indentation (Vega-Bermudez and Johnson, 1999).

It has been noted that the SAI responses to repeated skin indentation are remarkably invariant (Werner and Mountcastle, 1965; Wheat et al., 1995; Vega-Bermudez and Johnson, 1999). In fact, Vega-Bermudez and Johnson (1999) showed that in their experiments, regardless of the number of spikes emitted, the variability was of about one impulse per trial, which could not be

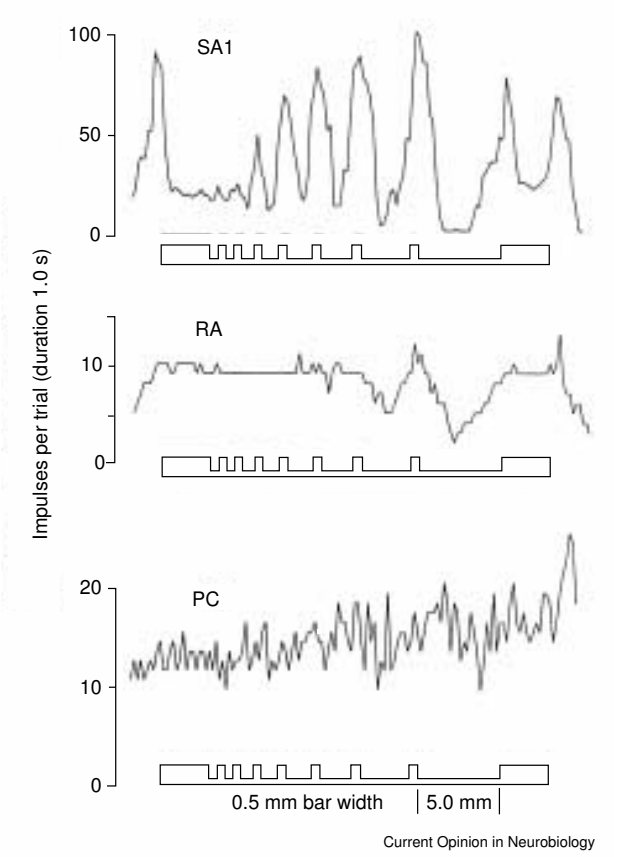

Figure 3.4: SAI, FAI and FAII responses to an aperiodic grating indenting the skin. The grating is shown in cross-section beneath each response profile. Gaps between bars are 0.5, 0.5, 0.75, 1.0, 1.5, 2.0, 3.0 and 5.0 mm wide. The grating indented the skin by 1 mm for 1 s, was raised and moved laterally 0.2 mm for the next indentation. The ordinate represents the number of action potentials evoked during each 1 s period. FAI and FAII afferents responded during the indentation phase only, which accounts for their smaller impulse counts. Testing progressed from right to left; the progressive decline in PC responses results from adaptation to the repeated indentations. (taken from Johnson, 2001)

accounted for by a renewal process (see section 3.1.3). While this leads to a robust rate coding mechanism, it also suggests that tactile information is encoded through more than a simple rate code (even one that is spatially modulated) and that temporal coding has to be explored as well.

3.2.2 Temporal coding of tactile information

In a recent microneurography study, Johansson and Birznieks (2004) have suggested that the timing of impulses from ensembles of human mechanoreceptor afferents can convey information about important contact parameters. The transfer of this information would occur faster than the fastest possible rate code, and possibly fast enough to account for the use of tactile signals in natural manipulation. In the context of this experiment, the timing of first spikes reliably conveyed information about the probe shape, as well as its application direction and force. Intuitively, this is explained by the fact that changes in contact parameters influence differently individual afferents in a population, which is reflected in different first-spike latencies. Variations in first spike latencies can be greater than 15 ms, which is significant compared to the 1 ms jitter observed when repeating the same indentation (Johansson and Birznieks, 2004). The high temporal reliability of mechanoreceptor responses (Edin et al., 1995; Vega-Bermudez and Johnson, 1999; Johansson and Birznieks, 2004) allows for an effective temporal coding mechanism.

Estimates of how early responses from a population of afferents contain enough information for the discrimination of contact parameters indicate that an FAI population is more efficient (*ie.* faster) than the SAI population in encoding these features (Johansson and Birznieks, 2004; Brasselet et al., 2011b). At the level of individual afferents, Saal et al. (2009) found that spike timings contained more information about the force direction (1.6 times more) and curvature (2.2 times more) of the probe than a rate code. Furthermore, the coding of surface curvature and force direction by means of spike timing and spike counts provided overall complementary information. The information content of SAI and FAI responses were broadly similar (with a slightly better result for SAI afferents), which was explained, according to the authors, by the chosen stimulation time course (frequency of approximately 4 Hz). This frequency constitutes the edge of both FAI and SAI sensitive bands.

3.2.3 Cuneate nucleus processing

Sensory information from the fingertips is relayed through the feed-forward cuneate network. The cuneate nucleus is often assumed to play only a minor role in the processing of tactile information along the somatosensory system. This

view is reinforced by observations of cortical neurons from S1 typically displaying the same coding scheme (*ie.* spatial modulation of the firing rate) as primary afferents (see fig. 3.5). Similarly to peripheral afferents, slow adapting cuneate neuron firing rates were found to increase with the indentation level and displayed very little variability (Douglas et al., 1978). Evidence of phase locking mechanisms has been found in the case of stimulation vibration frequencies of 10 to 50 Hz (Douglas et al., 1978), though it is uncertain how this plays a role in encoding coarser textures.

A recent computational study has suggested that the connectivity layout of the cuneate nucleus could help enhance the discriminability between spatio-temporal signals by providing an optimal context separation (Brasselet et al., 2009). Similarly, and supposing the existence of a temporal coding mechanisms at the peripheral level, Johansson and Flanagan (2009) have hypothesized that the cuneate network might act as a coincidence detector. Meanwhile, Navarro et al. (2007) developed a model of the cuneate nucleus which generated a new spatio-temporal code for transmitting information to the thalamus in a progressive way, starting with regions with higher contrast and finishing at those with lower contrast.

Cuneate neurons have been found to have complex firing patterns (Pubols et al., 1989; Canedo et al., 1998) with both tonic and bursting phases. In anesthetized animals (*ie.* cats and raccoons), some cuneate neurons, though not all, spontaneously emitted spikes in the absence of stimuli (Sanchez et al., 2006; Canedo et al., 1998; Pubols et al., 1989). This has led to the hypothesis, still to be verified, that some form of phase coding of tactile information could occur at the cuneate level.

Though new insights in the temporal coding in cuneate responses will probably be found, the current state of the art suggests that, similarly to primary afferents, surface structures are encoded in the spatial modulation of the firing rate. The isomorphic representation of spatial structures is maintained up to the cortical level (see fig. 3.5) where more important feature extraction occurs. Evidence of temporal coding have been found in the somatosensory cortex, notably in the rat barrel cortex (Petersen et al., 2002; O'Connor et al., 2013); however cortical firing rates have proved sufficient for performing discrimination tasks (O'Doherty et al., 2011; O'Connor et al., 2013) and feature extraction (Hsiao et al., 2002). In monkey somatosensory cortex S1, these two coding schemes have been found to account for different features of the stimulus (Harvey et al., 2013).

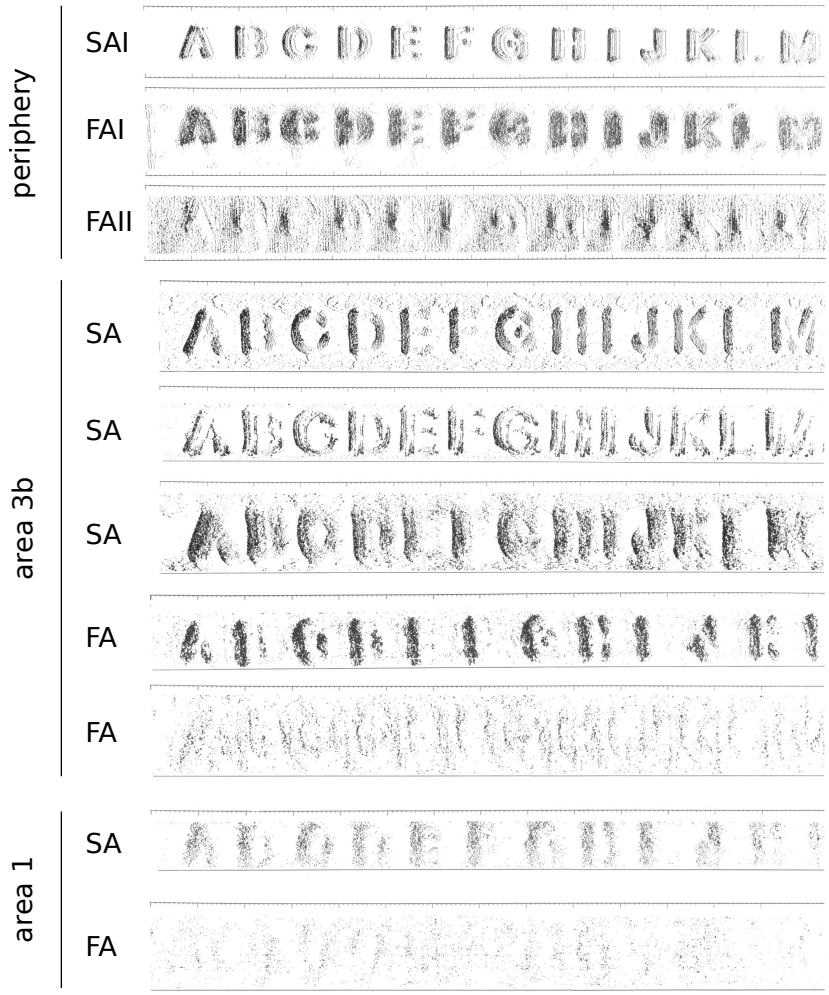

Figure 3.5: Spatial event plots reconstructed from single SA and FA neurons at the periphery and in areas 3b and 1 of S1 in an awake monkey. Letter height was 8.5 mm and the scanning velocity 50 mm/sec; contact force, 60 g. In area 3b, SA neurons best reproduced the isomorphic mapping observed at the periphery. This representation was noticeably degraded in area 1 of S1, suggesting that a change in the coding scheme, through feature extraction, occurs at that level. (adapted from Phillips et al., 1988*a*)

3.3 Conclusions

- Neural codes can be broadly distinguished into temporal codes and rate codes, depending on whether attention is paid to the precise timing of spikes, or to the number of spikes fired during an appropriately chosen temporal window.
- In the peripheral somatosensory system, SAI afferents have been found to best account for the encoding of stimuli spatial structures on a surface. This information is eventually complemented by FAI signals in the case of higher frequency stimulations and lower indentation levels.
- The encoding of form by SAI afferents most likely occurs under the form of a spatial modulation of the activity firing rate.
- The encoding mechanisms operated by the cuneate nucleus remain largely unknown. The coding scheme is likely to be similar to that of the primary afferent level.
- Evidence supporting the presence temporal coding mechanisms at the primary afferent and (to a lesser extent) cuneate level has been found.
- Both rate coding and temporal coding schemes have been observed in the somatosensory cortex, though firing rate codes remains the preferred approach to study cortical processing.

Chapter 4

Information analysis performed on primary afferent responses

Using human microneurography recordings, Johansson and Birznieks (2004) have shown that the timing of impulses from ensembles of mechanoreceptor afferents can convey information about important contact parameters. Brasselet et al. (2011b) uses metrical information theory to quantify the information content of spike train responses while accounting for different encoding schemes. The same method will be used for validating the results of the work presented in this manuscript and is employed in the current chapter to provide an illustrative analysis of primary afferent responses. This analysis constitutes a partial reproduction of the work of Brasselet et al. (2011b), as well as its extension to a population of SAI afferents.

4.1 Metrical information theory

Information theory is a powerful mathematical tool which is capable of quantifying how well it is theoretically possible to discriminate an input signal database, knowing only the corresponding output signals –*ie.* how much information about the input signals the output signals contain. This theoretical tool was first developed by Shannon (1948) in the context of a communication system as illustrated in figure 4.1. Since then it has been applied to many fields containing all sorts of signal communications and encoding-decoding schemes. This is notably the case in the field of neuroscience where it has been argued that the reliability of neural coding mechanisms can be analyzed in terms of information content (MacKay and McCulloch, 1952; Bialek et al., 1991; Rieke et al., 1999).

Shannon's information theory yields a considerable advantage over other

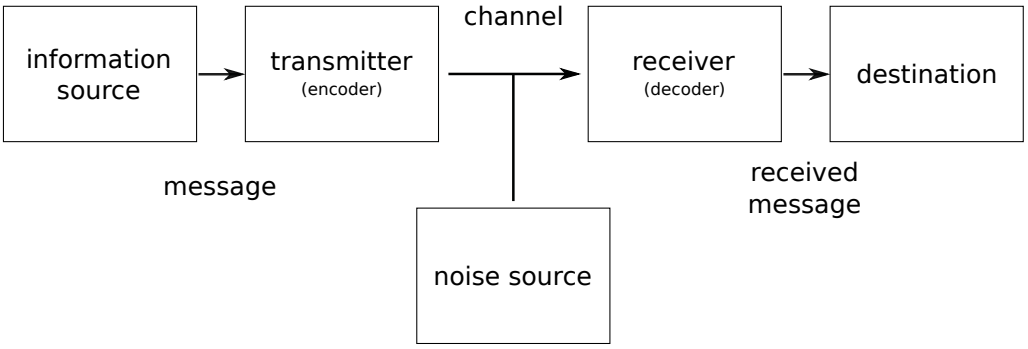

Figure 4.1: Basic scheme of a communication system. In the context of this study, both first and second order neural networks as well as the artificial skin can act as the channel. The information source is the Braille stimuli and the destination the discrimination results.

techniques in that it relies on a non-parametric probabilistic approach that makes no particular assumptions on the system and the signals being considered. As such, it distinguishes itself from classifiers and decoders which all make various assumptions on the signals being read in order to extract their informative content (Quiroga and Panzeri, 2009). However, contrary to classifiers, information theory only provides the amount of information available, not an actual scheme for extracting that information.

Information theory has grown to encompass different measures of information. The traditional measure is known as "Shannon Mutual Information" (Shannon, 1948). It provides an upper bound on the performance that can be expected from a classifier. Mathematically, mutual information is defined by the following equations:

$$I(R;S) = H(R) - H(R|S) \tag{4.1}$$

where

$$H(R) = -\sum_{r} p(r)\log_2\left(p(r)\right) \tag{4.2}$$

$$H(R|S) = \sum_{s} p(s)H(R|s) = -\sum_{s,r} p(r,s)\log_2\left(p(r|s)\right) \tag{4.3}$$

where $I(R;S)$ is the mutual information; $H(R)$ and $H(R|S)$ are the marginal and conditional entropies, respectively; R and S denote respectively the

response and the stimulus space; $p(r)$, with $r \in R$, is the response marginal probability; $p(s)$, with $s \in S$, the stimulus a priori probability; $p(r|s)$ and $p(r,s)$ the conditional and joint probabilities, respectively. Entropy values quantify how large the space of signals is, for instance a high $H(R)$ indicates that there are many possible response signals that could potentially be received. $H(R|S)$ reflects how much uncertainty on the response signals remains when the stimulus is known. Mutual information is therefore defined as the reduction of uncertainty brought by linking the responses to the stimuli through the communication or processing mechanisms.

When considering spike train signals, however, two responses are never exactly identical. Because mutual information is non-parametric, in this framework spike trains will always be considered unique –and consequently all equally probable– even when very similar. This has the consequence of leading to very high values of conditional and marginal entropies. The mutual information value remains correct as both entropy values react in the same way. However, entropy values may no longer reflect the variability in the signals such as the biological system sees them. This, taken by itself might lead to overestimating the decoding capacity of the nervous system. Considering signals to be simply identical or different also ignores the fact that some signals are more easily discriminated than others. While this is not necessarily a concern when conducting a pure information theoretical analysis, it might become a relevant problem when the aim is, for example, the study of a biological network.

To correct this, the metrical information theory was derived (Brasselet et al., 2011b). Unlike Shannon mutual information, this measure takes into account the metrical properties of the spike train space (Victor and Purpura, 1996; Schreiber et al., 2003; van Rossum, 2001) to assess how similar two responses are. Mathematically, metrical information $I^*(R;S)$ is defined by:

$$I^*(R;S) = H^*(R) - H^*(R|S) \tag{4.4}$$

where

$$H^*(R) = -\sum_r p(r)\log_2\left(\sum_{r'} p(r')\phi(r,r')\right) \tag{4.5}$$

$$H^*(R|S) = \sum_s p(s)H(R|s) = -\sum_{s,r} p(r,s)\log_2\left(\sum_{r'} p(r'|s)\phi(r,r')\right) \tag{4.6}$$

$$\phi(r,r') = H\Big(D_c - D(r,r')\Big) \tag{4.7}$$

The mathematical symbols used are the same as for Shannon mutual information (see equation 6.9). The function $\phi(r,r')$ measures the similarity between two responses, and it is defined as the Heaviside function of the spike train metric $D(r,r')$ between two spike trains $r,\ r' \in R$ (see section 4.2 for details on possible spike train metrics). For $D(r,r') < D_c$, responses $r,\ r'$ are considered as identical (i.e. $\phi(r,r') = 1$), otherwise they are considered as different. If $D_c = 0$, then the metrical version of entropies are identical their Shannon counterparts.

The critical distance D_c was established by comparing the distances between responses elicited by the same stimulus (known as intrastimulus distances) and responses elicited by different stimuli (named interstimulus distances). As explained by Brasselet et al. (2011b), D_c was set to the value at which the maximum intrastimulus distance –*ie.* the size of the largest cluster of responses from one class– becomes smaller than the minimum interstimulus distance –the smallest distance between clusters of responses from one class. In the case of neurotransmission, the relationship between intra- and interstimulus distance distributions tends to evolve over time as new spike waves arrive. While this process occurs, the distributions of intra- and interstimulus distances grow apart and eventually stop overlapping. At this point, the value of D_c can be determined, and the optimality condition is reached. The optimality condition corresponds to a maximal $I^*(R;S)$ along with a null (or minimal) $H^*(R|S)$. Conceptually, this means that not only do the output signals contain as much information as they can possibly have, but that there is a space in which the responses are unambiguously clustered –*ie.* the decoding of the output signals is very simple.

Figure 4.2 provides an example of the application of metrical information

theory to microneurography recordings performed on humans (Johansson and Birznieks, 2004). Shannon information is shown to accumulate faster, reaching its maximum approximately 13 ms before the metrical information does. However, contrary to metrical entropy, Shannon conditional entropy only stabilizes around 6.7 bits (not shown on the figure), suggesting that the optimality condition will never be reached.

4.2 Spike train metrics

Many different metrics have been proposed for quantitatively comparing spike trains (van Rossum, 2001; Quian Quiroga et al., 2002; Schreiber et al., 2003; Kreuz et al., 2007; Houghton and Sen, 2008; Wu and Srivastava, 2011). In this study, two different metrics were considered: the Victor-Purpura Spike distance, and its derivation: the the Victor-Purpura Interval distance. These two Victor-Purpura distances allowed to choose the temporal resolution with which spike times were compared, by the tuning of a cost parameter.

4.2.1 Victor-Purpura spike distance

The Victor-Purpura Spike distance (D_{spike} ,Victor and Purpura, 1996) was originally inspired by methods used to to quantify the difference between gene sequences (Sellers, 1974). The concept behind the algorithm is that the distance between two spike trains (and more generally any trains of comparable elements) is equal to the cost of transforming one train into another. The process of transformation occurs through successive elementary steps, each associated with a cost value. Computing the distance is therefore equivalent to finding the optimal sequence elementary steps for the transformation.

The transformation process between two spike trains is illustrated in figure 4.3. Elementary operations in the case of the Victor-Purpura Spike distance are:

- Removing or adding a spike for a cost of 1
- Displacing a spike for a cost proportional to the displacement (*ie.* $C_{VP} \times \delta t$)

C_{VP} is the cost parameter of the Victor-Purpura distance, it reflects the temporal precision considered when comparing the spike trains. Indeed, when displacing a spike, $C_{VP} \times \delta t$ is necessarily lower than 2, else it would be more

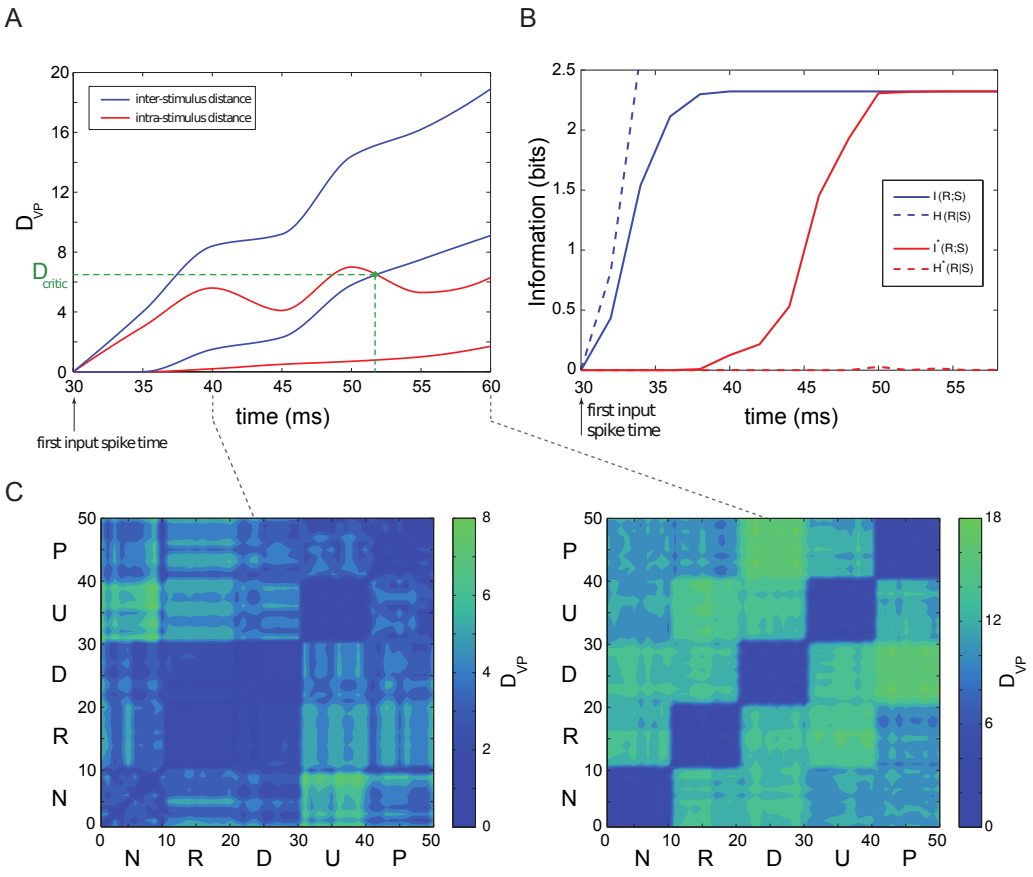

Figure 4.2: Application of information theory (metrical and Shannon) to microneurography recordings performed by Johansson and Birznieks (2004). Only the first spikes of 100 generated trials were used to discriminate between 5 different stimulation directions: proximal (P), ulnar (U), distal(D), radial (R) and normal (N). The Victor-Purpura distance D_{VP} was used to compute the distances between spike trains (Victor and Purpura, 1996). *A.* Evolution of the intra- and inter-stimulus distances as spikes flow in. The perfect discrimination condition is met about 40 ms after the stimulus onset, when the critical cutoff D_{critic} can be determined. *B.* Shannon mutual information (blue curves) and metrical information (red curves) over time. *C.* Distance matrices before (left) and after (right) the occurrence of perfect discrimination. Only 10 presentations per stimulus were considered to generate these matrices. Whereas at 40 ms some interferences exist in the input-output mapping, all the events are are well separated at 60 ms. (adapted from Brasselet et al., 2011*b*)

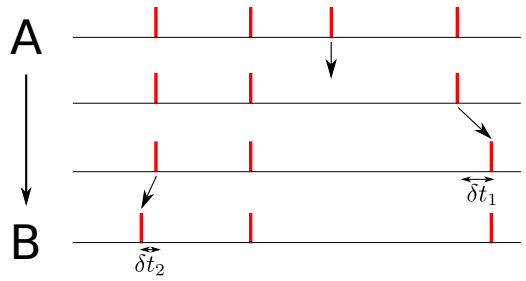

$$dist(A, B) = 1 + C\delta t_1 + C\delta t_2$$

Figure 4.3: Illustration of the transformation steps used to compute the Victor-Purpura distance between two spike trains A and B. From top to bottom: a spike is deleted for a unitary cost, then two spikes are successively displaced for a cost proportional to the displacement. The total distance is the sum of the costs of these operations.

efficient to simply perform a spike deletion followed by a spike creation operation (for a combined cost of 2). Consequently, spike displacements are always limited by $T = 2/C_{VP}$. In the case where $C_{VP} = 0$, then spikes can be displaced as much as necessary (*ie.* the timing of spikes is no longer relevant for comparing the two spike trains), and a spike count or rate comparison is performed.

4.2.2 Victor-Purpura interval distance

A subsequent metric relying of spike intervals ($D_{interval}$, Victor and Purpura, 1996) has been derived from the Victor-Purpura Spike metric. The logic behind it is identical, the only difference residing in that interspike intervals (instead of spike times spikes) are now considered as the composing elements of the spike train. The basic operations are similar with the addition and deletion of a spike (thereby cutting and interspike interval into two) and the elongation or shortening of an interval for a cost proportional to the length change. This operation is somewhat equivalent to displacing a spike, and in addition performing the same displacement to all subsequent spikes.

Interspike intervals are used to define the timing of spikes relative to the preceding spike occurrence. The use of this metric therefore implies taking into account the relative times instead of absolute times to describe the spatio-temporal pattern of spikes. This is relevant in conditions where the system does not have a temporal reference point for comparing spiking activity

–as is believed to be most mostly the case in biological sensory systems).

4.3 Microneurography recordings

A set of microneurography recordings was employed to study the encoding performance of the primary FAI and SAI afferent systems. The microneurography experiments (Hagbarth and Vallbo, 1968) were conducted by R. Johansson's team at UMEA University. The experiment consisted in percutaneously introducing an electrode in the radial nerve of awake subjects (near the level of the elbow). Subjects' arm were immobilized prior to the recordings and their nails glued to a fixed object in order to avoid possible proprioceptive effects on the discharge of mechanoreceptors. The tip of the electrode was placed close to a single axon so as to record the activity from a single mechanoreceptive afferent. Recorded afferents signals were pre-processed to determine the mechanoreceptor type (*ie.* FAI, SAI, FAII, or SAII, see section 2.2.2). Similar microneurography experiments have allowed to record the responses of a single afferent to various tactile stimulations, and so doing to precisely define the receptive field of individual mechanoreceptors, as well as characterize many of its dynamics (*eg.* fast adapting or slow adapting). Eventually it led to estimates of the fingertip's innervation properties such as the number of afferents, their density and their receptive field overlap.

For building the database on which was performed this analysis, a precise device was used to indent the fingertip's skin. Three stimulation probes with various curvature levels where applied at controlled levels of force, different directions and angles as well as following different time courses. The total database recorded by Johansson and Birznieks (2004) comprised 145 mechanoreceptors of all four different types, recorded in the presence of 111 different stimuli. However, a high level of precision was required for recording single afferents and was difficult to maintain for very long; consequently only a subset of all mechanoreceptor responses could be recorded for the entire set of stimuli. In this analysis, the activity from 60 FAI and 73 SAI afferents were recorded in response to 81 different stimuli. The database used here was an extended version of the database of 42 FAI mechanoreceptors Brasselet et al. (2011b) used in their study.

Stimuli were characterized through four different parameters (see fig. 4.4):

- The curvature of the probe: 0 m^{-1}, 100 m^{-1}, and 200 m^{-1}

- The magnitude of the force applied: 1 N, 2 N, and 4 N

- The direction of the force: ulnar, radial, distal, proximal, and normal

- The angle of the force application relative to the normal direction: 5°, 10°, and 20°

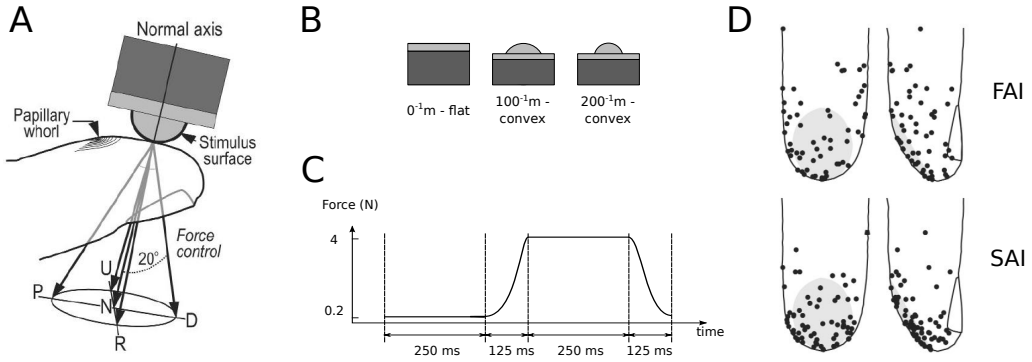

Figure 4.4: Experimental protocol during the microneurography recordings. *A.* A mechanical probe indented the fingertip skin following five different stimulation directions and various angles. *B.* Three probes with various curvatures were used. *C.* Plot of the stimulation's time course. The protraction phase lasted for 125 ms, the magnitude of the force was maintained for 250 ms, before gradually decreasing during the retraction of the probe (which lasted 125 ms). *D.* Populations of 60 FAI and 73 SAI afferents were recorded at different positions on the fingertip. (adapted from Johansson and Birznieks, 2004)

A database of 50 trials per stimulus was constructed by adding a temporal jitter to the recorded spike trains. Jitter values were taken following normal distributions whose standard deviations were derived from experimental recordings (Johansson and Birznieks, 2004). Jitter values were 0.8 and 1.1 ms for FAI and SAI responses respectively. Note that an approximation was made here, as the experimental values used for establishing the jitter only record first spikes. The same jitter quantity was added to subsequent spikes which probably led to an underestimation of activity variability in the database (Johansson and Flanagan, 2009).

4.4 Results

4.4.1 Spike metric comparison

A metrical information analysis was performed on responses of both FAI and SAI to 81 stimuli. The time of optimal discrimination (see section 4.1) was computed using both D_{spike} and $D_{interval}$ metrics over a range cost parameter (C_{vp}) values. Comparing results obtained with the two metrics allowed to asses the information content of two different coding schemes: a coding of stimulus information through absolute spike times (*ie.* D_{spike}), and one through relative spike times (*ie.* $D_{interval}$). Similarly to the analysis carried out by Brasselet et al. (2011b), metrical information was computed using both entire spike trains and first spike waves only. This analysis extends the work from Brasselet et al. (2011b) in that both populations of FAI and SAI afferents was considered, and in that the informative content of interspike intervals was also assessed. The results are presented in figure 4.5. The actual time course of the metrical information closely resembled that observed by Brasselet et al. (2011b) in their analysis of FAI responses (see fig. 4.2) and is therefore not represented here.

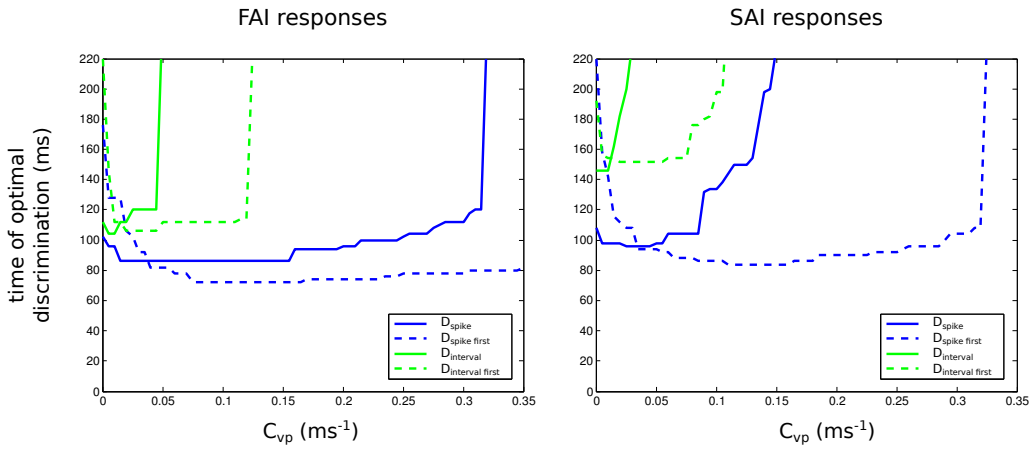

Figure 4.5: Optimal discrimination time over the spike metric parameter C_{vp} of FAI and SAI primary afferent populations (right and left panels respectively). D_{spike} and $D_{interval}$ metrics were considered (blue and green curves respectively), for entire spike trains (full line) and first spike (or interval) waves only (dashed line). Optimal discrimination times above 220 ms indicate that the optimality condition was never reached. For both populations, the best performance (*ie.* fastest optimal discrimination) was obtained when considering the absolute timings (*ie.* D_{spike}) of the first wave of spikes.

Optimally, all 81 stimuli could be discriminated 48 ms (FAI) and 64 ms (SAI) after the first spikes were emitted (at approximately t = 20 ms). Using the D_{spike} metric consistently led to higher performance in terms of reaching the optimal discrimination point. Gains of up to 20 ms (FAI) and 45 ms (SAI) could be obtained by considering the absolute timing of spikes rather than there relative latencies. Isolating the first wave of spikes led to a faster discrimination when using D_{spike} by approximately 20 ms in both populations, which points towards interference coming from subsequent spikes when performing a classification based on absolute spike timings. Conversely, the opposite was true regarding relative spike timings (*ie.* $D_{interval}$). A faster discrimination could be attained using all spike intervals instead of just the first interval. This suggests that some subsequent (short) interspike intervals contributed more to the information accumulation on the 81 stimuli than longer first spike intervals.

Both coding schemes displayed similar behaviors in response to C_{vp}. The C_{vp} cost parameter reflected the temporal precision at which the coding scheme was being considered. High cost values, indicating a very high temporal precision, systematically deteriorated the performance often completely preventing the optimality condition from being reached (*ie.* time values above 220 ms in fig. 4.5). Very low (or null) C_{vp} values, (*ie.* considering almost exclusively spike counts), also led to less than perfect performances. The best performances were reach at $C_{vp} = 0.16$ ms^{-1} in both afferent populations. As can be expected, a higher temporal precision level was tolerated when considering only the first spikes compared to entire spike trains. This is due to two complementary factors: as more spikes are emitted, the encoding capacity of the spike count increases, meaning that temporal coding might become, relatively, less and less useful; meanwhile, the addition of jitters on individual spikes deteriorates more, relatively, similar spike trains than highly dissimilar ones. The evolution of discrimination times of entire spike trains as the temporal resolution considered increases (*ie.* C_{vp} increases) reveals that although a performance gain is noticeable, it is not considerable (approximately 20 ms for the FAI population and 15 ms for the SAI population).

4.4.2 Afferent population comparison

Figure 4.5 reveals differences between FAI and SAI activity. Given the higher noise in the entire SAI spike trains (see section 4.3), the best performance was

reached for a lower C_{vp} values than was necessary in the FAI population. More generally, SAIs generally performed less well than FAIs at higher C_{vp} cost values. The performance difference between D_{spike} and $D_{interval}$ was considerably more marked in SAI responses than in FAI responses. Overall, and also in the best performing conditions, optimal discrimination was possible earlier with FAI responses than with SAI responses.

The performance difference between the two populations in accounting for individual features was also assessed. Metrical information theory was again used to estimate the time of optimal discrimination according to one feature: either the stimulation angle, the probe's curvature or the magnitude of the stimulation force, all other parameters being equal. The best time of optimal discrimination was recorded after performing an exhaustive search on C_{vp} values. For this analysis, the 50 trials were grouped by batches of five trials and the analysis carried out on each groups independently. Figure 4.6 shows the time of optimal discrimination for each specific stimulus feature.

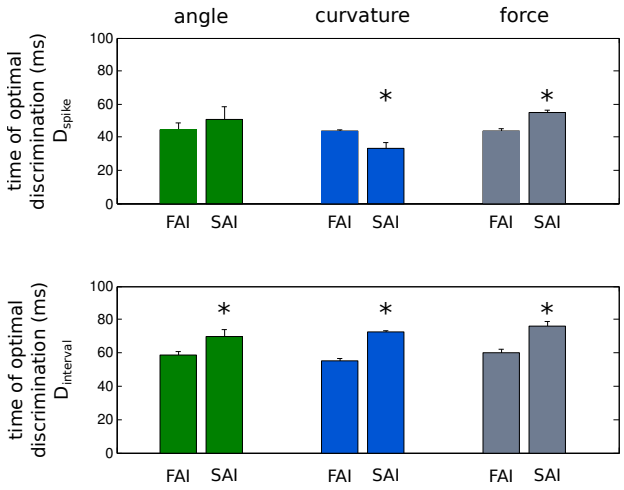

Figure 4.6: Optimal discrimination of specific stimulus features using the D_{spike} (top) and $D_{interval}$ (bottom) metrics. Error bars represent the standard deviation over 10 repetitions. Stars indicate a significant difference (Mann-Whitney U, $p < 0.01$).

In most cases, the FAI population outperformed the SAI population. Only for the encoding of curvature did the SAI population prove more efficient. Again, the D_{spike} metric proved more efficient in accounting for differences in responses to different features.

4.5 Conclusions

Previous studies have established the importance of temporal coding in peripheral afferent activity (Johansson and Birznieks, 2004; Saal et al., 2009). In particular, Brasselet et al. (2011b) used metrical information tools to assess the encoding capabilities of first spike waves of 42 FAI afferent responses to 81 stimuli. The current analysis reproduced and extended these results to a population of 60 FAI and 73 SAI afferents.

The results were coherent with previous studies and show that a perfect discrimination of all 81 stimuli could be performed using a spatio-temporal coding scheme in both FAI and SAI populations. However, the perfect discrimination time was delayed when either ignoring, or considering too precisely, the temporal structure of response patterns. Relying on first spikes waves only, as opposed to entire spike trains, allowed for a faster discrimination in optimal conditions. FAI and SAI populations followed a similar trend but FAI remained consistently more efficient in encoding information relevant to reach perfect discrimination. This was true when considering the entire 81 stimuli as well as, to a lesser extent, when accounting for individual stimuli features. The SAI population did manage to outperform the FAI population in encoding for the probe's curvature. SAI afferents have indeed been shown to encode surface curvatures (Goodwin and Wheat, 1999; Bisley et al., 2000), however, it is unclear whether that should translate into a faster discrimination as was found here.

In other sensory systems, it has been observed that the relative spike time could be highly informative about the stimulus (Gollisch and Meister, 2008). In the current analysis, representing the spatio-temporal structure of afferent activity using interspike intervals has been found to be sufficient to perform discrimination of the entire stimuli dataset, but also less efficient than using absolute spike times, especially in the case of SAI afferents. Similarly, spike counts contained sufficient information for an entire discrimination of all 81 stimuli, but was less efficient in that perfect discrimination was reached later than when considering the temporal patterns of the activity. However, the discrimination delay was only of about 15 ms when considering the SAI population response. Consequently, although taking into account the temporal structure allows for better performance, satisfactory performance could still be obtained through spike count based codes depending on the temporal constraints of the task being performed.

Part III

Closed Loop Neural Architecture for Fine Touch Discrimination

Chapter 5

Artificial tactile sensing

The third part of this manuscript will present a closed loop neural architecture capable of fine touch discrimination. The aim of the system is to perform tactile discrimination of 2D shapes on a surface (*ie.* coarse textures) in a dynamic scanning scenario. This is accomplished by relying exclusively on cutaneous information provided by a sensor array, and the same information should be used for deciding an appropriate movement policy.

The development of this artificial framework represents the main objective of the current thesis work and has been realized following a three-fold requirement: *(i)* neuro-mimetism, *(ii)* closed loop active sensing, and *(iii)* integration of modular processing components.

With such a requirement in mind, a neuromorphic processing scheme was adopted on the basis of the anatomo-functional and neural coding principles introduced in Part II. The well-known anatomy and neurotransmission mechanisms observed at the first stages of the somatosensory pathway were reproduced. Neural signals were fed to a classifier which algorithmically implemented a probabilistic discrimination function. The resulting probability estimates were used to devise fingertip moving strategies. Low-level motor control was supported by a bio-inspired model of the cerebellum. The system presented in Part III of this manuscript gave rise to different studies (Bologna et al., 2011, 2012; Pinoteau et al., 2012; Bologna et al., 2013), the results of which are included here. This work was part of a collaborative effort; the author's main contributions included the modeling of the first and second order neurons as well as the analysis of the their neuronal responses. The author was also responsible for the implementation, adaptation and integration of the different components of the complete architecture.

The present chapter reviews the state of the art from both a neural modeling and a robotic tactile sensing perspective, and helps position the novel architecture presented here with respect to previous studies.

5.1 Modeling of the peripheral somatosensory system

5.1.1 Computational models of primary afferents

Primary afferents have been the subject of many studies over the past decades (for review see Johnson and Hsiao, 1992; Johnson, 2004; Johansson and Flanagan, 2009) and along with it a number of models have been proposed to better reproduce and understand their dynamics. Previous works have especially focused on models of FAII (Freeman and Johnson, 1982; Bell and Holmes, 1992; Kim et al., 2010), FAI (Freeman and Johnson, 1982; Slavik and Bell, 1995; Looft, 1996; Bensmaia, 2002; Güçlü and Bolanowski, 2004; Sripati, 2006; Kim et al., 2010) and SAI (Freeman and Johnson, 1982; Slavik and Bell, 1995; Sripati, 2006; Lesniak and Gerling, 2009; Kim et al., 2010; Gerling et al., 2013) mechanoreceptor types. Most of these models relied on spiking neuron components to emulate the afferent activity. In fact, the computational model primarily chosen was the leaky integrate-and-fire neuron (Lapicque, 1907) which was adopted under various forms for emulating SAI dynamics especially (Freeman and Johnson, 1982; Slavik and Bell, 1995; Bensmaia, 2002; Lesniak and Gerling, 2009; Kim et al., 2010; Gerling et al., 2013). Meanwhile, Sripati (2006) used tensile strain in the skin to try to account for SAI activity, and receptive field deformation for FAI responses. Güçlü and Bolanowski (2004) chose to reproduce FAI activity using a Markov process in which neurons had a probability of switching between firing states.

These models were validated using a firing rate coding scheme, probably because these were the data most accessible in the literature. For instance, Lesniak and Gerling (2009) considered first spike latencies when analyzing their model's response but did not have data available to compare with. Concerning SAI neurons, the spatial modulation of the activity (see section 3.2.1) was often considered to evaluate the model (Lesniak and Gerling, 2009; Sripati, 2006). In some cases, this was indirectly estimated by taking into account spatial event plots (Johnson and Phillips, 1988). These are a form of representation consisting in displaying the recorded spikes onto the stimulus pattern in order to obtain a spatial image of the outgoing activity. A spatial modulation of the activity is directly visible on the plot as the stimulus shape is reproduced in the neural activity. One model in particular (Güçlü and Bolanowski, 2003) concentrated on

reproducing isomorphic properties of primary afferents.

Among these models, the most complete is perhaps the one from Kim et al. (2010) which uses a leaky integrate-and-fire neuron whose inputs are the filtered versions of the complete skin indentation signals (*ie.* indentation position and velocity for SAI afferents, and velocity alone for FAI). In order to add some limited stochasticity to the model, a Gaussian noise was added to the membrane potential. The model was validated by comparing its output spiking dynamics with recorded spike trains in terms of firing rate, spike distance –using the Victor-Purpura distance (Victor and Purpura, 1996)– and temporal jitter on spikes. The model was successful in capturing the response properties of mechanoreceptive afferents across a wide range of vibratory frequencies and in predicting the timing of individual spikes with a millisecond accuracy. The model also managed to reproduce spatial event plot representations of embossed characters. One of the main limitations of the model was its inability to account for nonlinearities in the response. This led to a divergence between predicted and observed responses of FAI and FAII afferents for large indentation amplitudes. SAI afferents, on the other hand, remained accurately predicted across stimuli of all amplitudes thanks to the linearity (in terms of rate) of their responses.

The input signals for these models were simulated either using spatial filters (Güçlü and Bolanowski, 2003, 2004) or by modeling mechanical deformations on the skin (Sripati, 2006; Lesniak and Gerling, 2009; Gerling et al., 2013). In the model presented by Freeman and Johnson (1982), a periodic stimulation signal representing the skin's vibrations was directly fed into the model's equation. In only one case were the received inputs generated by a physical tactile sensor (Spigler et al., 2012).

5.1.2 Computational models of the cuneate nucleus

Few computational studies of the cuneate nucleus have been carried out. The earliest model found, focused on reproducing the dynamics of individual cuneate cells. A multi-compartmental approach was adopted, with the Hodgkin-Huxley (Hodgkin and Huxley, 1952) mathematical model used to membrane potential dynamics. Model neurons successfully reproduced the spontaneous activity as well as the inhibited and desinhibited states observed experimentally. The model was subsequently integrated in a more complete cuneate network (Sánchez, Barro, Marino and Canedo, 2001) reproducing the anatomical properties of the biological

system. This network contained afferent excitation and inhibition of cuneate neurons –to create center-surround receptive fields–, recurrent lateral inhibition –so that only the neurons with the highest input in a region could be activated–, and recurrent lateral excitation –to sensitize neurons with overlapping receptive fields. The network properties allowed the cuneate model to act as an edge detector, and later as a motion detector (Sanchez et al., 2002). Another iteration of this model allowed to faithfully reproduce both tonic and oscillatory firing modes of cuneate neurons (Sánchez et al., 2003). The same model eventually allowed not only feature extraction of edges and motion, but also a progressive transmission of the information prioritizing regions with higher contrast and finishing with those with lower contrast (Navarro et al., 2005, 2006). In all these studies, afferent inputs to the cuneate network were represented by ionic currents.

The functional properties of the cuneate nucleus model from Sánchez, Barro, Marino and Canedo (2001) were implemented in a robotic collision avoidance task (Sanchez, Mucientes and Barro, 2001). The cuneate nucleus then acted as a spatial and a temporal filter of the environment –in this case seen through sonar data– to select salient regions in a trajectory while removing persistent objects irrelevant for the task.

Another approach has been adopted by Brasselet et al. (2009), who fed spatio-temporal activity patterns from microneurography recordings into a feed forward network of cuneate-like cells with plastic connections. No lateral or inhibitory connections were implemented in the model. The result was the emergence of a network with very few functional connections but high efficacy synapses, similar to what has been observed in the decerebrated cats (Bengtsson et al., 2013).

No studies were found to model bio-mimetically both first two stages of the peripheral somatosensory system. Bankman et al. (1989), however, did proposed a model of the entire ascending somatotosensory system to account for the isomorphic encoding observed at the cortical level (see section 3.2.3). To do so, it relied on a three layer feed forward neural network with inhibitory lateral connections, mimicking the different processing stages of the biological system (see section 2.1).

5.2 Bio-inspired solutions for fine touch sensing in robots

5.2.1 Bio-inspired tactile sensors

An increasing body of literature has called for the development of biologically inspired tactile sensing systems (Lederman and Pawluk, 1992; Howe, 1993; Dargahi and Najarian, 2004; Maheshwari and Saraf, 2008; Dahiya et al., 2010; Loeb et al., 2011a; Dahiya and Valle, 2013; Yousef et al., 2011) for robotic applications. In their review, Dahiya et al. (2010) have compiled a 11 properties of the biological system that should serve as design criteria for tactile sensing in general robotic systems:

1. The tactile system is composed of many sensor types with different functional roles (Johnson, 2001). In robotics, this should be emulated by relying on miniaturized sensors optimized for the extraction of one particular contact feature in addition to multi-functional ones. In the case of fine touch, coarse structures are encoded by SAI afferents (see section 3.2.1) and other receptors types (*ie.* FAI and FAII) are only useful for encoding very fine textures.

2. The spatial resolution of sensor arrays should depend on its function and location. On fingertips designed for fine touch, the spatial period should be approximately 1 mm (Johnson and Hsiao, 1992).

3. Tactile sensing should be highly sensitive and have a wide dynamic range (Dario, 1991). This is especially relevant for manipulation tasks. For discriminative touch, the dynamic range can be lower, as long as it is sensitive enough to detect the spatial structure of the surface.

4. Sensors should be able to account for both static and dynamic stimulations. This allows to scan a surface –as opposed to raising, moving, and lowering the sensor– when performing fine touch explorative task. It is also noteworthy that SAI mechanoreceptors are 10 times more sensitive when delivered a dynamic stimulation than they are to a static one (Johnson and Hsiao, 1992).

5. Robotic tactile sensors should respond quickly, especially when involved in a closed control loop. Considering the somatosensory system as a benchmark, each touch element should respond within 1 ms from the stimulus delivery.

6. As in humans, tactile information should be processed at different levels in

order to lighten the computation load of the central processing unit. Additionally, preprocessing the sensory data may also help optimize the transfer of relevant information.

7. Depending on its use, sensory information should be transfered via different pathways and processed at different speeds and/or with different priority (this point can be discarded in the case of fine touch sensing).

8. To emulate the visco-elastic properties of the skin, sensors may be embedded into or covered with elastic material. This may have varying effects (*eg.* on force and spatial sensitivity) depending on the material chosen and the sensor type; however it allows to increase the contact area and is especially helpful in manipulation tasks.

9. A covering layer on the sensors can also be used to support, enhance or correct some of their properties. This is somewhat akin to the role of papillary ridges on the fingertip, which are believed to contribute to the encoding properties of mechanoreceptors (Scheibert et al., 2009).

10. Much like the skin, robotic taxels should be robust, flexible, conformable, stretchable, and soft. This property should be modulated according to the environment the robot is designed to interact with.

11. Sensors should preferably have linear responses and low hysteresis. However, human mechanoreceptors do not comply with these two requirements. Dahiya et al. (2010) argue that these drawbacks are compensated by a large number of receptors which allow the central nervous system to still extract enough information. Yet it is also probable that non-linearity and hysteresis support the neural coding mechanisms and account for part of the preprocessing evoked in point **6**.

When considering tactile sensing of spatial patterns, only a few of the properties evoked in this list are truly essential. The sensor must be able to encode vibrations (for very fine textures) or spatial indentation patterns (for coarser patterns). In this second case, a high spatial resolution is required to detect small spatial modulations. In both cases, an important temporal resolution is necessary to properly encode and convey the information. Finally, being responsive to dynamic stimulations (especially) is necessary for encoding fine textures (Katz, 2013) and advised (if only to simplify the movement policy) for coarser textures as well.

Over the past years, many new sensors satisfying several of these properties have been designed (for reviews see Maheshwari and Saraf, 2008; Dahiya et al., 2010; Loeb et al., 2011a; Yousef et al., 2011) and used in texture discrimination tasks (Lin et al., 2009; Oddo et al., 2011; Engel et al., 2006).

5.2.2 Neuromorphic processing of tactile signals

A number of tactile sensors have drawn a parallel between their dynamics and function, and those of cutaneous mechanoreceptors (Shimojo and Ishikawa, 1993; Lin et al., 2009; Oddo et al., 2011; Engel et al., 2006). This was generally linked to the stimulus features being extracted by the sensor; however, the processing (if any) operated on the sensory signals prior to classification was rarely neuromorphic. Similarly, and under certain circumstances consequently, the classification processes were always implemented algorithmically, although the use of Bayesian processes (*eg.* Fishel and Loeb, 2012) or non spiking neural networks (*eg.* Germagnoli and Magenes, 1996; Caiti et al., 1995) may somewhat reflect real biological processing mechanisms (Pouget et al., 2013).

A few studies have attempted to process tactile information using biologically inspired neural networks. Dario et al. (2000) have developed an impressive system for grasping and recognizing objects based on anthropomorphic principles. The robotic hand was capable of integrating visual information of the grasped object edge, proprioceptive information on the arm configuration, and tactile information on the contact, for processing by a neural network with a reinforcement learning paradigm. More recently, Ratnasingam and McGinnity (2011b) designed a system capable of object recognition based on spiking neural networks. In this study, spatio-temporal patterns of spikes encoded the joint angles (*ie.* proprioceptive information) as the object was grasped in the robotic hand, and processed by a feed forward network. In a subsequent study, the system's performance was tested using different neural coding schemes (Ratnasingam and McGinnity, 2011a).

Spigler et al. (2012) provide an example of neuromorphic processing of fine touch signals from a robotic tactile sensor. Signals from a 2×2 MEMS array were converted into trains of action potentials through an Izhikevich neuron model (Izhikevich, 2003). The tactile sensor provided 16 channels to transduce mechanical stimulation features at a density equivalent to that of SAI afferents on the fingertip (*ie.* approximately 70 units/cm^2). The system was tested by passively scanning fine textures and performing a discrimination of surfaces by

comparing the output spiking signal's spectrograms. This work therefore proposes a neuromorphic processing of tactile information emulating that performed by first order neurons in the peripheral somatosensory system.

5.2.3 Closed-loop tactile discrimination

Touch is an interactive sense. Hence, object's tactile properties are extracted by performing a series of movements. In humans, experimental psychologists have identified six such exploratory behaviors: compliance is determined by applying pressure, surface texture is assessed through lateral sliding movements (see chapter 3), static touch is for temperature, enclosure is used to estimate shape and volume, hefting is used to determine wieight, and the exact shape is found through contour following (Lederman and Klatzky, 1987, 1993).

Numerous examples of active sensing in closed-loop robotics exist. They primarily focus on tactile perception of object shape and grasp-related control (Howe, 1993; Asfour et al., 2008; Saal et al., 2010; Petrovskaya and Khatib, 2011; Chitta et al., 2011; Romano et al., 2011; Bekiroglu et al., 2011). Meanwhile, texture discrimination using tactile sensors has also been extensively studied (Howe and Cutkosky, 1993; Oddo et al., 2011; Sinapov et al., 2011a; Decherchi et al., 2011; Jamali and Sammut, 2011; Spigler et al., 2012). In particular, (Sinapov et al., 2011a) has demonstrated that using multiple exploratory movements can greatly increase (from 65% to 80%) the recognition rate of the system.

Instead, fewer works have sought to discriminate fine or coarse textures using closed-loop systems. Shimojo and Ishikawa (1993) provides an example of active sensing system in which a spatial filtering operated by the tactile sensor changes characteristics depending on its motion. A parallel with efference copy (Blakemore et al., 2000) is drawn by the authors with the motor system signaling the sensory system to adapt to the motion performed.

A closed-loop in which motion policy is modulated by tactile percepts is proposed by Fishel and Loeb (2012). In this study, a multi-modal bio-mimetic tactile sensor was used to provide the system with sensory inputs about a texture being scanned. Bayesian inference was used to discriminate between textures. The estimated probabilities also allowed to devise a movement policy that would optimally separate ambiguous textures in order to perform the

discrimination. In a subsequent application, a reinforcement learning mechanism was added to the system (Xu et al., 2013).

Although bio-mimetic in their sensors and in their exploration policy (Loeb et al., 2011a), no closed-loop system was used in their system to operate a neuromorphic processing of tactile signals.

5.3 Conclusions

In this chapter an overview of the existing models of first and second order afferents has been given together with a summary of the current trend in development of touch sensors and closed-loop robotic implementations for tactile signals discrimination.

From the neural modeling point of view, multiple precise models reproducing the dynamics of primary afferents have already been established, along with two groups of modeling studies on the cuneate network. However, these models have rarely been combined into an integrative processing stream, furthermore with input signals originating from a tactile sensor.

From the neuro-robotics perspective, many bio-inspired sensors reproducing several of the mechnaoreceptors properties now exist. Yet, a neuromorphic framework for the processing of these signals has only rarely been considered. Similarly, although it has been extensively observed in humans, and despite the numerous studies on texture discrimination, few systems adopt active sensing strategies to optimize their performance.

The work presented in what follows is therefore novel in that it combines many composing elements which not only have been studied separately, with different aims and approaches, but have also never been built into an integrative neuro-robotic system.

Chapter 6

Closed loop neural architecture

The current chapter provides a presentation of the developed closed loop neural architecture for processing fine touch information. The modules composing the system will be described individually, as well as how they were integrated in the complete neuro-mimetic framework. The system was tested in a Braille reading. Its performance will be described in chapter 7.

6.1 System overview

The closed loop architecture of the neural architecture (illustrated in fig. 6.1) was designed in a modular nature so that each element could be individually studied and replaced. An artificial touch sensor acted as the fingertip skin to provide analog information on the tissue deformations generated by the stimuli. The signals were transduced into spiking activity by a network of primary neurons acting as mechanoreceptors and primary afferents. The neuronal activity generated was relayed and processed by a network of second order neurons emulating the role of the cuneate nucleus of the brainstem. The outgoing spiking activity was used for tactile discrimination by a probabilistic classification system which generated a probability distribution for the stimulus being scanned. The shape of this distribution was used by a high-level controller to shape the active sensing policy of the system. A low-level controller, following a cerebellar like structure, allowed fine tuning of the movement to ensure that the trajectory followed by the fingertip resembled that which was desired.

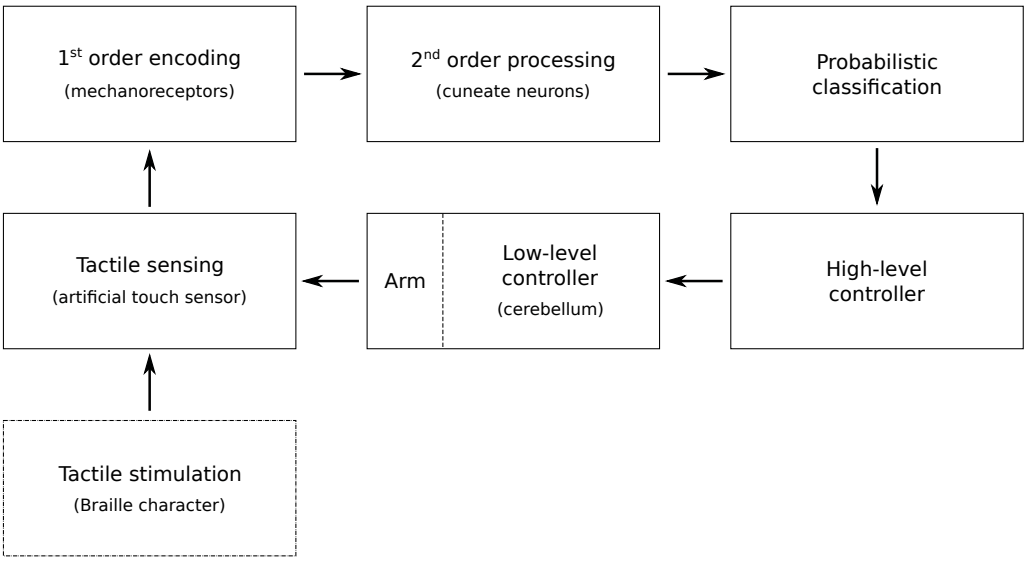

Figure 6.1: A schematic representation of the closed loop system. Clockwise, starting at the bottom left: Braille character-like tactile used as stimuli indent the artificial touch sensor. A network of first-order neurons mapped the analogue readouts of the touch sensor onto spiking (mechanoreceptor-like) spatiotemporal patterns. Then, a downstream network of second-order neurons processed the primary afferent signals (emulating the cuneate nucleus' function) prior to their transmission to a probabilistic classifier. The estimated posterior probability distribution across stimuli population allowed a high-level controller to modulated the sensing process by adapting the scanning speed of the fingertip. Finally, a cerebellar-like neural controller provided low-level adjustments of motor commands before their actual execution by the hand-arm platform.

6.2 Tactile stimuli and artificial skin models

6.2.1 Stimulus alphabet

The fine touch discrimination performance of the system was tested on a Braille reading task. Braille is a tactile writing system developed in 1824 by Louis Braille for visually impaired and blind individuals. Braille characters are formed by a pattern of raised dots spread over the two columns and three lines that compose individual cells. In its standard form (also known as Grade 1 Braille), each cell corresponds to a single letter (see fig. 6.2) or punctuation symbol. Higher levels of Grade introduce abbreviations and contractions to the traditional alphabet. Over time, the Braille alphabet has evolved into multiple standards and been adapted to fit different languages. Although the size and spacing of the dots vary depending on the standard, these variations rarely exceed 0.5 mm in inter-dot

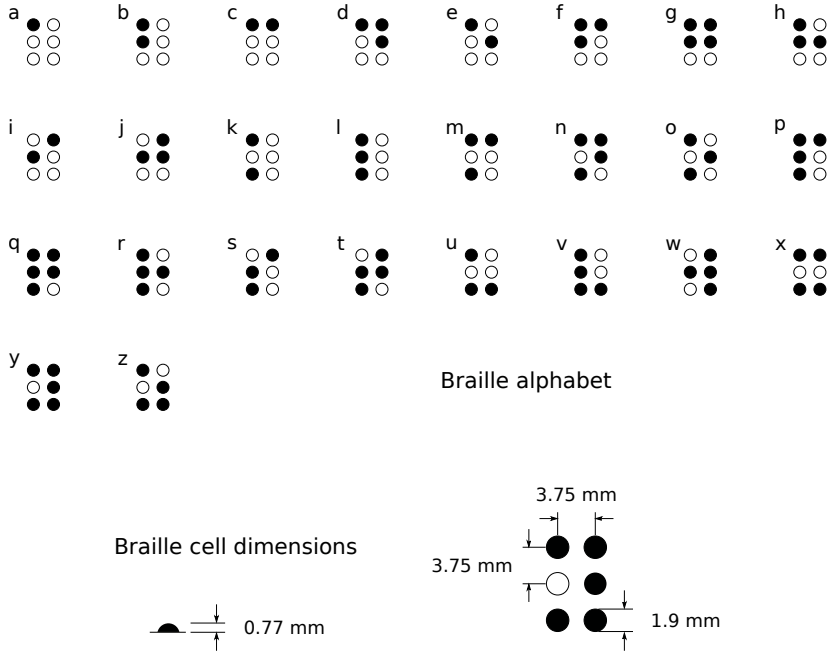

Figure 6.2: Braille cells used as stimuli. *Top.* The 26 lower-case characters of the standard Braille alphabet. *Bottom.* Dimensions of the scaled Braille cells and dots used in the stimulation protocol.

dimensions (generally comprised between 2.2 and 2.6 mm), and 2 mm for inter-cell spacings (generally higher than 6 mm). Regardless of the standard, and given the dimensions considered, Braille reading can certainly be regarded as a fine touch discrimination task. It is important to note however that although Braille was used as stimulus, other dot patterns might just as well have been considered. In particular, no attempt has been made to organize Braille letters in order to be syntactically correct, nor was syntax or semantics ever taken into account to help in the discrimination of the characters.

The alphabet used in the stimulation protocol was composed of the 26 lower-case characters of Grade 1 (or standard) Braille. The choice was made to use a scaled version ($1 : 1.7$) of the Braille cells from the "American National Library for the Blind" standard. This scaling was necessary to effectively simulate the responses primary afferents would have to raised Braille dots given the larger size of the sensors composing the artificial skin. Had the scaling not been made, Braille cells would have been comparatively smaller relative to the fingertip, making the reading task noticeably more complicated. Manufacturing constraints did impose some slight variations in the final size of the Braille dots used, however these were

of the order of a tenth of millimeter and therefore had little consequence on the performance of the system. The final dimensions of the Braille characters are illustrated in figure 6.2.

6.2.2 The artificial touch sensor

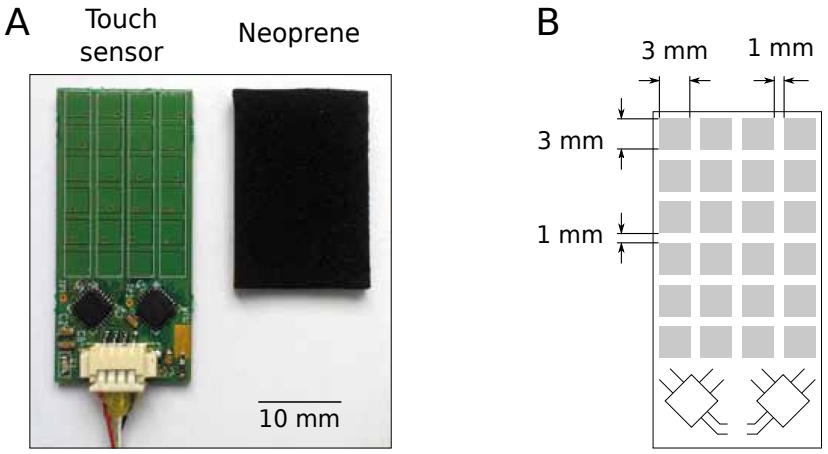

Figure 6.3: The artificial fingertip consisted of 24 capacitive sensors distributed following a 6 × 4 array configuration. *A.* A neoprene patch positioned over the touch sensor modulated mechanical indentations. *B.* Dimensions of the artificial fingertip (with individual sensor size and inter-sensor distances).

The artificial skin used for this system was a prototype developed at the Italian Institute of Technology consisting of an array of 24 capacitive sensors (Cannata et al., 2008; Bologna et al., 2010). The issue of hysteresis often observed in capacitive sensors (Loeb et al., 2011b), only occurred here when saturating the sensor with a high indentation force. A 2.5 mm thick neoprene layer (fig. 6.3 A.) covered the entire array to protect the underlying sensors during mechanical indentation as well as to passively modulate the exerted pressure. Each sensor had here a square form with a side dimension of 3 mm and was separated from its neighbors by 1 mm spacings (fig. 6.3 B.). The sensors were arranged following a rectangular grid layout with 6 lines and 4 columns, making the sensitive surface total at 18 × 23 mm^2. When the spatial rescaling applied to the Braille characters is taken into account, the density of sensors on the artificial skin reached 17 $sensor/cm^2$.

A preliminary study was carried out to characterize and validate the tactile sensor prior to its use in the closed-loop fine touch architecture. Two different

experimental protocols were carried out to investigate the basic response properties of the sensors.

The first experiment aimed at studying the response of the device to a static stimulation, in the sense that the position of the mechanical indentation did not vary while the stimulation was performed. A 4 mm diameter cylindrical probe, mounted on a load cell (see fig. 6.4 A.), was used to indent the neoprene at regular positions. The probe was lowered to indent the neoprene at a given intensity, when the sensor response stabilized, the value was recorded. The probe was then raised again, moved horizontally 0.2 mm to the next position and lowered again onto the neoprene. In total, the touch sensor was stimulated at 6161 different positions over the entire array surface according to a regular grid layout (with a 0.2 mm step). Results showed that each sensor's receptive field was Gaussian-shaped with a peak amplitude of 200 $\pm$ 3.3 fF (mean $\pm$ std) and width 2.5 $\pm$ 0.044 mm. This procedure also allowed us to test the stability of the device, as well as the homogeneity property of its sensor responses across different positions in the array. It was possible to observe a small degree of overlapping between the sensors' receptive fields, probably due to the superficial neoprene layer. The testing was repeated for multiple indentation levels and observed the same Gaussian-like receptive fields with equivalent widths and peak amplitudes proportional to the indentation intensity. In the conditions of maximal indentation of the neoprene, the recordings showed a high signal-to-noise ratio (50 dB) for each of the 24 sensors.

The second experimental protocol sought to similarly characterize the touch sensor responses, but to a stimulus moving dynamically over the sensors. The fingertip was mounted on the mobile section of a motorized linear stage named 8MT195 and commercialized by Standa Ltd. The mounted device was then made to travel over a Braille line of 6 different characters (see fig. 6.4 B.). The artificial fingertip was rubbed over the Braille dots at a speed of 15 mm/s during 200 recording trials. For this experimental setup, only one indentation level was used. It was calibrated to achieve an appropriate signal-to-noise ratio (32 dB) while minimizing possible interferences due to the visco-elastic properties of the neoprene. Averaging over all recorded responses to the dynamical stimuli, a Gaussian shaped receptive field with a peak amplitude of 42.88 $\pm$ 8.9 fF (mean $\pm$ std) and a width of 2.9 $\pm$ 0.32 mm appeared. Receptive field overlap was observed to be higher than in the static stimulation protocol.

The analog response of each sensor had an intensity proportional to the

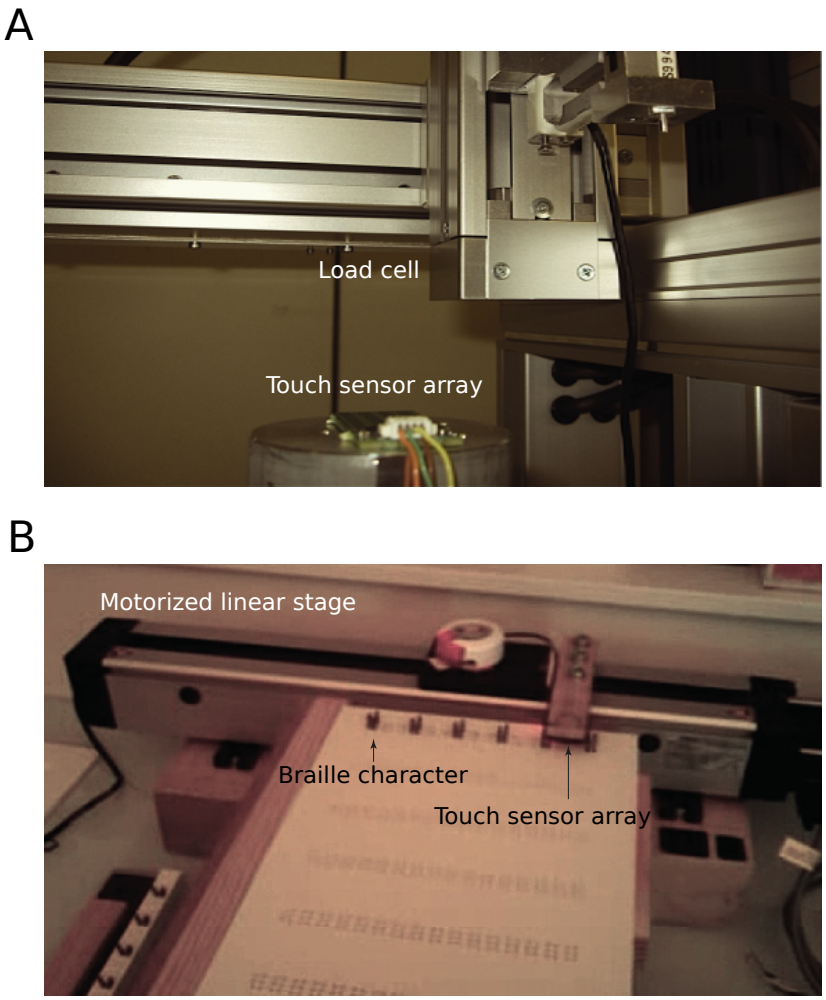

Figure 6.4: *A.* The static stimulation setup consisted of a load cell allowing the touch sensor to be stimulated at different positions and with different indentation forces. *B.* The dynamic stimulation setup consisted of a motorized linear stage (commercialized by Standa Ltd), with the artificial sensor mounted on its mobile section scanning a line of Braille characters at 15 mm/s.

indentation level. Consequently, stimulating a sensor at the periphery of its receptive field was equivalent to applying the stimulus at its center but with a lower intensity. As the intensity level on the stimulation did not vary in all other experimental protocols, the response intensity was informative on the position of the stimulation point. With a very high signal to noise ration observed in both protocols, the localization of the stimulus should theoretically prove fairly easy to extract. However, the acquisition frequency of each capacitive pad was 20 Hz, which created added a level of imprecision in the case of dynamic stimulations.

These testing experiments allowed to build a dataset of analog responses which served as a basis for developing a simulated version of the artificial touch sensor. A family of 24 noisy Gaussian kernels were spread over the input space based on the spatial distribution of the real array. Each kernel modeled the response profile of an individual sensor, with white noise added to the amplitude and width of the response, 2.5 fF and 0.1 mm respectively. Also, a Gaussian noise on the position of each simulated stimulus (std = 0.1 mm) accounted for possible positional errors during real stimulation conditions.

6.3 Processing of tactile signals

6.3.1 First order neurons

The analog signals generated by the sensors of the artificial skin where converted into biomimetic spiking signals patterns by a network of modeled neurons. These first order neurons acted as a population of cutaneous fingertip slow adapting type I (SAI) mechanoreceptors, converting analog skin deformations following mechanical indentations onto spiking spatiotemporal patterns. The precise response of each first order neuron was implemented through a leaky-integrate and fire model (Lapicque, 1907), and their membrane potential dynamics were determined by the differential equation:

$$C \cdot \frac{dV_i(t)}{dt} = -g \cdot \Big(V_i(t) - V' \Big) - k \cdot A_i(t) \tag{6.1}$$

in which C = 0.5 nF denotes the membrane capacitance and g = 25 nS the passive conductance, resulting in a membrane time constant equal to $\tau = C/g$ = 20 ms. V'=-70 mV is the resting membrane potential. The term $k \cdot A_i(t)$ represents

the depolarizing input current, whose intensity was computed by multiplying the analog response of the i^{th} touch sensor: $A_i(t)$ (measured in femtoFarads) by a gain factor k = -390 pA/fF. Each first order neuron received current input signals from a single sensor (see fig. 6.5 for a representation of the connectivity layout). These parameter values were determined by comparing the output spike trains of simulated first order neurons against microneurography recordings of human mechanoreceptor responses Johansson and Birznieks (2004).

Each neuron emitted an action potential whenever its membrane potential $V_i(t)$ reached a threshold value $V_{\text{th}}(t)$. Immediately after a spike event, the neuron was hyperpolarized to $V_i(t) = V_{\text{reset}}$ = -100 mV, and the dynamics of its membrane potential frozen during a refractory period Δt_{ref} = 2 ms. We also modeled the spiking adaptation phenomenon by means of a "threshold fatigue" Chacron et al. (2003), which consisted in increasing the threshold V_{th} by 50 mV following each neuron's discharge, making it harder for the neuron to spike again (i.e. bounding its response firing rate). In the absence of spikes, V_{th} decreased exponentially back to its resting value V'_{th} following the equation:

$$\frac{dV_{\text{th}}(t)}{dt} = -\frac{V_{\text{th}}(t) - V'_{\text{th}}}{\tau_{\text{th}}} \tag{6.2}$$

where τ_{th} = 100 ms, and V'_{th} = -50 mV. No noise input was added to this neuronal model, and the output spike times were therefore entirely determined by the input signal from the sensor and previous activity of the neurons.

6.3.2 Second order neurons

The processing of afferent signals was carried out by a downstream network of second order neurons (see fig. 6.5), modeling a population of brainstem cuneate cells. The cuneate nucleus constitutes the first relay mediating peripheral-to-central transmission of tactile signals originating from the fingertips (see section 2.3). The neural model used in this study was derived from a previous work based on neurophysiological data from cat cuneate neurons (Brasselet et al., 2009; Bengtsson et al., 2013).

Each cuneate neuron received its inputs from either one or several adjacent mechanoreceptors through non-plastic synapses. On average, 1.9 ± 0.6 (mean ± std) mechanoreceptive afferents connected with every second-order neuron. As

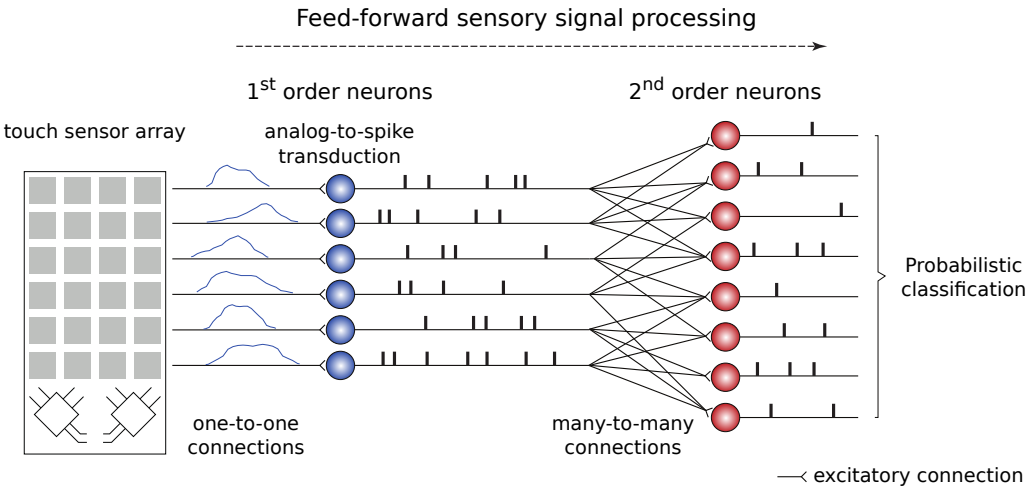

Figure 6.5: The implemented ascending somatosensory pathway. From left to right: the analog outputs from the artificial touch sensor stimulated a network of 24 first-order neurons according to a one-to-one projection layout. This early processing stage allowed analog sensory inputs following mechanical indentation to be converted into spike train patterns, mimicking fingertip mechanoreceptors. A downstream network of 49 spiking neurons then decoded and re-encoded primary afferent signals, acting as a sub-population of second-order cuneate neurons in the brainstem. The spatiotemporal output of this second-order network served for a probabilistic classification of fine touch stimuli.

seen in section 2.3, this sparse connectivity is coherent with physiological observations that very few (less than ten) functionally contribute inputs to individual cuneate cells (Bengtsson et al., 2013). All connections were excitatory and designed to create a purely feed forward network. The excitatory projections from first to second order neurons followed a scheme that resulted in second order receptive fields such as those illustrated in figure 6.6. The smaller receptive fields combined with high synaptic efficacy allowed topographical information from the mechanoreceptors to be maintained at the level of the second order output space. At the same time, the dimension and shape of the other receptive fields, combined with the synaptic weight distribution of the mechanoreceptor-to-cuneate projections, led to some cuneate neurons to act as partial coincidence detectors (Hopfield, 1995) capable of accounting for both single primary neuron activation and multiple co-activations, thus enriching their coding dynamics.

Cuneate neurons were modeled according to the spike-response model (Gerstner and Kistler, 2002), with the incorporation of a noise model, known as escape noise. The escape noise model relies on a stochastic process which

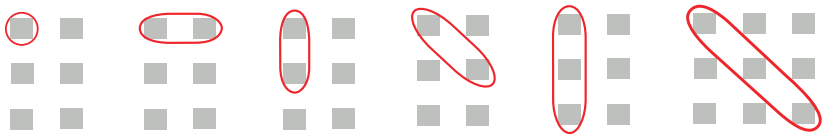

Figure 6.6: Sample of receptive fields (projected on the 24 sensors of the artificial fingertip) of the second order neurons. The many-to-many connection scheme used to drive second-order neurons resulted in receptive fields sampling either unitary or multiple primary afferent activity (up to three adjacent mechanoreceptors).

computes a spiking probability depending on the difference between the membrane potential and the spike threshold. In can therefore lead to some spontaneous activity or to the suppression of a spike which would normally have been emitted.

Whenever multiple afferent spikes excited the neuron within a short time window, they induced a compound membrane potential depolarization equal to:

$$V(t) = V' + \sum_{i,j} w_{\mathrm{i}} \cdot \Delta V(t - \hat{t}_{\mathrm{i}}^{\mathrm{j}}) \tag{6.3}$$

$$\Delta V(t) \propto \sqrt{t} \cdot \exp(-t/\tau) \tag{6.4}$$

with $V' = -70$ mV denoting the resting potential, i the presynaptic neurons, and j indexing the spikes emitted by a presynaptic neuron i at times $\hat{t}_{\mathrm{i}}^{\mathrm{j}}$. The synaptic weight w_{i} of the projection from the presynaptic unit i was taken so as to guarantee a reliable transmission of primary afferent signals and avoid a saturation of the second order neurons' activity. The values were fixed at $w_{\mathrm{i}} = 0.04$ and $w_{\mathrm{i}} = 0.028$ for connections belonging to cuneate units with receptive fields regrouping one and two/three mechanoreceptive units respectively (see fig. 6.6). The function $\Delta V(t)$ represented a unitary EPSP (excitatory postsynaptic potential), with $\tau =$ 2 ms indicating the decay time constant of the EPSP profile.

At each time step, the spiking probability $p(t)$ of the neuron depended on the following functions:

$$p(t) = 1 - \exp\Big(- f(t) \cdot R(t) \Big) \tag{6.5}$$

$$f(t) = r_0 \cdot \log\left(1 + \exp\left(\frac{V(t) - V_{\mathrm{th}}}{V_{\mathrm{f}}}\right)\right) \tag{6.6}$$

$$R(t) = \frac{(t - \hat{t} - \tau_{\mathrm{abs}})^2}{\tau_{\mathrm{rel}}^2 + (t - \hat{t} - \tau_{\mathrm{abs}})^2} \, H(t - \hat{t} - \tau_{\mathrm{abs}}) \tag{6.7}$$

with $f(t)$ denoting the instantaneous firing rate, determined by the constant $r_0 = 11$ Hz, the threshold potential $V_{\text{th}} = -65$ mV, and a gain factor $V_{\text{f}} = 0.1$ mV. The function $R(t)$ determined the refractoriness property of the neuron, with $\hat{t}$ indicating the time of the last spike emitted, $\tau_{\text{abs}} = 3$ ms the time constant of the absolute refractory period, $\tau_{\text{rel}} = 9$ ms the time constant of relative refractory period, and H the Heaviside function.

6.3.3 Probabilistic classification of tactile percepts

After being converted and processed by the two first neural stages, tactile signals were classified online by a trained Naïve Bayesian Classifier (NBC) (McCallum and Nigam, 1998). The NBC belongs to the family of probabilistic classifiers relying on Bayes' rule to compute a multinomial posterior probability distribution for sample classes (Duda et al., 2001). The NBC's computations are performed with the underlying hypothesis that input features are independent from one another. This simplification allows the NBC to provide a fast classification and making it suitable for applications requiring frequent estimations of class posterior probabilities and strict execution-time constraints. It is also not the first time an NBC process has been applied to neural data (Truccolo et al., 2008).

The NBC was trained on a database of simulated second order cuneate activity. The database consisted of the cuneate responses to 100 repetitions for each of the 26 Braille characters (where 1 repetition means to 1 complete scan of the letter by the artificial touch sensor). These data points were generated by swiping the fingertip over the characters at a constant speed of 30 mm/s. For analysis purposes only, the same protocol was used to also train the NBC based on the first order activity that drove cuneate responses in the database mentioned above.

For each letter, and for every repetition of that letter, a binning procedure mapped the spatiotemporal patterns provided by the cuneate population onto spike count class vectors. This was done in a cumulative manner, meaning that bin width increased incrementally such that $b_i = i \times \Delta t$ (see fig. 6.7), where b_i is the width of the i^{th} bin and Δt the temporal bin increment. All bins sampled the neural responses starting from the time of the first spike emitted by the cuneate network. Consequently, larger bins also took into account the activity already counted in previous, smaller temporal bins. Every dimension of the spike count vector corresponded to the activity of a single cuneate neuron. Hence,

the resulting feature vectors had the same dimension as the second order neuron population. The resulting spike count vectors formed a dataset that was used to train the NBC.

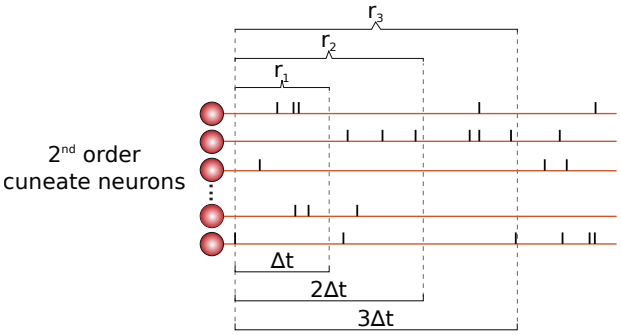

Figure 6.7: The output spiking activity of the cuneate network was binned by means of incrementally increasing time windows $i \times \Delta t$, with $i = 1, 2, \ldots, n$, and mapped onto spike count class vectors r_i.

During the training, the NBC computed the likelihood of many (a few hundreds) response classes vectors for each character. Each class effectively represented the response activity to that letter at a given point of the scanning process. Later, during recognition, the NBC estimated the posterior probability of a letter as the sum of the posterior probabilities of each response class vectors corresponding to that letter. For example, in the context depicted in fig. 6.7 A., the recorded cuneate activity r was obtained with the fingertip scanning the letter x. The response vectors corresponding to bins $\Delta t, 2\Delta t, \ldots, n\Delta t$ would then be labeled as r_{x_1}, $r_{x_2}, \ldots, r_{x_n}$. The resulting training set (composed of all response vectors r_{x_i}) would serve the NBC to compute the likelihoods $p(r_{x_i}|x)$, $\forall i$. Finally, the posterior probability of x would simply be computed as $p(x|r) = \sum_i p(x|r_{x_i})$.

A preliminary analysis was carried out to study the influence of the bin width on recognition rates and speeds (see fig. 6.8 A. and B., respectively). These results were obtained by using a range of Δt values to train the NBC on the basis of 100 repetitions per letter, and then to test its classification performance on a probe set of 50 repetitions per letter. Based on these results, we could select a bin width of $\Delta t = 1$ ms for running the NBC in the system, and we observed a very rapid convergence of the training process, in terms of both recognition rate and recognition time, after only about 10 repetitions per letter in the training set.

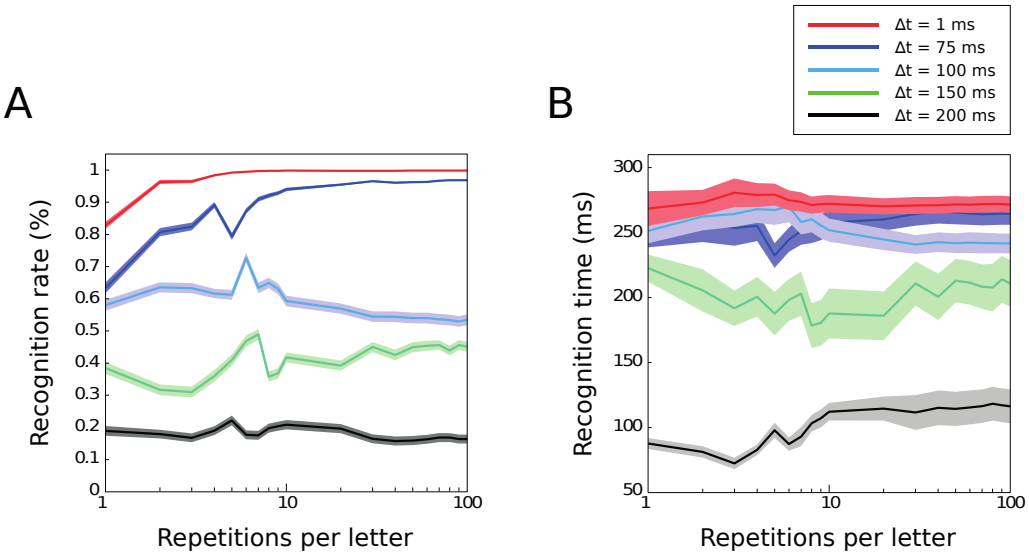

Figure 6.8: *A.* Recognition rate (mean ± s.e.m.) as a function of the size of the training base in terms of number of repetitions (scans) per letter. Different curves correspond to different bin widths. These results where obtained by applying the NBC on a test base of 50 repetitions per letter. *B.* Recognition time (mean ± s.e.m.) as a function of the training base size. Again, different curves correspond to different bin sizes. These results were obtained using the same testing base as in A.

The NBC training procedure used for recognizing the Braille letters involved a sample base of 100 trials for each Braille character. Comfortably above the minimum of 10 trials found during the preliminary analysis. The timeset for the temporal bin window however was set to $\Delta t = 4$ ms, which nonetheless remained fairly close to the optimal value of $\Delta t = 1$ ms found previously. The NBC computed the posterior probability of a letter being read to correspond to a known character class every time a new bin of activity was received, meaning every 4 ms. For online classification, the computed probability distribution (across all Braille characters) was averaged over a 40 ms history. A classification event was considered to have occurred as soon as the peak of the mean probability distribution exceeded the 90% threshold. Naturally, the classification of the letter being read corresponded to the letter linked to the class with the peak average posterior probability.

6.4 Closed loop control

6.4.1 High-level speed controller

The shape of the posterior probability distribution estimated by the NBC across all Braille letters evolved over time as the artificial fingertip scanned a given character. The ongoing degree of "peakedness" of this probability distribution provided a simple and effective basis to optimize the scanning speed control. The "peakedness" of a probability distribution is reflected by the value of its kurtosis. A high kurtosis value indicates that one probability is standing out relative to the others. The null kurtosis value corresponds to a Gaussian distribution and negative values reflect the fact that the probability distribution is almost flat or uniform. The fact that the posterior probability distribution computed by the NBC was multinomial helped ensure that when the probability of one letter rose, that of the other letters would decrease, thereby enhancing the creation of peaks (whether local or global).

A decision making module monitored the evolution of the excess Kurtosis index $k(t)$ of the NBC's output average probability distribution on a 4 ms timestep basis. The fingertip scanning speed $v(t)$ was then modulated according to:

$$\dot{v}(t) = \frac{k(t) - k(t-1)}{C \cdot v(t)} \tag{6.8}$$

where $\dot{v}(t)$ denotes the scanning acceleration (in $\mathrm{cm/s^2}$), and C a constant factor tuned to 600 $\mathrm{cm^2/s^2}$. An increase of the $k(t)$ function indicated a narrowing of the distribution, reflecting a decrease in the uncertainty of the probabilistic classification of the character being scanned. The high-level controller consequently increased the scanning speed proportionally to the gradient value. By contrast, a decrease of $k(t)$ indicated a broadening of the estimate distribution, which induced a deceleration of the fingertip.

6.4.2 Low-level controller

In order to compensate for errors during the execution of movements, the closed-loop architecture incorporated a low-level controller responsible for online sensorimotor adaptation. The low-level controller consisted of a spiking neural network mimicking the role of the cerebellum in fine movement control and

coordination (Ito, 1974; Thach et al., 1992; Miall et al., 2001; Attwell et al., 2002).

In agreement with Marr-Albus-Ito theory (Marr, 1969; Albus, 1971; Ito and Kano, 1982), the model assumed that the cerebellum could learn internal representations of sensorimotor interactions through its multiple microcomplexes (Wolpert et al., 1998). Four microcomplexes were implemented, respecting the anatomo-functional properties of their biological counterparts (see fig. 6.9). Input signals entered the cerebellar network via the mossy fibers (MFs), which were connected by excitatory synapses to both the granule cells (GCs) and the deep cerebellar nuclei (DCN). Purkinje cells (PCs) received excitatory inputs from both GCs (via the parallel fibers, PFs) and inferior olive (IO) neurons (via the climbing fibers, CFs). PCs inhibited the DCN cells, which formed the output of the microcircuit model. The microcomplex model adopted was taken from a previous work by Passot et al. (2012, 2013).

The cerebellar microcomplexes were trained to act as forward predictor models (Ito, 1984; Miall et al., 1993; Wolpert and Miall, 1996) meaning that they could predict the outcomes of motor commands prior to their actual execution. These predictions allowed the motor commands to be finely adjusted online, notably avoiding otherwise inaccurate movement execution such as local drifts in trajectories. The training adapted the input-output dynamics of the microcomplexes through long-term plasticity mechanisms which acted as follows. MFs excited DCN neurons via all-to-all constant connections; hence, without inhibition from PCs, the output of the microcircuit was constant and did not depend on the input. In order for the output to be meaningful, the strength of the inhibitory output of PCs should depend on the input conveyed by MFs via GCs and PFs. The GC layer provided a sparse representation of the MF inputs –the number of GC neurons was 100 times larger than that of MFs and the MF-GC connection probability was only 0.04 (*ie.* each MF innervated 400 GCs and each GC received 4 MF afferents, on average, in agreement with anatomical data, Eccles et al., 1967; Jakab and Hamori, 1988; Chadderton et al., 2004). A sparse coding representation served to optimize the encoding capacity and information transmission from MFs to PCs (D'Angelo and De Zeeuw, 2009). The synapses between PFs (*ie.* GCs' output fibers) and PCs were the only plastic synapses implemented in the microcircuit model, they learned to translate the inputs into PC outputs (that inhibited the DCN). Bidirectional long-term plasticity (*ie.* potentiation, LTP, and depression, LTD) modified the

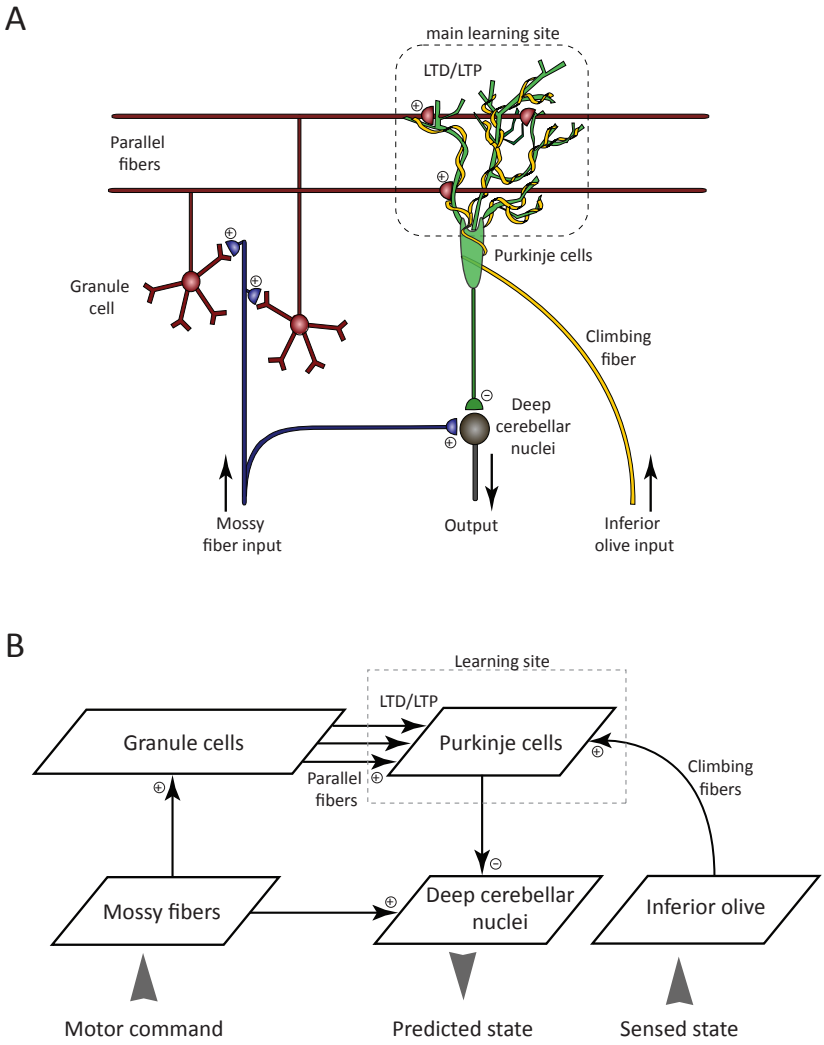

Figure 6.9: *A.* A simplified scheme of a cerebellar microcomplex, adapted from Medina et al., 2002. Information enters the cerebellum via two neural pathways: the mossy fibers convey multimodal sensorimotor signals, whereas climbing fibers are assumed to convey error-related information. Granule cells process and transmit sensorimotor inputs to Purkinje cells. Error-related signals also converge onto Purkinje cell synapses, where long-term modifications (i.e. long-term potentiation, LTP, and depression, LTD) occur. *B.* Model of the cerebellar microcomplex circuit. Each box represents a population of spiking neurons.

efficacy of PF-PC synapses and shaped the input-output dynamics of the microcomplex (see fig. 6.9 B.). LTP was implemented as a non-associative mechanism (Lev-Ram et al., 2002), such that every incoming PF spike triggered a synaptic weight increase. Conversely, LTD was modeled as a supervised associative mechanism with the teaching signal conveyed by CFs (output fibers of the IO neurons). This is in accordance with experimental data showing that conjunctive inputs to a PC from PFs and CFs tend to depress PF-PC projections (Ito and Kano, 1982; Wang and Linden, 2000; Safo and Regehr, 2008). The training signal from the CFs reflected the difference between the desired position for the hand and its actual position. The actual position was computed algorithmically, though it represented the proprioceptive knowledge (here supposed perfectly accurate) of the hand-arm's position.

A more comprehensive description of the cerebellar microcomplex model can be found in Passot et al. (2012).

6.4.3 Hand-arm robotic platform

The closed-loop system was test using a simulated 2 degrees of freedom arm with noisy dynamics, taken from Carrillo et al. (2008). The arm model included two joints (shoulder, elbow), with the arm end-point carrying the simulated touch sensor described in Sec. 6.2.2. The four cerebellar forward models learned to predict the future angular position and velocity of each of the two joints. During movement control, the predicted joint states allowed to algorithmically estimate what the arm end-point position (in Cartesian coordinates) would be. A trajectory generator Carrillo et al. (2008) compared the desired and predicted position of the arm end-point and updated the motor commands consequently. Note that the wrist joint was not included in the model, instead the simulated arm would only compute the sensor's position (at the arm's end-point), while the sensor's orientation was considered constant.

The performance of the overall Braille reading system was also tested in a real-world scenario. For this preliminary experiment, the artificial touch sensor Cannata et al. (2008) was fixed on the index digit of the DLR-HIT hand 2 (Liu et al., 2008) which was mounted on the DLR light-weight robot III (LWR) (Albu-Schäffer et al., 2007a). Both the LWR robot and the DLR-HIT hand were operated in impedance control mode Albu-Schäffer et al. (2007b), which ensured stability even in physical contact situations as was required by this task. The fingertip

was rubbed over a Braille line comprising seven different characters at a constant speed of 30 mm/s. This preliminary robotic validation gave rise to a real-time and online Braille reading demonstrator in the framework of the European project 'Sensopac', no. IST-028056-IP (fig. 6.10).

For the real-world robotic setup, the fine control of the arm joints was left to the robotic controller instead of the cerebellar model described above (see section 6.4.2). The traveling speed imposed to the sensor was constant, however, if an error in the trajectory was detected, corrective movement commands were sent to the robotic platform. Notably, errors of a few millimeters in the trajectory could be detected using feedback from the sensor, allowing for some form of high-level control. Still, compared to the simulated arm, noise in the pitch and roll dynamics of the real arm-hand platform remained marginally compensated, which increased the probability of inhomogeneous and discontinuous contacts between the fingertip and Braille characters.

6.4.4 Technical implementation details

All modules containing spiking neuron models –that is the first-order and second-order neurons, as well as the neurons of the cerebellum– where implemented using the C++ programming language. Furthermore, both the cuneate nucleus model and the cerebellum were implemented through the EDLUT (Event-Driven neural simulator based on LookUp Tables)[1] simulation environment (Ros et al., 2006). EDLUT was designed for efficient simulation of complex neural network models and takes advantage of both time-driven and event-drive procedures to guarantee a fast computation and update of neural state variables (Garrido et al., 2011). Thanks to its properties, the EDLUT environment provided the system with the computational efficiency required for neurobotic applications.

The Naïve Bayesian Classifier and high-level controller were run as Matlab scripts. Every component of the system was designed as a separate module, capable of being run independently or removed from the system altogether. Different modules communicated between each other using "Transmission Control Protocol/Internet Protocol" (TCP/IP), except for the robotic hand-arm platform which was controlled through a "User Datagram Protocol" (UDP)

[1]EDLUT is an open source project freely available at http://edlut.googlecode.com.

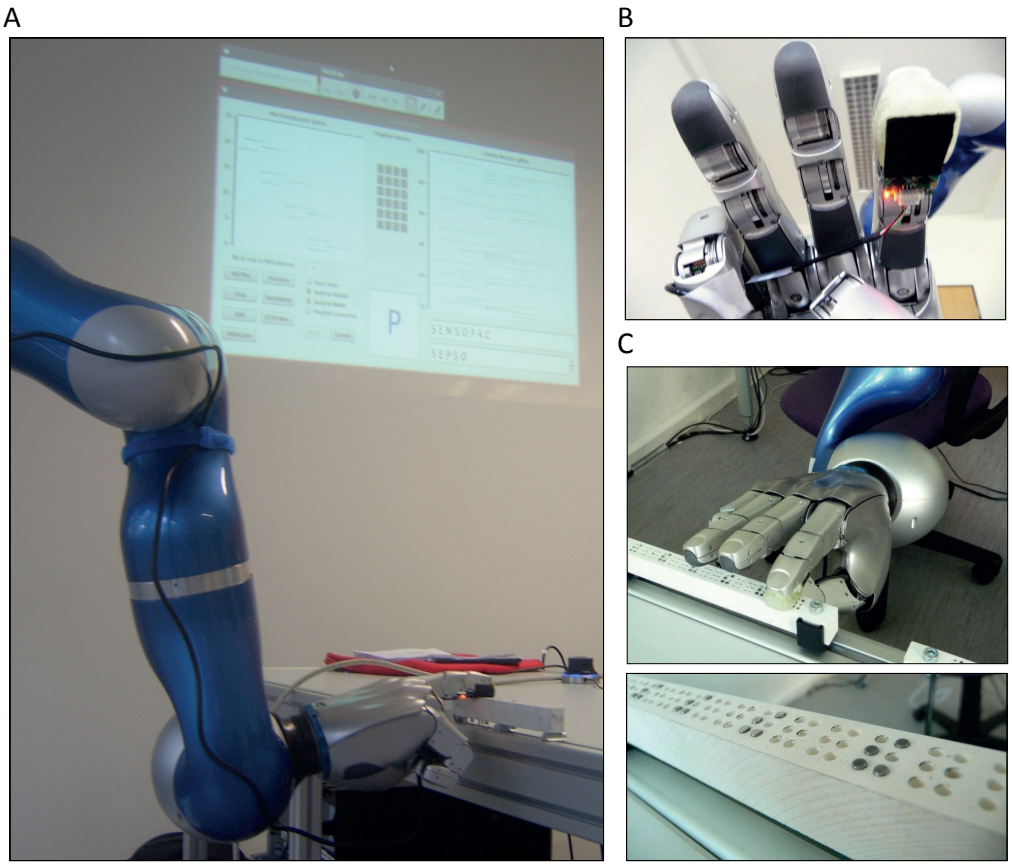

Figure 6.10: Preliminary validation on a real robotic platform performing real-time Braille reading. *A.* The arm-hand robotic platform performing online and real-time Braille reading. *B.* The artificial touch sensor was fixed on the robotic hand DLR-HIT hand II. *C.* The robotic hand-arm sliding over a Braille line. *D.* A scaled Braille character line.

interface.

The running frequency of the entire system had to be adapted to suit the temporal constraints of individual modules. The artificial fingertip had an acquisition frequency of only 20 Hz, well below the temporal precision required for fine touch discrimination. To compensate, sensor values were interpolated between two acquisition times, allowing the spatiotemporal patterns from the neuron models to remain temporally precise. The simulated version of the sensors was designed to run at 1000 Hz, allowing it not to be a limiting factor for the online execution of the rest of the system.

6.5 Analysis tools

6.5.1 Metrical information theory

Before studying the the Naïve Bayesian Classifier's performance, it was necessary to first assess the quantity of information which was transmitted (or lost) by the first and second order neurons. Doing so was important in oder to understand which part of the discrimination results was the due to the choice of classifier, and which was due to the loss of information along the modeled ascending pathway.

To do so, an information theory framework was adopted. Information theory is a powerful mathematical tool which is capable of quantifying how well it is theoretically possible to discriminate an input signal database, knowing only the corresponding output signals –*ie.* how much information about the input signals the output signals contain. A more comprehensive description of the information theory tools used is provided in section 4.1.

It is recalled here that metrical information $I^*(R;S)$ is defined by:

$$I^*(R;S) = H^*(R) - H^*(R|S) \tag{6.9}$$

where

$$H^*(R) = -\sum_r p(r)\log_2\left(\sum_{r'} p(r')\phi(r,r')\right) \tag{6.10}$$

$$H^*(R|S) = \sum_s p(s)H(R|s) = -\sum_{s,r} p(r,s)\log_2\left(\sum_{r'} p(r'|s)\phi(r,r')\right) \tag{6.11}$$

$$\phi(r,r') = H\Big(D_c - D(r,r')\Big) \tag{6.12}$$

where $I(R;S)$ is the mutual information; $H(R)$ and $H(R|S)$ are the marginal and conditional entropies, respectively; R and S denote respectively the response and the stimulus space; $p(r)$, with $r \in R$, is the response marginal probability; $p(s)$, with $s \in S$, the stimulus a priori probability; $p(r|s)$ and $p(r,s)$ the conditional and joint probabilities, respectively. The function $\phi(r,r')$ measures the similarity between two responses, and it is defined as the Heaviside function of the Victor-Purpura distance $D(r,r')$ between two spike trains $r,\ r' \in R$ (see section 4.2.1, Victor and Purpura, 1996. The Victor-Purpura distance allowed to choose the temporal resolution with which spike times were compared, by tuning a cost parameter. The term D_c is the cutoff parameter, named critical distance. For $D(r,r') < D_c$, responses $r,\ r'$ are considered as identical (i.e. $\phi(r,r') = 1$), otherwise they are considered as different. If $D_c = 0$, then the metrical version of entropies are identical their Shannon counterparts.

When considering metrical information theory, the optimality condition corresponds to a maximal $I^*(R;S)$ along with a null (or minimal) $H^*(R|S)$. Conceptually, this means that not only do the output signals contain as much information as they can possibly have, but that there is a space in which the responses are unambiguously clustered –*ie.* the decoding of the output signals is very simple.

6.5.2 Braille pattern complexity

With the control loop closed, the system is able to devise movement strategies to scan the different Braille charcters. A complexity measure was found to model the 'shape' of Braille characters and see if and how it influenced the system movement strategies.

Several complexity measures have been established in the field of psychophysics to describe visual (Alexander and Carey, 1968; Chipman, 1977; Yodogawa, 1982) and vibro-tactile stimuli (Horner, 1991). The objective of these different measures was to link an objective quantity to the complexity perceived by a human subject (Aksentijevic and Gibson, 2012). Such measures have also been applied to study the Braille alphabet, however this has been done by concentrating solely around the number of dots as an estimator of complexity (Nolan and Kederis, 1969; Newman et al., 1984). However, other complexity measures for dot patterns exist (Ichikawa, 1985) and could be adapted to Braille character patterns. Similarly to the process used by Ichikawa (1985), the correlation between Braille letter complexity and movement policy was estimated as a linear combination of two complexity measures: the number of dots *Dot* (Nolan and Kederis, 1969), and the number of subsymmetries *Sym* (Alexander and Carey, 1968). The number of subsymmetries was computed as follows:

$$C = \alpha \cdot Dot + (1 - \alpha) \cdot Sym \tag{6.13}$$

where

$$Sym = \sum_{x=1}^{X} \sum_{y=1}^{Y} \Big(\sum_{i=1}^{X-x} \sum_{j=1}^{Y-y} i \cdot j \cdot NSym_{(x,y)}(i,j) \Big) \tag{6.14}$$

with $\alpha = 0.94$. The Sym function counted the number of symmetries of each rectangular sub-grid of the Braille character matrix and added them in a sum weighted by the area of the sub-grid; with X and Y referring to the size of the first and second cell dimensions respectively (i.e. 2×3 in the case of Braille cells), and $NSym_{(x,y)}(i,j)$ being the number of symmetries observed in the rectangle of size $i \times j$ at position (x,y). The symmetries considered consisted in vertical, horizontal, and central symmetries for all sub-grid dimensions, as well as both diagonal symmetries when $i = j$.

Chapter 7

Results

The current chapter presents the behavior of the neural architecture in a real world scenario. A Braille reading task was used to: *(i)* quantify the information content of first and second order neuron activity, *(ii)* assess the performance of the implemented classifier, *(iii)* and estimate the robustness of the high and low-level controllers.

7.1 First order neuron responses

7.1.1 Model response characterization

The model first order neuron responses were first characterized and compared to real mechanoreceptor responses. To do so, experimental protocols used during microneurography recording sessions were reproduced in simulation. The two protocols consisted in delivering a passively applied stimuli indenting the human fingertip while recording different mechanoreceptor response. These studies were carried out by Phillips et al. (1990) and Birznieks et al. (2001) respectively.

Topological mapping

In the first experimental protocol (Phillips et al., 1990), a series of moving Braille characters were passively sensed by fixed fingertip. The Braille characters were dynamically swiped at 60 mm/s over the receptive field of a recorded mechanoreceptor following the distal-proximal direction. Once the stimulus exited the receptive field, its position was shifted by 0.2 mm along the radial-ulnar axis, and the process repeated. This procedure allowed the so called Spatial Event Plot (SEP, Phillips et al., 1988b) to be constructed from the recorded mechanoreceptor spikes. A SEP consists in displaying the recorded spikes onto the stimulus pattern in order to obtain a spatial representation of

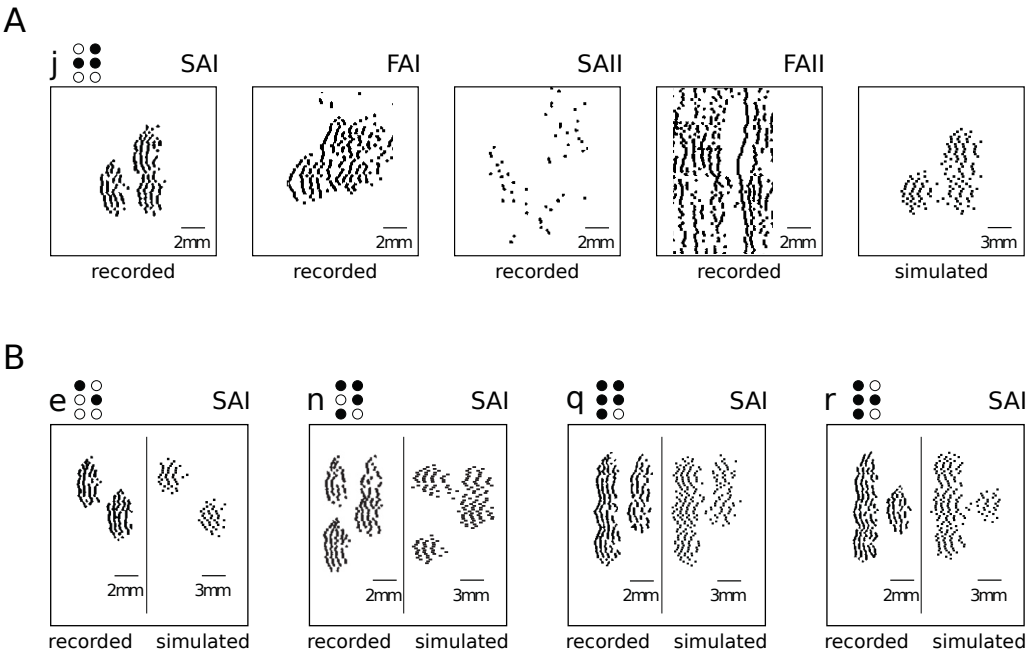

Figure 7.1: *A.* Comparison between the spatial event plots of responses from the four different mechanoreceptor types in the human glabrous skin to a Braille "J" stimulus. Note the scale difference (1:1.7) between recorded and simulated responses (as explained in section 6.2.1). *B.* Different examples of spatial event plots of human SAI mechanoreceptor responses to scanned Braille characters, and their simulated counterparts. (recorded spatial event plots were adapted from Phillips et al., 1990)

the outgoing activity. This representation is made possible through the precise knowledge of the stimulus position at each time point as well as the precise timing of the spikes. Examples of the results are illustrated in figure 7.1. Simulated SEPs, which illustrated the spatiotemporal characteristics of a first order neuron response to a moving Braille stimulus, were qualitatively most similar to those of slow adaptive type I (SAI) human mechanoreceptors (see fig. 7.1 A.).

Receptive field sizes were estimated by computing the areal extent of the fiber's response cluster to an isolated dot. Recorded and simulated afferents were found to have comparable receptive field sizes at respectively 4.8 $\pm$ 1.2 mm^2 (mean $\pm$ std) and 4.7 $\pm$ 1.5 mm^2 after correcting for the scale difference. However, due to mechanical constraints, the modeled receptive fields had very little overlap and consequently covered the artificial fingertip with a density of 17 units/mm^2, one fourth of the 70 units/mm^2 reached by their biological counterparts (Phillips et al., 1990). Furthermore, simulated mechanoreceptor SEPs in response to Braille dots

seemed to remain more symmetrical then those of their biological equivalents (see fig. 7.1 B.). The distortion observed on the recorded SEPs is likely due to the compression of the fingertip's skin as the stimulus is dynamically swiped over it. Though not entirely inexistent –thanks to the neoprene layer– this phenomenon remains marginal at best in the artificial fingertip. Nonetheless, they showed a topological stimulus-response mapping, an important property for the encoding of fine spatial discontinuities (Johansson and Flanagan, 2009).

Response dynamics

Figure 7.2 shows an example of discharge pattern recorded from a simulated first order neuron in response to a single dot stimulus moving at 30 mm/s. Responses are shown as a raster plot of spike times (middle) and the corresponding PSTH (bottom) during 150 stimulation trials. The analog output signal from the indented touch sensor serves as depolarizing current to the model neurons (top).

Like SAI mechanoreceptors, the neuron responded with a sustained activity exclusively during the entire indentation time. Furthermore, the spike timing reliability of the firing pattern was high at the onset of the protraction stimulation phase and decreased with time, as was observed for human SAI mechanoreceptors (Johansson and Flanagan, 2009) and more generally in central neurons (Mainen and Sejnowski, 1995).

The second experimental protocol (Birznieks et al., 2001) was then simulated. This allowed to compare both first spike jitter and interspike interval (ISI) distributions of the model SAIs against the experimental data (see fig. 7.3) reported in Johansson and Birznieks (2004). Despite a time lag of about 2 ms, there was no statistically significant difference between the two distribution shapes (Kolmogorov-Smirnov, $p > 0.076$). Indeed, when accounting for the 2 ms delay, no statistical difference between the two distribution medians was observed (Mann-Whitney U, $p > 0.11$). Note that to estimate the distribution of first spike jitters, Johansson and Birznieks (2004) computed the standard deviation of first spike latencies for five repetitions of every stimulus. Consequently, supposing that first spike times (elicited by the same stim lus) follow a normal distribution, and observing that the mean jitter recorded was bout 0.8 ms, it can be deduced that 99% of first spikes were within a 3 ms neighborhood around the mean recorded latency. Under the same assumptions,

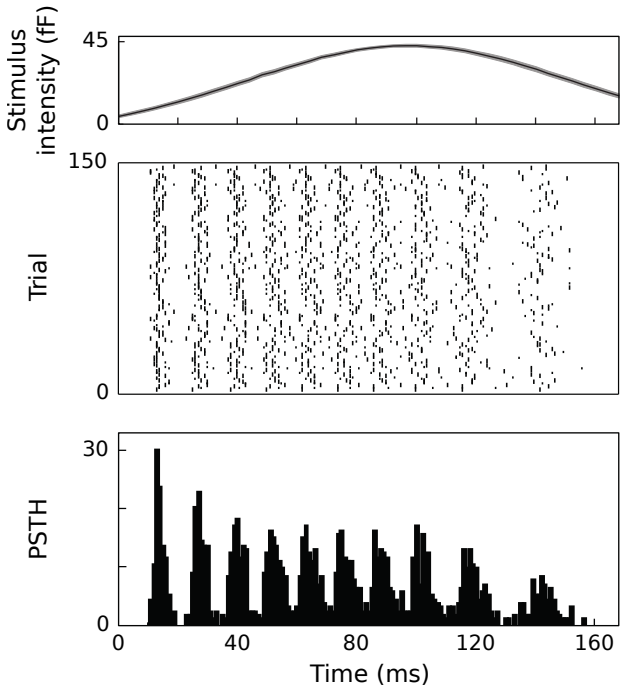

Figure 7.2: Raster plot (middle) and corresponding Peristimulus Time Histogram (PSTH, bottom) of 150 responses of a simulated first order neuron to a single dot stimulus moving at 30 mm/s (top), showing a stronger and better timed activity at the onset of the stimulus. (adapted from Bologna et al., 2013)

the 2 ms second difference observed on the model jitter distribution leads to 99% of first spikes being in a 9 ms neighborhood around the mean latency. This is a significant difference and –considering the amount of information the precise timing of first spikes yields (Johansson and Birznieks, 2004)– a drawback for the system performance.

Nonetheless, when comparing the ISI distributions from simulated and real mechanoreceptor responses (see fig. 7.3 B.), the medians of the two distributions were not statistically different (Mann–Whitney U test, $p > 0.16$). Consequently, firing rates of model and real SAI are likely to be found in a similar range. However, the ISI variability of model neurons was smaller than in recorded SAI afferents. This difference may reflect the viscoelastic properties and more complex dynamics of the human skin as compared to the artificial finger.

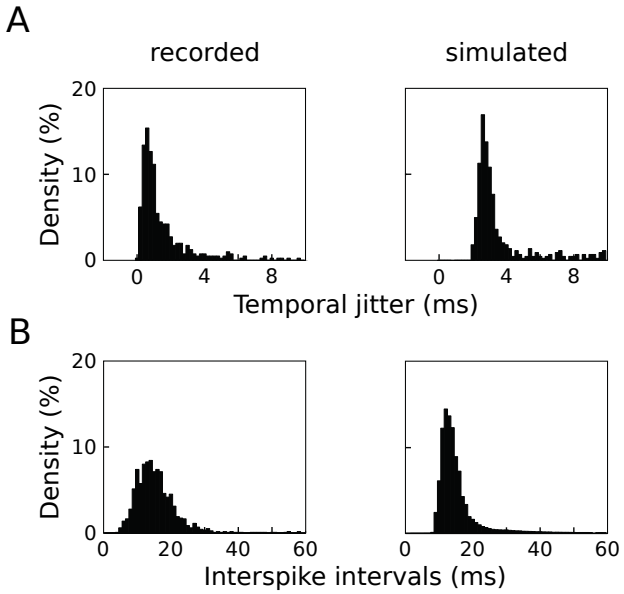

Figure 7.3: Distributions of standard deviations of first-spike latencies (top) and interspike intervals (bottom) for both real SAI (left) and simulated (right) mechanoreceptor responses. Data for the real SAI mechanoreceptor was recorded by Johansson and Birznieks (2004).

7.1.2 Information content of responses to static indentation

An information theoretical analysis was performed to assess the information encoded in first order neuron responses to 26 distinct Braille characters sensed statically. During a protraction phase, Braille characters were gradually pressed on the fingertip where they then stayed immobile during 250 ms before being gradually lifted. Both protraction and retraction phases lasted 125 ms. The evolution of metrical information over time was monitored to quantify how rapidly after the stimulus onset a perfect discrimination of all Braille stimuli could be achieved. Considering that the implemented classifier –*ie.* the Naïve Bayesian Classifier, see 6.3.3– would only use spike counts to discriminate between different signals, the cost parameter of the Victor-Purpura distance was set to 0 for this theoretical analysis. The results are illustrated in figure 7.4.

Within 100 ms of the stimulus onset the maximum intra-stimuli distance becomes smaller than the minimum interstimuli distance (see fig. 7.4 A., top), thereby satisfying the condition for an error-less stimulus reconstruction –*ie.*

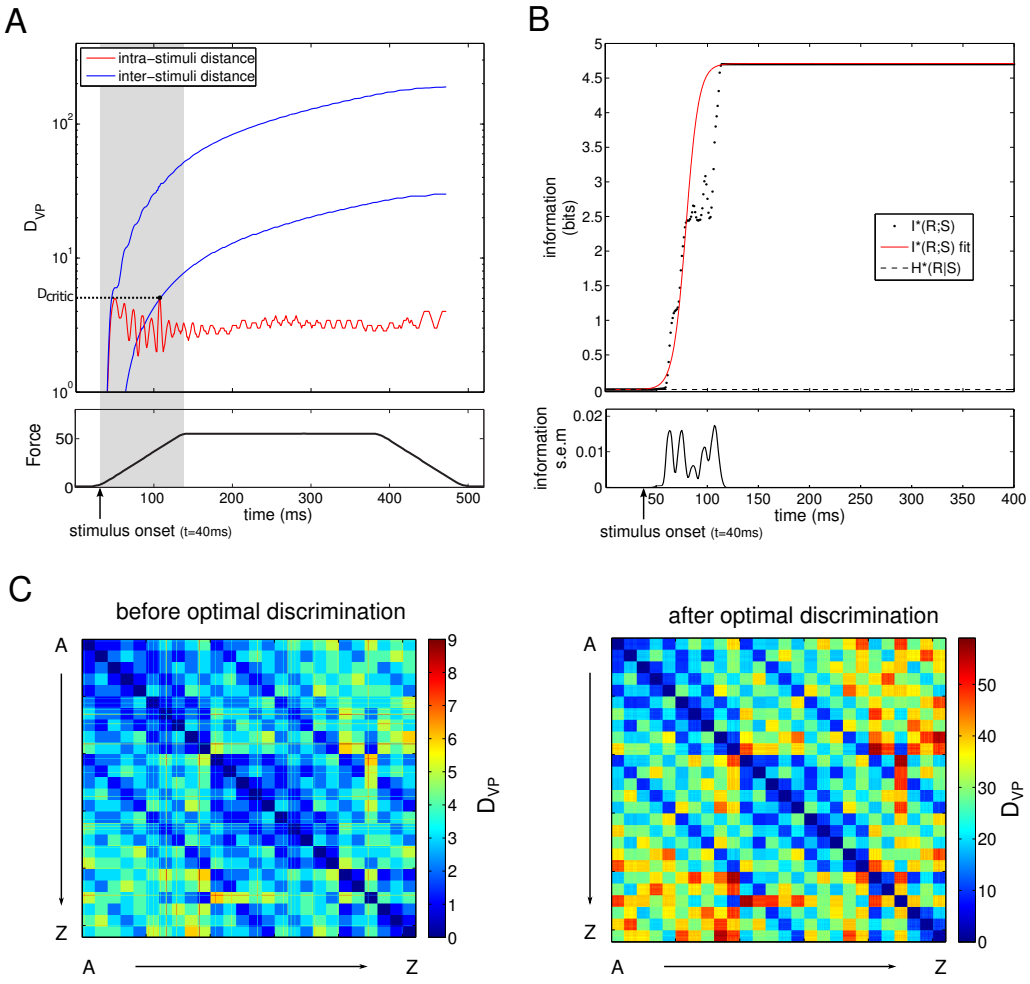

Figure 7.4: Metrical information analysis of primary afferent responses to static Braille stimuli. *A. Top:* Evolution of maximal and minimal interstimulus and maximal intrastimulus distances over time (blue and red curves respectively) on a semilogarithmic scale. The minimal intrastimulus distance is approximately zero during the entire stimulus duration and has not been reported. Twenty repetitions per stimulus are used. Perfect discrimination is achieved within about 100 ms of stimulus onset. The critical distance used for computing the metrical Information and Entropy is indicated by D_{critic}. *Bottom:* The time course of the stimulus indentation force shows that the perfect discrimination is reached well before the end of the protraction phase (t < 125 ms). *B. Top:* The metrical information (black dots: data; continuous red line: sigmoidal fit) converges to its maximal value after about 100 ms, while the metrical conditional entropy (dashed black line) remains equal to zero. *Bottom:* information variability, measured as mean standard error, over time. *C.* Distances between mechanoreceptor responses before (left matrix) and after (right matrix) the perfect discrimination condition is reached. Twenty repetitions for each character are used and distances computed for all 520^2 spike train pairs. Each line shows the distances between a single response to a stimulus and all other responses. Intrastimulus distances are grouped into small squares (20-sample side) along the diagonal and become remarkably smaller than the others (i.e. interstimulus distances) after the optimal discrimination point is reached (right matrix). (taken from Bologna et al., 2011)

maximal metrical information $I^*(R;S)$ and zero conditional entropy $H^*(R|S)$ (see fig. 7.4 B., top). The metrical information reaches a maximal value of 4.7 bits, meaning that enough information is present to discriminate all $2^{4.7} = 26$ stimuli. Consistently with a previous decoding analysis performed on real primary afferent recordings (Johansson and Birznieks, 2004), a fast and complete discrimination could theoretically occur before the end of the indentation protraction phase (see fig. 7.4 A., bottom), which corresponds to the period after which the time precision of spikes deteriorated. This study was performed on 12 batches of 20 repetitions for each Braille character. Despite the relatively small sample size, the error remained surprisingly small (see fig. 7.4 B., bottom). This suggests that despite a lower temporal precision than in the biological system, model signals were still quite robust and highly reproducible.

Figure 7.4 C. also reports two examples of distance matrices between simulated mechanoreceptor responses before (left) and after (right) the occurrence of the perfect discrimination condition. For t $<$ 100 ms (left matrix) responses to different stimuli can have relatively small distances, which produces interferences impairing the decoding process. By contrast, for t $>$ 100 ms (right matrix) all the initially overlapping contexts becomes well separated, removing all interferences across inputs and leading to 100% accuracy in the discrimination process. Note the different colormap scales used to represent spike train distances D_{VP} before and after the occurrence of the optimality condition.

7.1.3 Information content of responses to dynamic stimulation

For the second information theoretical analysis, the simulated data was obtained by dynamically delivering the stimuli. All 26 Braille characters moved laterally over the fingertip at a constant velocity of 15 mm/s. Figure 7.5 illustrates the sensor, mechanoreceptor and cuneate neurons outputs as the letter “y” was scanned following the dynamical protocol.

The evolution of maximal and minimal intra- and interstimulus distances over time was once again investigated (see fig. 7.6). The condition of perfect discrimination of all 26 Braille inputs was reached after about 700 ms from stimulus onset. As predicted by metrical information theory, this condition

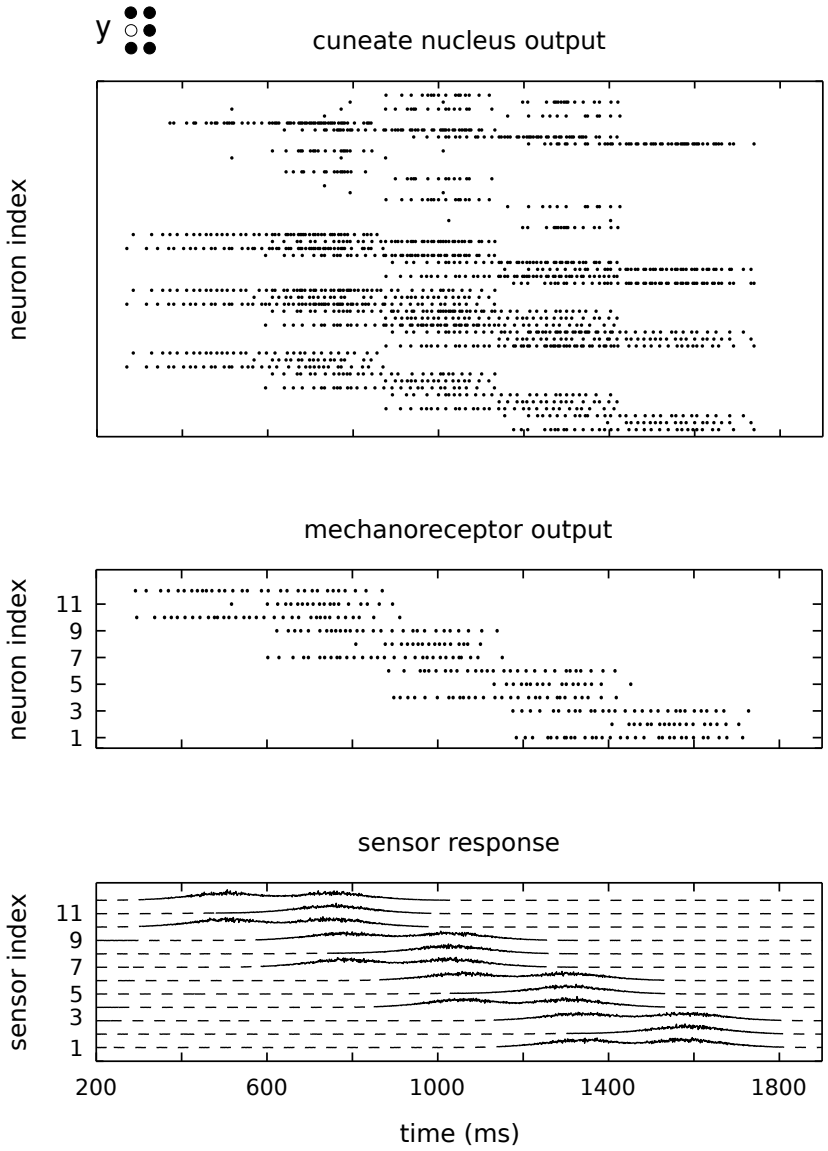

Figure 7.5: Example of sensor (bottom) responses to a dynamically delivered (at 15 mm/s) stimulus 'y', and the corresponding mechanoreceptor (middle) and cuneate (top) activity during the entire stimulation period. Given the one to one connectivity between mechanoreceptors and sensors (see section 6.3.1), neuron indexes shown in the central plot correspond to sensor indexes in the bottom plot. Differently, given many to many connectivity of the cuneate nucleus, the indexing of cuneate neurons was omitted for the sake of clarity. (adapted from Bologna et al., 2011)

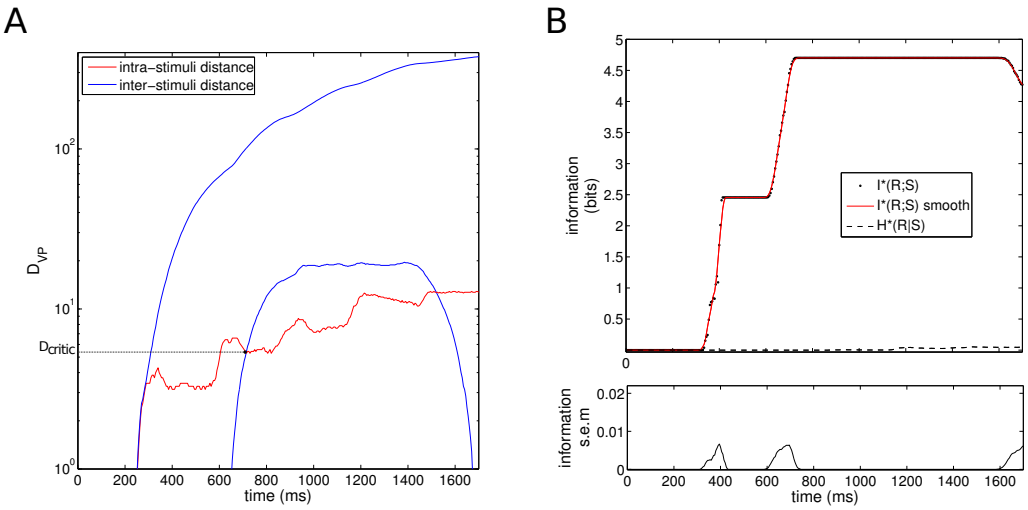

Figure 7.6: Metrical information analysis of primary afferent responses to dynamic Braille stimuli. *A.* Evolution of maximal and minimal interstimulus and maximal intrastimulus distances over time (blue and red curves respectively) on a semilogarithmic scale. The minimal intrastimulus distance is approximately zero during the entire stimulus duration and has not been reported. The critical distance used for computing the metrical information and entropy is indicated by D_{critic}. Sixty repetitions per stimulus are used. Perfect discrimination occurs 700 ms after the stimulus onset. Note that at the end of the stimulus application the minimum interstimulus distance becomes smaller than the maximum intrastimulus distance, indicating that interferences between similar stimuli impair the discrimination process. *B. Top:* The time course of information (grey circles: data; continuous red line: sliding window smoothing) and of conditional entropy (dashed black line) confirms that perfect discrimination of all 26 Braille characters is achieved at time t $\approx$ 700 ms. *Bottom:* information variability, measured as mean standard error (s.e.m.), over time. (adapted from Bologna et al., 2011)

corresponds to maximum information and zero conditional entropy (see fig. 7.6 B.). As could be expected, the metrical information curve (red line) exhibits a plateau starting at around 400 ms and lasting for about 120 ms. This corresponds to the stimulation phase during which the first column of Braille dots is already in contact with the fingertip while the second column does not yet stimulate any sensor. The information value at plateau is about half of the total amount of information transmitted, meaning that the first column of dots is enough to discriminate between $2^{2.6} = 6$ different groups of Braille characters. This study was carried out on the same sample size as for the analysis in static condition (see section 7.1.2). As observed for the static scenario, the error remained small (see fig. 7.6 B., bottom).

Figure 7.6 B. shows a drop in the amount of metrical information after 1500

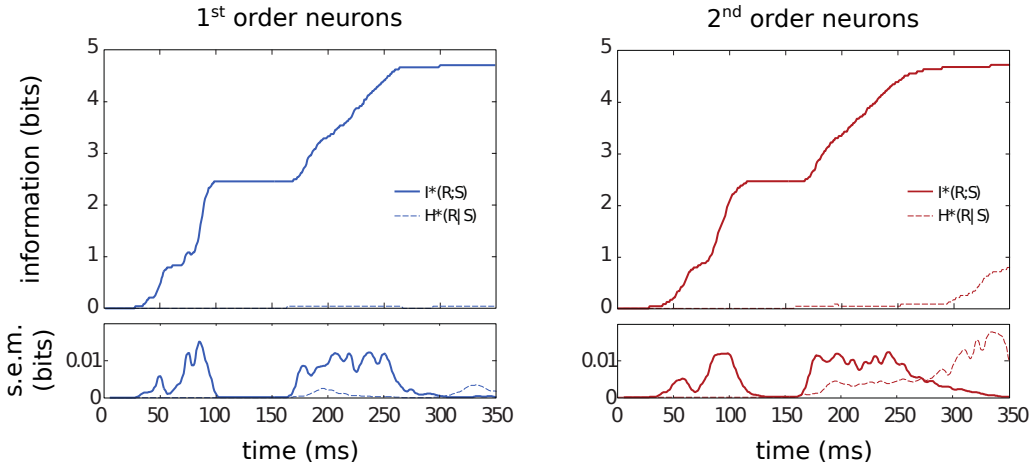

Figure 7.7: Time course of metrical mutual information (solid curve) and conditional entropy (dashed curve) at the output of first order neurons (left) and cuneate neurons (right), as the fingertip scans the entire Braille alphabet at 30 mm/s during 200 trials. The bottom diagrams display the time course of the s.e.m. for both metrical information and conditional entropy. (adapted from Bologna et al., 2013)

ms. This reflects an increasing interference between the spike count of different Braille characters, making it impossible to correctly discriminate them. This is linked to the dot pattern organization of certain symmetrical Braille characters which creates an ambiguity that cannot be resolved by the first order neurons (see section 6.2.1).

7.2 Second order neuron responses

7.2.1 Information content of neural responses

The theoretical information analysis carried out on first order neuron outputs (see sections 7.1.2 and 7.1.3) was also applied to the second order neuron responses with similar results. In both static and dynamic stimulation conditions, the information dynamics were identical to those observed in first order neurons. In the static indentation condition, perfect discrimination of all Braille stimuli occurred approximately within 100 ms of stimulus onset, just as for the primary afferent level (see section 7.1.2).

Figure 7.7 shows a comparison between the information evolution at the

primary afferent and cuneate neuron output level. The stimulation protocol consisted in scanning the entire 26 character Braille alphabet at a constant speed of 30 mm/s during 200 trials. As such, with the exception of the speed value –which rose from 15 mm/s to 30 mm/s– it was the same protocol as described in section 7.1.3. At the mechanoreceptor level (fig. 7.7, left), a complete discrimination of all Braille characters occurred within 350 ms of stimulus onset, at which point the optimality condition was verified (see section 4.1). As when tested at 15 mm/s, the information curve exhibited a plateau after about 100 ms and lasting approximately 75 ms. Simulated cuneate outputs displayed a similar information content profile (fig. 7.7, right), according to which a perfect discrimination of the inputs occurred as rapidly as at the first order neuron level. Yet, the redundancy of second order neuron responses was slightly larger, as is reflected by the non-zero conditional metrical entropy after 350 ms.

As observed in section 7.1.3 (see fig. 7.6 B.), also in the dynamic scenario, primary afferent processing led to a drop in the information as the dynamic stimulation progressed (though the information drop occurs beyond the plot's axisin fig. 7.7). This, however, was not the case for cuneate output signals. The processing by the cuneate network therefore allowed the information curve to be monotonic during the entire stimulation phase.

7.2.2 Information content as a function of velocity

The theoretical analysis of cuneate responses was extended to consider the effect of different scanning velocities on the systems performance. To do so, the information content of cuneate responses and the discrimination time –*ie.* time taken to converge to the maximal information, or the optimal discrimination point when possible– were computed as a function of 16 scanning velocities in the range [5 - 90] mm/s. For speed values between 5 - 50 mm/s, the time necessary to achieve maximum discrimination decreases exponentially (see fig. 7.8 A.). Within the same speed range, the information remained constant at its maximum value. For higher reading velocities, recognition time stabilized between 400 and 500 ms, but a significant reduction in information content occured, making a complete stimulus discrimination impossible. These results show the existence of a trade-off between scanning speed and discrimination capabilities, with an optimal velocity range for single Braille character recognition of 40 - 50 mm/s (see fig. 7.8 B.).

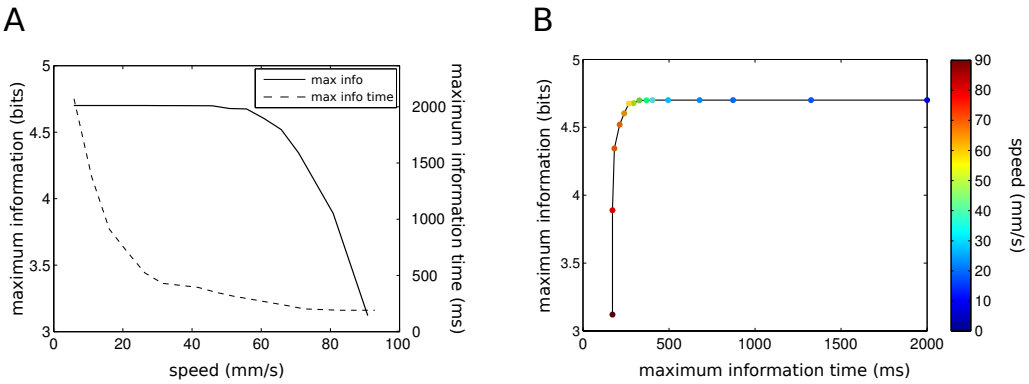

Figure 7.8: Cuneate responses information content as a function of velocity. *A*. Maximal metrical information (solid line) and time necessary to reach the information maximum (dashed line) plotted against the scanning velocity. *B*. Maximal information as a function of recognition time. Both diagrams show the optimal velocity range, in terms of scanning speed and discrimination accuracy, to be 40 - 50 mm/s. (adapted from Bologna et al., 2011)

7.2.3 Probabilistic classification of neural responses

Even if after 350 ms both mechanoreceptor and cuneate responses contained enough information to discriminate all Braille letters theoretically, this is no guaranty that the implemented probabilistic decoder could benefit from the processing carried out at the cuneate level to improve on the classification performance. The above stimulation protocol was extended by varying the fingertip speed within the range [10 - 80] mm/s (by steps of 10 mm/s). For each speed value, the fingertip scanned all 26 Braille characters for 100 trials. The performance of the Naïve Bayesian Classifier was comparable when decoding first and second order neuron responses at movement speeds lower than 30 mm/s (fig. 7.9, top). By contrast, processing at the cuneate level led to a statistically significant increase of 12% in the classification performance at 30 mm/s (Mann-Whitney U, $p < 0.01$), with respect to what was obtained at the mechanoreceptor level. Such an improvement in performance was even larger for higher scanning speeds, showing that cuneate processing enhanced the generalization and robustness of the classification process in the presence of speed modulations. Figure 7.9 (bottom) shows the non classification rate –*ie.* how often, on average, the system was unable to classify a Braille letter during scanning. This measure is related to the mean number of reversal movements during the Braille reading, which consisted in backtracking the fingertip to

rescan a letter that had not been recognized. In accordance with the above results, for scanning speeds higher than 30 mm/s, the non classification rate was significantly larger when decoding first order neuron responses than cuneate activity.

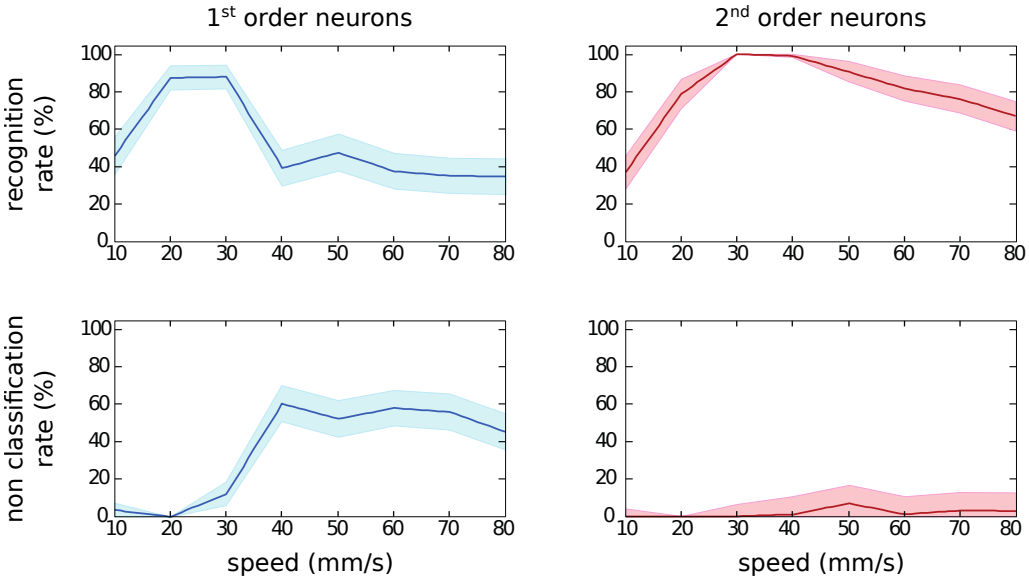

Figure 7.9: Mean recognition rate (top) and non-classification rate (bottom) when using the Naïve Bayesian Classifier to decode first-order activity (left column) and cuneate responses (right column) at different Braille scanning speeds. (adapted from Bologna et al., 2013)

7.2.4 Mediation of Braille character interference

To explain this performance difference, the influence of Braille dot arrangement on possible recognition rate was studied. Some Braille dot arrangements are likely to evoke similar mechanoreceptor responses due to the homogeneous structure of the artificial touch sensor. For instance, symmetrical letters (*eg.* 'e' & 'i', 'd' & 'f', 'h' & 'j' and 'r' & 'w') would activate the same subset of sensors, increasing the probability of cross-character interference during scanning. This was illustrated by performing a principal component analysis (PCA) of both first order and cuneate responses obtained at a scanning speed of 30 mm/s (see fig. 7.10). It can be observed that while the separation between the clusters of responses to letters 'e' and 'i' at the first order level decreased over time, it remained fairly constant for the cuneate responses. The reduced interference between symmetrical letters

at the second order level partially explains the corresponding better classification performance at higher speeds (fig. 7.9). In the context of the full Braille alphabet, an early discrimination was prevented by interference from letters with identical first dot columns (*eg.* 'a', 'c' & 'd' for letter 'e'). In the case of first order neuron responses, subsequent interference by symmetrical characters left only a small time window available for the classification to occur. This was reflected by the notable drop in the information available at the output of first order neurons towards the end of the scanning phase (see section 7.1.3 and fig. 7.6). For high scanning speeds, this window shortened and the classification performance decreased consequently. By contrast, cuneate processing avoided this effect and maintained a higher performance at increased speeds.

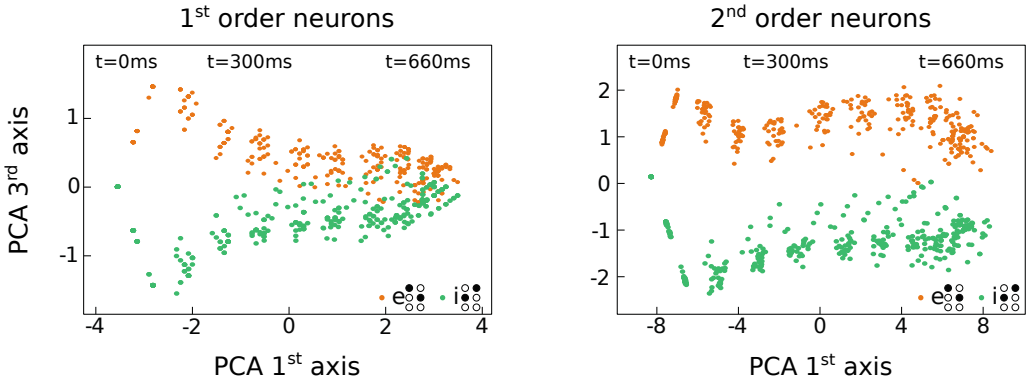

Figure 7.10: Principal component analysis on mechanoreceptor (left) and cuneate (right) responses to Braille character 'e' and 'i'. In both cases, the response clusters are projected onto the first and third principal component plane (the second component did not contain any information for distinguishing the two responses). (adapted from Bologna et al., 2013)

7.2.5 Cuneate network processing

The processing operated by the cuneate network was therefore essential for preventing interference between dot patterns in the spike count coding scheme. For all cuneate neurons, an individual input spike was enough to generate an outgoing action potential. This is coherent with observations of high synaptic efficacy at the cuneate level (Hsiao and Yau, 2008). However, neurons often have a non-linear dynamic and it was observed that the one-to-one ratio in input-output spikes was not preserved when considering entire spike patterns.

Typically, input firing rates higher than 40 Hz, led to an outgoing activity that was significantly lower than the ingoing one (see fig. 7.11, blue curve). This was due to the adaptation mechanism implemented in the neuronal model used (see section 6.3.2).

One of the consequences of this property of the model was that while maintaining a high synaptic efficacy, the cuneate network could also act as a coincidence detector. Indeed, the co-activation of two first order neurons connecting to the same cuneate neuron led to a noticeably different activity pattern –and ultimately to a different spike count– than two successive activation of one of these same first order neurons. For example, the dot pattern of the Braille character 'c' is composed of two neighboring dots (see section 6.2.1), which successively activates two adjacent mechanoreceptors as the character is scanned by the fingertip at 30 mm/s for 100 repetitions. The cuneate neurons that were co-activated fired 16.3 $\pm$ 1.9 (mean $\pm$ std) whereas neurons that were successively activated had a total of 20.9 $\pm$ 1.2 (mean $\pm$ std) outgoing spikes (Mann-Whitney U, $p < 10^{-3}$). Had the neurons acted as linear integrator of spikes, the difference would not have been significant and the spike count could not have carried information about co-activations.

A more thorough analysis was carried out by recording the output spike count to different input firing rates. Spike trains lasted for 5 seconds and were generated randomly, following a Poisson process at different constant firing frequencies. The analysis was performed with 50 repetitions per input frequency (which varied from 10 to 150 Hz by step of 10 Hz). When a cuneate neuron was connected to more than one mechanoreceptor, inputs were delivered to either one, two or three of its synapses. In that case, correlated spike trains, built by adding random jitters to a Poisson spike train, were also delivered to each input synapses. The jitters were taken from a Gaussian distribution with a 3 ms standard deviation in order to reflect the jitter values found in the model mechanoreceptors (see fig. 7.3). Values of standard deviation of up to 10 ms were also tested and yielded similar results.

The outgoing activity firing rate is plotted in figure 7.11. As mentioned previously, output spike counts did not vary linearly with the frequency of the input. Furthermore, cuneate neurons connected to multiple mechanoreceptors (red and green curves in fig. 7.11) responded differently when only one, two or three of these mechanoreceptors fired simultaneously. This could be expected given that, for a given input frequency, using two input channels would result in

actually doubling the input spike count. For uncorrelated input spike trains, output activities were indeed indistinguishable between a single input at a given frequency and two inputs at half of that frequency (fig. 7.11 A). However, this was not true for correlated inputs, in which case the two different input scenarios could be recognized through the outgoing spike count (fig. 7.11 B). In effect the cuneate network acted as a coincidence detector. This allowed cuneate neurons to account for co-activations and encode the information in the spike counts, thereby resolving the performance issues arising from the interference between characters (see section 7.2.4).

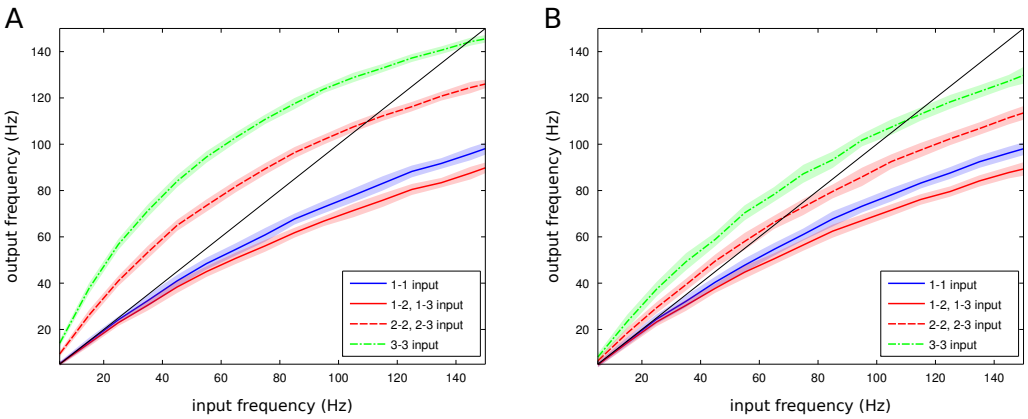

Figure 7.11: Input-output frequency transfer function of the cuneate network. Spike trains, lasting for 5 seconds, were generated randomly, following a Poisson process at different constant firing frequencies. Different curves display different stimulation scenarios –for individual neurons– represented, in the legends, by a two digit code: "$n_{in} - n_{co}$", n_{in} being the number of active input synapses and n_{co} the number of mechanoreceptor-to-cuneate connections the neuron has (*ie.* the total number of input synapses). Cases "1-3" and "2-3" overlap perfectly with cases "1-2" and "2-2" respectively, and are not represented on the plot. *A.* Inputs were uncorrelated Poisson spike trains. The different input scenarios were indistinguishable by the system as output spike counts were identical for an input at frequency f and two inputs at a frequency $f/2$. *B.* Correlated inputs were generated by adding a 3 ms jitter to the same Poisson spike train. All scenarios are here distinguishable from a spike count perspective. In effect, the cuneate network acted as a coincidence detector.

7.3 Online classification of Braille characters

Using the simulation environment, the complete closed loop system was tested in an online classification task of Braille stimuli. This involved a probabilistic classification process decoding the tactile signals processed by the first and second

order neural networks, as well as a high and a low level controller modulating the scanning velocity and thereby closing the active sensing loop.

7.3.1 Classification performance

The performance of the entire closed loop system –including high- and low-level movement control– was tested in a Braille reading task. The artificial fingertip scanned multiple Braille lines containing 8 letters each, for a total of 200 trials (*ie.* repetitions) per letter. During the scanning, the feed-forward networks of first and second order neurons provided the probabilistic classifier (*ie.* Naïve Bayesian Classifier) with continuously evolving spiking responses. Using the cumulative spike count of these responses, the classifier estimated online the posterior probability distribution. In the ideal case, this distribution converges towards a narrow single peaked shape, thereby allowing the classification of the Braille character to be achieved.

Figure 7.12 A. shows the time course of two examples of posterior probability distributions corresponding to the scanning of the letter 'r' (top) and 'e' (bottom). In the first example, early cuneate activity did not allow the probabilistic classifier to distinguish between 'r' and other Braille characters with a similar dot arrangement (*ie.* 'l', 'p', 'q', 'v'). Nevertheless, as the fingertip progressed over the character, the probability distribution started to peak, indicating a decrease of uncertainty, until a correct classification became possible.

As shown by the confusion matrix in figure 7.12 B. and by the distribution in figure 7.12 C., the overall online classification performance was characterized by a recognition rate of 95 $\pm$ 1.5 % (mean $\pm$ s.e.m.), a non classification rate (*ie.* reversal movement rate) of 1 $\pm$ 0.4 %, and a false positive rate of 4 $\pm$ 1.3%.

7.3.2 Speed modulation

The speed modulation which determined the active sensing policy was a function of the evolution of the posterior probability distribution through time (see section 6.4.1). Figure 7.13 A. displays the time course of the posterior probability distribution (top) and of the corresponding finger acceleration profile (bottom) while scanning a line with three letters ('d', 'y', and 'n'). Over the

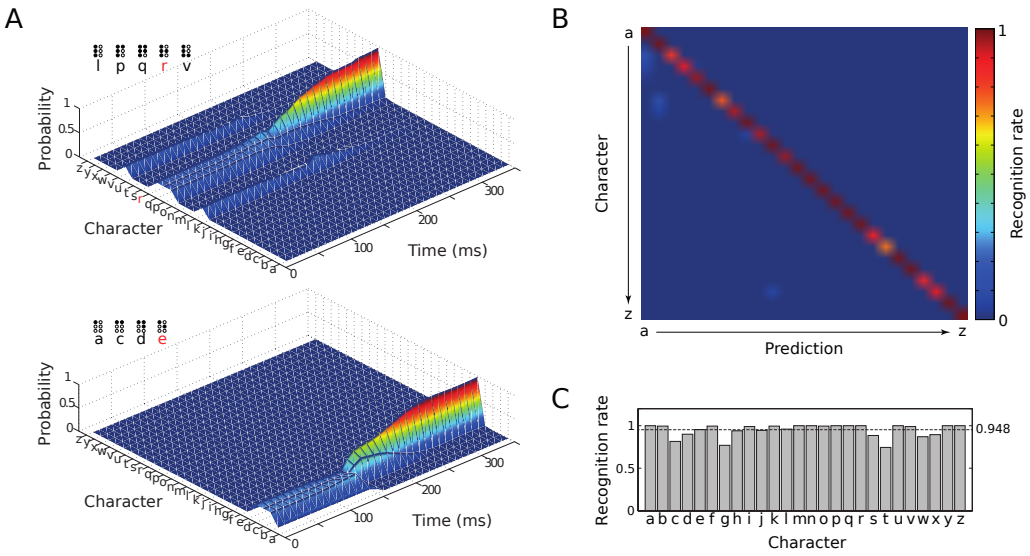

Figure 7.12: *A.* Time course of the posterior probability distribution estimated by the Naïve Bayesian Classifier when scanning the Braille letter 'r' (top) and 'e' (bottom). *B.* Confusion matrix showing the recognition rate and cross-letter interference during online probabilistic classification of Braille characters. The protocol involved 200 scanning trials for each of the 26 letters. *C.* Mean recognition rate distribution across the Braille alphabet. (adapted from Bologna et al., 2013)

entire Braille reading task, the mean number of finger accelerations (both positive and negative) per letter was equal to 11.8, which is of the same order of magnitude as that observed in human Braille reading experiments (Hughes, 2011; Hughes et al., 2011). Importantly, the movement policy (and consequently the number of accelerations) varied significantly depending on the letter being scanned (see fig. 7.13 B., top; Kruskal-Wallis ANOVA, $p < 0.01$). In addition, a significant correlation between the distribution of Braille character complexity (see section 6.5.2) and the distribution of the number of accelerations per letter was found (fig. 7.13 B., bottom; Spearman's $\rho = 0.66$, $p < 10^{-3}$).

7.3.3 Robustness to position errors

During Braille reading, the low-level cerebellar controller adjusted the trajectory of the fingertip online. The training of the cerebellar network was carried out over 10 sessions. Each session consisted of 10 trials during which the fingertip (*ie.* the end-point of the 2 degree of freedom arm carrying the artificial touch sensor, see section 6.4.3) had to scan a Braille line containing 8 evenly spaced characters, at a constant command speed of 30 mm/s. After training, the

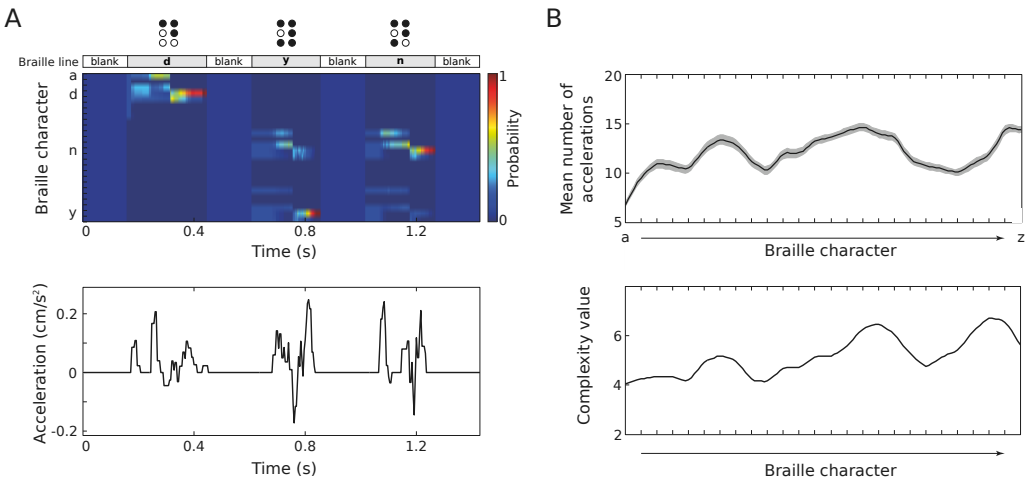

Figure 7.13: *A. Top:* example of evolution of the posterior probability distribution estimated by the Naïve Bayesian Classifier as the fingertip was scanning a Braille line with three letters. *Bottom:* corresponding online fingertip acceleration profile. *B. Top:* mean number of accelerations (both positive and negative) per letter, averaged over 200 repetitions (solid line: mean; gray area: s.e.m.). Accelerations smaller than 0.1 mm/s^2 were filtered out for this analysis. *Bottom:* complexity value of the different Braille characters. (adapted from Bologna et al., 2013)

output of the cerebellar network provided a good estimator of the noisy arm dynamics Passot et al. (2013). This allowed motor commands to be tuned online and the movement accuracy to be improved accordingly. The mean position error, computed as the discrepancy between desired and actual fingertip trajectory, decreased significantly through cerebellar training, from 0.81 ± 0.04 mm (mean ± s.e.m.) to 0.54 ± 0.04 mm (Mann-Whitney U, $p < 0.01$).

Figure 7.14 A. shows a sample of fingertip trajectory (top), the corresponding PSTH (center) of the cerebellar output (*ie.* the activity of simulated neurons in the deep cerebellar nuclei, DCN), and two examples of DCN spikegrams. Figure 7.14 B. shows a fingertip trajectory, averaged over 10 trials, with and without cerebellar-dependent adaptation (blue and red curve, respectively). The cerebellar online adjustment proved effective at reducing fingertip oscillation amplitudes.

To study the influence of position inaccuracies on the classification performance, a line of Braille characters was swiped over the immobile fingertip at 30 mm/s. After 80 repetitions of each letter, the Braille line was shifted along the distal-to-proximal axis by 0.5 mm, and the process repeated. This shift corresponded to a fingertip position change along the Y axis in the active sensing scenario. Note that in this protocol, the positions of the Braille lines and

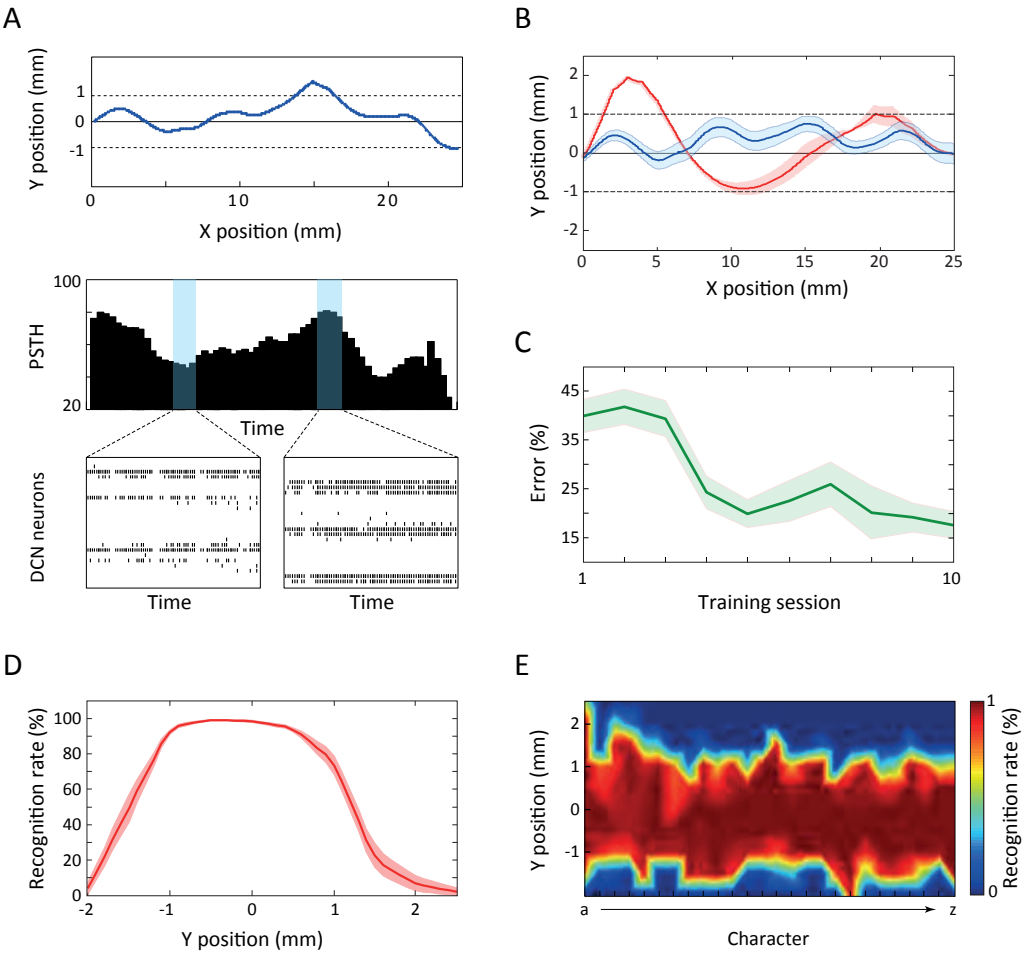

Figure 7.14: *A.* Example of fingertip trajectory (top), corresponding PSTH (center) of the cerebellar output (*ie.* activity of simulated deep cerebellar nucleus –DCN– units), and raster plots of DCN spike trains at two different moments of the trajectory (bottom). *B.* Fingertip trajectory samples before and after training of the cerebellar low-level controller (red and blue curve, respectively). Solid lines indicate mean trajectories averaged over 10 trials, whereas shaded areas delimit the corresponding s.e.m. values. *C.* Mean percentage of points of a trajectory exceeding the ±1 mm boundary as a function of cerebellar training sessions. *D.* mean recognition rate, averaged over all Braille characters and 80 repetitions per character, as a function of the Y position of the finger (the shaded area represents the s.e.m.). *E.* distribution of recognition rates across all Braille letters for different Y positions. (taken from Bologna et al., 2013)

of the fingertip were tightly controlled and no trajectory errors could occur. Consequently, this protocol allowed to quantify the system's classification performance as a function of the position along the Y axis (see fig. 7.14 D.). The mean classification performance remained high within the ±1 mm range, but decreased sharply beyond these boundaries. The best recognition rate of

99% occurred at Y positions of 0 and -0.5 mm (Mann-Whitney U, $p > 0.4$). A more in depth look at the system's performance depending on the Braille letter (fig. 7.14 E.) revealed that the recognition rate of individual letters tended to follow an all-or-none pattern, with few intermediate values.

Taking into account this observation, the percentage of times the fingertip trajectory exceeded a ±1 mm bounded region was recorded (dashed lines in fig. 7.14 B.). The resulting error, averaged over 10 trials, decreased significantly through cerebellar training (see fig. 7.14 C.; Mann-Whitney U, $p < 10^{-3}$). About 82% of the positions belonging to a finger trajectory fell, on average, within the ±1 mm boundary by the end of training.

7.4 Preliminary robotic implementation

The system performance was tested in a preliminary experiment in which a robotic hand-arm platform equipped with the artificial fingertip had to solve a Braille reading task (see section 6.4.3). In this implementation, speed modulation signals from the the high-level controller were ignored, and the low-level algorithmic controller of the robotic system was used to replace the cerebellar model. The scanning speed of the fingertip was maintained broadly constant at 30 mm/s, though corrective signals were occasionally sent to account for trajectory errors.

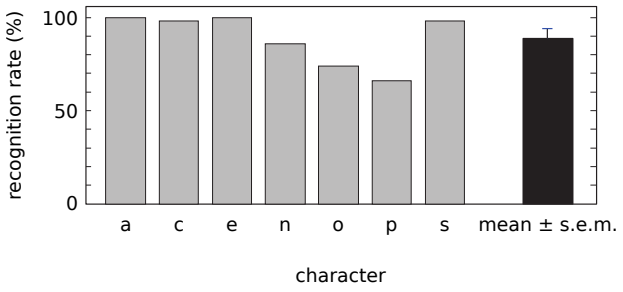

Figure 7.15: Mean recognition rate distribution across a subset of Braille letters, and mean ± s.e.m. values. (adapted from Bologna et al., 2013)

The system implementation was tested on a subset of representative Braille characters (*ie.* 'a', 'c', 'e', 'n', 'o', 'p', 's'), for which 150 trials were recorded per character. As in the simulated version, the first and second order neural networks mediated feed-forward processing of tactile signals prior to their use for

probabilistic classification. The Naïve Bayesian Classifier was trained through the same offline procedure used for the simulated data. Among the 150 trials, 100 were randomly selected for training and 50 kept as a testing database. The mean classification rate, averaged over the 7 characters, was $89 \pm 5.3\%$ (mean $\pm$ s.e.m.; fig. 7.15), with a false positive rate of $11 \pm 5.3\%$.

Part IV

Conclusions

Chapter 8

Conclusions

The work carried out in the context of this thesis led to the development of a closed-loop neural architecture for fine tactile sensing. A computational model of mechanoreceptive afferents and of the cuneate network was established on the basis of the neural coding principles observed at these stages of the somatosensory system. The output signals of these models were analyzed using theoretical tools in order to assess the quality of the encoding. Second order output signals were also fed to a probabilistic classifier tasked with decoding the tactile information. A closed loop system was built by associating the mechanoreceptor model with an artificial fingertip, whose position was modulated according to the classification results. In addition, a neuro-mimetic model of the cerebellum was used for the low-level control of the fingertip position. This architecture was tested using a real robotic implementation for which the capacitive sensors were fixed to a robotic hand-arm system to act as the artificial skin of the fingertip.

The current chapter first provides a summary of the main results and contributions of this study. The second section is centered around a discussion on the achievement of the main objective and the future directions of this research.

8.1 Main results and contributions

8.1.1 Mechanoreceptor model

Tactile processing at the early stages of the somatosensory pathway was emulated by converting the analog readouts into mechanoreceptor-like responses. The analog inputs were informative of the skin deformation induced by the texture being read. These inputs were built using an artificial touch sensor also used during the robotic implementation of the architecture. A

preliminary characterization of these sensors was carried out, and a computational model was derived to simulate their response to different stimuli. Thanks to the sensor model, analog inputs could be simulated offline, under various conditions, in order to test the mechanoreceptor model.

A leaky integrate-and-fire model was used as basis for generating mechanoreceptive output signals. This type of model had already been successfully used to model the activity of FAI and SAI mechanoreceptive afferents (Lesniak and Gerling, 2009; Kim et al., 2010; Gerling et al., 2013). Leaky integrate-and-fire neurons allowed to accurately reproduce mechanoreceptor properties while meeting the computational requirements for performing the task online. Each model first-order neuron was connected to a single capacitive sensor (either physical or simulated) to receive skin deformation information.

The developed model managed to capture some of the known properties of SAI mechanoreceptors. Though both SAI and FAI primary afferents are involved in fine touch discrimination, SAI have been shown to better capture the spatial discontinuities for textures of Braille-like size and likely transmit most of the information relevant in this case (Phillips et al., 1992; Johnson, 2001; Hsiao and Yau, 2008). Model neurons were tuned to have similar spatial modulation properties as their biological counterparts, notably thanks to comparable receptive field sizes. Firing rates where broadly the same, although a little more contained in the case of the model SAIs, and the temporal precision of spikes was lower by 2 ms in the case of the model. As the leaky integrate-and-fire model used did not contain a noisy component, the poorer temporal precision was the consequence of the variability of the analog signal from the sensors.

An analysis of the model's output spike trains using information theory tools –adapted to the study of spike train-like signals and previously used on human microneurography recordings of peripheral afferents (Brasselet et al., 2011b)– showed that a sufficient amount of information was conveyed in these signals for a full discrimination of all 26 Braille-like stimuli. The time of optimal discrimination –defined as the time of maximal metrical information and of minimal conditional entropy– was reached around 300 ms after the stimulus. However, this discrimination time was constrained by the fact that both columns of dots in the Braille character had to be read before the maximal information could be reached. In comparison, when the focus was placed on the first column of Braille dots only, optimal discrimination occurred some 100 ms

after the stimulus onset. This was consistent with the finding that the spatiotemporal structure of mechanoreceptor responses provides highly relevant information about the stimulus (Brasselet et al., 2011b).

8.1.2 Cuneate nucleus model

Primary afferent signals were processed by a network of second order neurons embodying the biological cuneate nucleus. The neural architecture of this network was founded on a previous modeling work in which the spike-response model was used to capture the properties of cuneate neurons. The EDLUT simulation environment (Ros et al., 2006) underlying the implementation of the model allowed for a quick computation of the neural dynamics.

Following the literature on the subject, the network was composed of a single layer of neurons (see section 2). The connectivity between first and second order neurons was fixed at a low rate, as has been observed in the functional synapses of the biological system (Bengtsson et al., 2013). This limited number of functional connections was complemented by high synaptic weights allowing a cuneate spike to be generated for every input spike. The model did not include lateral inhibitory neurons, nor the resulting center-surround receptive fields which have been documented in the literature (Canedo and Aguilar, 2000). However, this shortcoming most likely had little consequence on the output of the cuneate neurons given the chosen set of stimuli and the sensor layout. Indeed, this complex receptive field structure has been shown to enhance perceptual contrast and allow the most active output neurons to limit the activity of less active neighbors (Kandel et al., 2000); yet, given the lack of consequential overlap between the sensors receptive' fields, individual Braille dots rarely activated more than one sensor at a time. Consequently, in the case of the dot arrangements used as stimuli, and given the characteristics of the sensors, contrast levels were already very high.

No information loss was observed at the output of the model cuneate, and all stimuli remained theoretically discriminable. A small delay in the information transfer –relative to first order neuron signals– was observed when considering the precise spatiotemporal structure of the output signals. This is likely the consequence of the slightly noisy dynamics of cuneate neurons. The sparse connectivity between first and second order neurons allowed the cuneate network to act as a coincidence detector, as has been discussed by Johansson

and Birznieks (2004) and Johansson and Flanagan (2009). The result was a remapping of the information contained in the spatiotemporal structure of primary afferent spike trains into the rate coding scheme. This allowed to increase the maximal separability and resolve ambiguities that might arise downstream, where the probabilistic classification occurred.

8.1.3 Discrimination process

Downstream of the simulated cuneate layer, a Naïve Bayesian classifier performed stimulus pattern recognition. The Naïve Bayesian is a relatively simple classification process which can outperform more sophisticated algorithms in some categorization tasks. Its simplicity stems from the underlying hypothesis that the system variables are independent. This assumption is seldom verified in real world applications, however this does not seem to significantly deteriorate the classification performance. This is likely due to the fact that the statistical dependencies between the attributes often either cancel themselves out or are evenly distributed among classes (Zhang, 2004). Furthermore, even though the values of the posterior probabilities computed by the Naïve Bayesian classifier may be inaccurate, significant differences are likely to remain true. In the case of categorization tasks, the class with a significantly higher posterior probability is often the correct class for the data sample considered, regardless of the precise value of its probability (Domingos and Pazzani, 1996, 1997).

The probabilistic approach used for performing the classification allowed for an efficient discrimination of 95 $\pm$ 1.5 % (mean $\pm$ s.e.m.) of all Braille stimuli online in simulation, and of 89 $\pm$ 5.3% (mean $\pm$ s.e.m.) in the case of the real robotic implementation. It also provided the tools necessary for estimating online how close the systems was to being able to perform the discrimination. This was later used to devise a movement policy for guiding the fingertip movements.

8.1.4 Finger kinematics

The action perception loop was closed by a high- and a low-level controller. The high-level controller relied on the posterior probability distribution computed by the Naïve Bayesian classifier to modulate the movement velocity. When the system detected that the discrimination point was drawing nearer –*ie.* that the amount of information was increasing rapidly– the scanning speed of the finger

was augmented. Reciprocally, if the level of doubt increased, the movement speed was decreased.

The low-level controller used for fine tuning the movement was implemented through a spiking neural network model of the cerebellum. This model was derived from a previous work by Passot et al. (2013) using the same micro-complex structure. The cerebellar networks were formed through a semi-supervised learning protocol to act as forward predictors. In effect, this allowed trajectory errors to be anticipated and corrected preemptively. After learning, the cerebellar model was capable of maintaining the fingertip within less than 1 mm from the desired position during 85% of the character scanning time. This ±1 mm boundary was found to be the spatial resolution allowing the system to perform optimally. The fine tuning operated by the cerebellum also gave rise to an increased number of accelerations and decelerations in the fingertip movement.

While performing a Braille reading or scanning task, the human finger undergoes an important number of speed modulations, the origins of which are not well understood. Several mechanisms (*eg.* sensorimotor, semantic, linguistic) undoubtedly play an important role in building the final trajectory, but the extent of their contributions is still unclear (Hughes, 2011; Hughes et al., 2011). For example, sublexical mechanisms were shown to influence the number of accelerations only in specific reading conditions (Hughes, 2011). Without seeking a comprehensive explanation for the origin of finger accelerations, this platform was used to investigate if a simple probabilistic approach could account for the influence of texture complexity and local ambiguities on finger kinematics. Results showed a number of accelerations that were coherent with experimental observations (Hughes, 2011) as well as significantly correlated with the complexity of Braille dot patterns.

8.2 Limitations and perspectives

The closed loop system presented in this manuscript was developed following a neuro-engineering approach and can be extended to further investigate *(i)* the neural bases of fine touch processing and active sensing, *(ii)* neuromorphic-like solutions for humanoid robotics built on the efficiency principles behind tactile coding, and ultimately *(iii)* biologically plausible sensory feedbacks for haptic

neuro-prosthetic applications. In the following sections, limitations of the current system to its application in real world environments will be discussed. Its performance will be compared to that of other fine touch discrimination robotic devices and possible improvements will be considered. Along the same line, the neural architecture and its individual components will be questioned, and possible future developments discussed.

8.2.1 System performance

The chosen probabilistic classifier allowed to efficiently discriminate 95 ± 1.5% (mean ± s.e.m.) of all Braille stimuli online in simulation, and 89 ± 5.3% (mean ± s.e.m.) in the case of the real robotic implementation. While this is not an unsatisfactory performance, it was obtained while testing the system in a restrained environment. Indeed, only 26 spatial patterns (of identical intensity) were used as stimuli and the surface scanning was carried out only along one dimension (*ie.* following the Braille line). By comparison, Fishel and Loeb (2012) managed to obtain a 95.4% recognition rate when choosing from a database of 117 different textures. Other modern texture discrimination devices demonstrated similar (*ie.* close to 95% or higher) performances (Giguere and Dudek, 2011; Oddo et al., 2011; Jamali and Sammut, 2011; Sinapov et al., 2011b). The two tasks are not quite comparable as the fine touch sensing carried out by the closed loop system consists in spatial pattern recognition instead of texture recognition –although both systems could probably be used for the discrimination of gross texture. Nonetheless, it suggests that the performance should be tested on a larger database than that used here. Given the observed properties of the system (notably the precise somatotopic encoding of stimuli patterns), it is likely that the current system's performance would be maintained for a greater number of patterns; the only constraint being that the finger and neural networks be scaled up with the size of the patterns being scanned.

The system did account for a limited amount of noise in its trajectory. This position error exponentially affected the performance of the system, which fell from 99% to 95% (recognition rate) when passing from a perfect trajectory to the noisy arm simulation, and then to 89% during the implementation on an actual robotic arm. The near perfect performance of the system in an ideal situation (*ie.* perfect trajectory) leads to believe that neither the neuro-inspired processing nor the simple classifier are responsible for the system's fall in performance.

Limiting the position error is therefore essential for maintaining the overall performance of the system. However, this objective is unlikely to be reached realistically, and, in real world applications, increasing the robustness of the classification to position errors is a more efficient solution. To do so, either a more extensive database must be created, or some feature extraction mechanism must be considered.

Using a probabilistic classifier also provided the tools necessary for estimating online how close the system was to being able to perform the discrimination. This was later used to devise a movement policy for guiding the fingertip movements. The movement policy did not increase the classification rate but allowed an increase in the recognition speed. Other systems have relied on policies which actively select movements to better discriminate between different possibilities and facilitate the classification (Xu et al., 2013; Fishel and Loeb, 2012; Saal et al., 2010) similarly to what is observed in human behavior (Loeb et al., 2011b). Learning mechanisms, which gradually increase the performance of the robotic systems, have also been tested (Xu et al., 2013) and could help optimize discrimination behaviors in evolving environments.

8.2.2 Neuromorphic processing of fine touch information

The current system was designed to reproduce the neural bases of fine touch processing, and transfer the efficiency and performance principles of the biological system onto a neuro-robotic platform. To this effect, the first two stages of processing were modeled after the peripheral ascending somatosensory system. However, both these networks relied either directly or indirectly on signals originating from the artificial touch sensor.

Concerning the overall system's performance, the artificial touch sensor's properties proved to be a limiting element. Although providing signals with very little noise (see section 6.2.2), its spatial and temporal resolution were low with respectively 5.8 sensor/cm^2 (when no rescaling is taken into account) and an acquisition frequency of 20 Hz. The size of the sensors by themselves was suitable (after rescaling the Braille characters), but the lack of overlap between sensitive areas of the capacitive pads was responsible for the lower spatial resolution. The neoprene layer spread over the sensors did dampen the shape of receptive fields, and led to a noticeable but still small overlap. Arguably, a higher overlap could also allow for more redundancy in the information encoded

(multiple sensors recording the same indentation point on the skin), thereby providing a means for averaging out part of the temporal imprecision in the signals.

The system's primary afferent model was based on leaky integrate-and-fire neurons, which have proven to be a suitable model for reproducing the deterministic nature of mechanoreceptor responses (Lesniak and Gerling, 2009; Kim et al., 2010; Gerling et al., 2013). Most of these models use filtering techniques or mechanical simulations to create the skin deformation signals fed into the leaky integrate-and-fire neuron. Here, this role was played by the artificial fingertip and its particular dynamics. Consequently, the temporal imprecision of the touch sensor's signals was inherited by the mechanoreceptor model. Outgoing spike trains were shown to be less precise by a few milliseconds than that of their biological counterparts.

The system's modular architecture makes it possible to easily modify individual components. Given the current system's limitations, one such modification should consist in introducing a more efficient transduction technology (Maheshwari and Saraf, 2008) to replace the current sensors. Notably, a higher acquisition frequency is required to increase the temporal precision of spiking signals (Johansson and Flanagan, 2009). Besides increasing the system's theoretical performance (Brasselet et al., 2011b), more biologically accurate dynamics could allow to reproduce and study different coding strategies. It has notably been suggested that primary afferents might encode stimulus features to create an isomorphic representation of the stimulus space (Brasselet et al., 2011a). Such a coding scheme would constitute an important improvement for characterizing and possibly recognizing unknown stimuli.

Introducing new transduction technologies could also help increase the spatial resolution and sensor density of the fingertip. In particular, linking multiple, very small, sensors to single mechanoreceptors should permit to imitate the irregular and inhomogeneous receptive fields observed in the glabrous skin (Johansson, 1978; Vallbo and Johansson, 1984; Phillips et al., 1992). Recent experimental evidence suggests that the pattern of hotspots on the receptive field might help extract stimulus shape features as early as the primary afferent level (Pruszynski et al., 2011). A temporal coding scheme would allow such feature extraction to remain compatible with the topological (or isomorphic) representation of stimulus shapes observed up till cortical areas (Phillips et al., 1988a). This may increase the encoding capabilities of single mechanoreceptive afferents and perhaps serve

as a basis for the known stimulus orientation selectivity of somatosensory cortical responses (Hsiao et al., 2002). The mechanoreceptor model would benefit from the implementation of this feature, if only to generate more bio-mimetic signals. However, it should also prove useful in helping to better understand how and with what advantages both encoding schemes can be combined; or conversely, how this early processing might be disadvantageous for distinguishing certain stimuli.

The choice was made to model SAI primary afferents as those are most likely to be involved in the transduction of detailed spatial features (Phillips et al., 1990; Srinivasan and LaMotte, 1987; LaMotte and Srinivasan, 1987; Hsiao and Yau, 2008). This was helped by the properties of the touch sensors with their sharp, well-defined receptive fields and their ongoing "tonic" response (see section 2.2.2 for a comparison with primary afferent functional properties). However, concentrating on only one mechanoreceptor type both ignores the contribution from the other types in extracting specific features of the stimulus and simplifies the processing of informative signals in the higher areas of the nervous system. This limitation has been noticed in the field of robotics and some sensors now integrate components for recording different sub-modalities (Castelli, 2002; Dahiya et al., 2010; Loeb et al., 2011b). This is not an issue in the current context as SAI neurons are best suited to extract the only relevant information –the location of the Braille dots– but it does limit the possible application of the architecture to other contexts without prior modification.

In this study, the cuneate nucleus network was fixed following a sparse connectivity paradigm (see section 6.3.2). While this proved essential to resolve signal ambiguities (see section 7.2.4), the connectivity layout was ultimately arbitrary and resulted in cutaneous receptive fields unlikely to closely resemble experimental observations, although basic properties were maintained. This is notably reflected by the absence of center-surround receptive fields, although there is little chance that their absence played a significant role in the system's performance (see section 8.1.2). Complementing the current excitatory dynamics with lateral inhibitory connections (Sánchez, Barro, Marino and Canedo, 2001; Sánchez et al., 2003) and a sensor with a higher spatial resolution would allow to generate more complex receptive fields. Furthermore, the addition of plasticity mechanisms capable of shaping the connectivity layout (and indirectly the receptive fields) could lead to both a more robust robotic system (adaptable to the stimulus base considered) and would allow to test hypotheses as to how and why cuneate receptive fields are defined. Indeed,

though the underlying mechanisms are still poorly understood, an increasing amount of experimental evidence suggests that a cuneate network reshaping occurs following afferent injury (Millar et al., 1976; Pettit and Schwark, 1993; Darian-Smith and Ciferri, 2006).

Similarly, the cuneate activity patterns were simplified in the model (Pubols et al., 1989; Canedo et al., 1998) and the spontaneous activity displayed by some cuneate neurons (Sanchez et al., 2006; Canedo et al., 1998; Pubols et al., 1989) was not implemented. A probabilistic discrimination based on spike counts would still have been possible had this been modeled, but its performance would have decreased with the added noise on the signal. A new classifier, relying on the more precise spatio-temporal structure of the cuneate spike trains, could be implemented perhaps using mechanisms relying on precise spike times such as spike timing dependent plasticity (STDP, Bi and Poo, 1998). STDP is a Hebbian learning mechanism (Hebb, 1949) induced by tight temporal correlations and has been extensively observed in many central brain regions (for a review see Sjöström et al., 2008). This learning rule has already been used in unsupervised spike pattern recognition tasks (Masquelier and Thorpe, 2007; Masquelier, Guyonneau and Thorpe, 2009), and has proven to be extremely robust to noise induced by spontaneous activity (Guyonneau et al., 2011; Masquelier et al., 2008). The STDP rule might also be capable of exploiting the sustained oscillatory 20 Hz component observed in cuneate activity (Marino et al., 999), if a phase coding mechanism is confirmed at this level (Masquelier, Hugues, Deco and Thorpe, 2009). Actual implementations of this rule in circuit systems using memristors as synapses has also been considered (Serrano-Gotarredona et al., 2013), suggesting that its addition to a neuro-robotic system could even take place at the hardware level.

8.3 Final considerations

This manuscript presents a neural architecture capable of fine touch discrimination. The processing of tactile information was based on neural coding properties of the peripheral somatosensory system. Networks of spiking neurons were used to replicate the processing operated on biological signals before discrimination. Beyond the possible application of this framework to investigating the neural bases of fine touch processing and providing

neuromorphic-like solutions for humanoid robotics, the principles upon which this system was designed will contribute to building biologically plausible sensory feedbacks for haptic neuroprosthetic applications.

Bibliography

Adrian, E. D. (1926a), "The impulses produced by sensory nerve-endings: Part 4. Impulses from pain receptors", J Physiol , Vol. 62, pp. 33–51.

Adrian, E. D. (1926b), "The impulses produced by sensory nerve endings: Part I", J Physiol , Vol. 61, pp. 49–72.

Adrian, E. D. and Zotterman, Y. (1926a), "The impulses produced by sensory nerve endings: Part 3. Impulses set up by touch and pressure", J Physiol , Vol. 61, pp. 465–483.

Adrian, E. D. and Zotterman, Y. (1926b), "The impulses produced by sensory nerve-endings: Part II. The response of a single end-organ", J Physiol , Vol. 61, pp. 151–171.

Aksentijevic, A. and Gibson, K. (2012), "Complexity equals change", Cogn Syst Res , Vol. 15, pp. 1–16.

Albu-Schäffer, A., Haddadin, S., Ott, C., Stemmer, A., Wimbock, T. and Hirzinger, G. (2007a), "The DLR lightweight robot: design and control concepts for robots in human environments", Industrial Robot: An International Journal , Vol. 34, pp. 376–385.

Albu-Schäffer, A., Ott, C. and Hirzinger, G. (2007b), "A unified passivity-based control framework for position, torque and impedance control of flexible joint robots", Int J Rob Res , Vol. 26, pp. 23–39.

Albus, J. S. (1971), "A theory of cerebellar function", Math Biosci , Vol. 10, pp. 25–61.

Alexander, C. and Carey, S. (1968), "Subsymmetries", Percept Psychophys , Vol. 4, pp. 73–77.

Amassian, V. E. and Giblin, D. (1974), "Periodic components in steady-state activity of cuneate neurones and their possible role in sensory coding", J physiol , Vol. 243, pp. 353–385.

Arabzadeh, E., Zorzin, E. and Diamond, M. E. (2005), "Neuronal encoding of texture in the whisker sensory pathway", PLoS Biol , Vol. 3, p. e17.

Asfour, T., Azad, P., Vahrenkamp, N., Regenstein, K., Bierbaum, A., Welke, K., Schroeder, J. and Dillmann, R. (2008), "Toward humanoid manipulation in human-centred environments", Rob Auton Syst , Vol. 56, pp. 54–65.

Attwell, P. J., Cooke, S. F. and Yeo, C. H. (2002), "Cerebellar function in consolidation of a motor memory", Neuron , Vol. 34, pp. 1011–1020.

Bair, W. and Koch, C. (1996), "Temporal precision of spike trains in extrastriate cortex of the behaving macaque monkey", Neural Comput , Vol. 8, pp. 1185–1202.

Bair, W., Koch, C., Newsome, W. and Britten, K. (1994), "Power spectrum analysis of bursting cells in area mt in the behaving monkey", J Neurosci , Vol. 14, pp. 2870–2892.

Bankman, I. N., Johnson, K. O. and Hsiao, S. S. (1989), A neural network model of transformations in the somatosensory system, in 'Proc IEEE Annual International Conference of Engineering in Medicine and Biology Society', pp. 2060–2061.

Bekey, G. A. (2005), Autonomous robots: from biological inspiration to implementation and control, MIT Press, Cambridge.

Bekiroglu, Y., Laaksonen, J., Jorgensen, J. A., Kyrki, V. and Kragic, D. (2011), "Assessing grasp stability based on learning and haptic data", IEEE Trans Robot , Vol. 27, pp. 616–629.

Bell, J., Bolanowski, S. and Holmes, M. H. (1994), "The structure and function of pacinian corpuscles: a review", Prog Neurobiol , Vol. 42, pp. 79–128.

Bell, J. and Holmes, M. (1992), "Model of the dynamics of receptor potential in a mechanoreceptor", Math Biosci , Vol. 110, pp. 139–174.

Bengtsson, F., Brasselet, R., Johansson, R. S., Arleo, A. and Jörntell, H. (2013), "Integration of sensory quanta in cuneate nucleus neurons in vivo", PloS ONE , Vol. 8, p. e56630.

Bensmaia, S. (2002), "A transduction model of the meissner corpuscle", Math Biosci , Vol. 176, pp. 203–217.

Bensmaia, S. J., Craig, J. C., Yoshioka, T. and Johnson, K. O. (2006), "Sa1 and ra afferent responses to static and vibrating gratings", J Neurophysiol , Vol. 95, pp. 1771–1782.

Bensmaia, S. J., Denchev, P. V., Dammann III, J. F., Craig, J. C. and Hsiao, S. S. (2008), "The representation of stimulus orientation in the early stages of somatosensory processing", J Neurosci , Vol. 28, pp. 776–786.

Bensmaia, S. J. and Hollins, M. (2003), "The vibrations of texture", Somatosens Mot Res , Vol. 20, pp. 33–43.

Berkley, K. J., Budell, R. J., Blomqvist, A. and Bull, M. (1986), "Output systems of the dorsal column nuclei in the cat", Brain Res , Vol. 396, pp. 199–225.

Berry, M. J., Warland, D. K. and Meister, M. (1997), "The structure and precision of retinal spike trains", Proc Natl Acad Sci USA , Vol. 94, pp. 5411–5416.

Bi, G. Q. and Poo, M. M. (1998), "Synaptic modifications in cultured hippocampal neurons: dependence on spike timing, synaptic strength, and postsynaptic cell type", J Neurosci , Vol. 18, pp. 10464–10472.

Bialek, W., Rieke, F., de Ruyter van Steveninck, R. R. and Warland, D. (1991), "Reading a neural code", Science , Vol. 252, pp. 1854–1857.

Birznieks, I., Jenmalm, P., Goodwin, A. W. and Johansson, R. S. (2001), "Encoding of direction of fingertip forces by human tactile afferents.", J. Neurosci. , Vol. 21, pp. 8222–8237.

Bisley, J. W., Goodwin, A. W. and Wheat, H. E. (2000), "Slowly adapting type i afferents from the sides and end of the finger respond to stimuli on the center of the fingerpad", J Neurophysiol , Vol. 84, pp. 57–64.

Blake, D. T., Johnson, K. O. and Hsiao, S. S. (1997), "Monkey cutaneous sai and ra responses to raised and depressed scanned patterns: effects of width, height, orientation, and a raised surround", J Neurophysiol , Vol. 78, pp. 2503–2517.

Blakemore, S.-J., Wolpert, D. and Frith, C. (2000), "Why can't you tickle yourself?", Neuroreport , Vol. 11, LWW, pp. R11–R16.

Bologna, L. L., Brasselet, R., Maggiali, M. and Arleo, A. (2010), Neuromimetic encoding/decoding of spatiotemporal spiking signals from an artificial touch sensor, in 'Proc International Joint Conference on Neural Networks', pp. 1–6.

Bologna, L. L., Pinoteau, J., Brasselet, R., Maggiali, M. and Arleo, A. (2011), "Encoding/decoding of first and second order tactile afferents in a neurorobotic application", J Physiol Paris , Vol. 105, pp. 25–35.

Bologna, L. L., Pinoteau, J., Garrido, J. and Arleo, A. (2012), Active tactile sensing in a neurorobotic braille-reading system, in 'Proc 4th IEEE RAS & EMBS International Conference on Biomedical Robotics and Biomechatronics (BioRob)', pp. 1925–1930.

Bologna, L. L., Pinoteau, J., Passot, J.-B., Garrido, J. A., Vogel, J., Ros-Vidal, E. and Arleo, A. (2013), "A closed-loop neurobotic system for fine touch sensing", J Neural Eng , Vol. 10, p. 046019.

Brasselet, R., Johansson, R. and Arleo, A. (2009), "Optimal context separation of spiking haptic signals by second-order somatosensory neurons", Adv Neural Inf Process Sys , Vol. 22, pp. 180–188.

Brasselet, R., Johansson, R. S. and Arleo, A. (2011a), Isometric coding of spiking haptic signals by peripheral somatosensory neurons, in J. e. a. Cabestany, ed., 'LNCS - Advances on Computational Intelligence', Vol. 6691, Springer, pp. 528–536.

Brasselet, R., Johansson, R. S. and Arleo, A. (2011b), "Quantifying neurotransmission reliability through metrics-based information analysis", Neural Comput , Vol. 23, pp. 852–881.

Brooks, R. (1991), "New approaches to robotics", Science , Vol. 253, pp. 1227–1232.

Burgess, N. and O'Keefe, J. (1996), "Neuronal computations underlying the firing of place cells and their role in navigation", Hippocampus , Vol. 6, pp. 749–762.

Burgess, P. R., Wei, J. Y., Clark, F. J. and Simon, J. (1982), "Signaling of kinesthetic information by peripheral sensory receptors", Annu Rev Neurosci , Vol. 5, pp. 171–87.

Caiti, A., Canepa, G., De Rossi, D., Germagnoli, F., Magenes, G. and Parisini, T. (1995), "Towards the realization of an artificial tactile system: fine-form discrimination by a tensorial tactile sensor array and neural inversion algorithms", IEEE Trans Systems, Man and Cybernetics , Vol. 25, pp. 933–946.

Canedo, A. and Aguilar, J. (2000), "Spatial and cortical influences exerted on cuneothalamic and thalamocortical neurons of the cat", Eur J Neurosci , Vol. 12, pp. 2515–2533.

Canedo, A., Martinez, L. and no, J. M. (1998), "Tonic and bursting activity in the cuneate nucleus of the chloralose-anesthetized cat", Neuroscience , Vol. 84, pp. 603–617.

Cannata, G., Maggiali, M., Metta, G. and Sandini, G. (2008), An embedded artificial skin for humanoid robots, in 'Proc IEEE International Conference on Multisensor Fusion and Integration for Intelligent Systems', pp. 434–438.

Carlson, M. (1981), "Characteristics of sensory deficits following lesions of brodmann's areas 1 and 2 in the postcentral gyrus of macaca mulatta", Brain Res , Vol. 204, pp. 424–430.

Carr, C. E. (1993), "Processing of temporal information in the brain", Annu Rev Neurosci , Vol. 16, pp. 223–243.

Carr, C. E., Heiligenberg, W. and Rose, G. J. (1986), "A time-comparison circuit in the electric fish midbrain. I. Behavior and physiology", J Neurosci , Vol. 6, pp. 107–119.

Carrillo, R. R., Ros, E., Boucheny, C. and Coenen, O. J. (2008), "A real-time spiking cerebellum model for learning robot control", Biosystems , Vol. 94, pp. 18–27.

Castelli, F. (2002), "An integrated tactile-thermal robot sensor with capacitive tactile array", IEEE Trans Industry Applications , Vol. 38, pp. 85–90.

Cauna, N. (1954), "Nature and functions of the papillary ridges of the digital skin", Anat Rec , Vol. 119, pp. 449–468.

Chacron, M. J., Pakdaman, K. and Longtin, A. (2003), "Interspike interval correlations, memory, adaptation, and refractoriness in a leaky integrate-and-fire model with threshold fatigue", Neural Comput , Vol. 15, pp. 253–278.

Chadderton, P., Margrie, T. W. and Häusser, M. (2004), "Integration of quanta in cerebellar granule cells during sensory processing", Nature , Vol. 428, pp. 856–860.

Chase, S. M. and Young, E. D. (2007), "First-spike latency information in single neurons increases when referenced to population onset", Proc Natl Acad Sci USA , Vol. 104, pp. 5175–5180.

Cheema, S., Fyffe, R., Light, A. and Rustioni, A. (1984), "Arborizations of single corticofugal axons in the feline cuneate nucleus stained by iontophoretic injection of horseradish peroxidase", Brain Res , Vol. 290, pp. 158–164.

Chipman, S. F. (1977), "Complexity and structure in visual patterns", J Exp Psychol Gen , Vol. 106, pp. 269–301.

Chitta, S., Sturm, J., Piccoli, M. and Burgard, W. (2011), "Tactile sensing for mobile manipulation", IEEE Trans Robot , Vol. 27, pp. 558–568.

Cole, J. (1995), Pride and a Daily Marathon, MIT Press, Cambridge.

Connor, C. E. and Johnson, K. O. (1992), "Neural coding of tactile texture: comparison of spatial and temporal mechanisms for roughness perception", J Neurosci , Vol. 12, pp. 3414–3426.

Costanzo, R. M. and Gardner, E. P. (1980), "A quantitative analysis of responses of direction-sensitive neurons in somatosensory cortex of awake monkeys", J Neurophysiol , Vol. 43, pp. 1319–1341.

Crapse, T. B. and Sommer, M. A. (2008), "Corollary discharge across the animal kingdom", Nat Rev Neurosci , Vol. 9, Nature Publishing Group, pp. 587–600.

Dahiya, R. S., Metta, G., Valle, M. and Sandini, G. (2010), "Tactile sensing – from humans to humanoids", IEEE Trans Robot , Vol. 26, pp. 1–20.

Dahiya, R. S. and Valle, M. (2013), Robotic Tactile Sensing: Technologies and System, Springer.

D'Angelo, E. and De Zeeuw, C. I. (2009), "Timing and plasticity in the cerebellum: focus on the granular layer", Trends Neurosci , Vol. 32, pp. 30–40.

Dargahi, J. and Najarian, S. (2004), "Human tactile perception as a standard for artificial tactile sensing–a review", Int J Med Robot , Vol. 1, pp. 23–35.

Darian-Smith, C. and Ciferri, M. (2006), "Cuneate nucleus reorganization following cervical dorsal rhizotomy in the macaque monkey: its role in the recovery of manual dexterity", J. Comp. Neurol. , Vol. 498, pp. 552–565.

Darian-Smith, I. (1984), Handbook of Physiology, American Physiological Society.

Dario, P. (1991), "Tactile sensing: Technology and applications", Sensors and Actuators A: Physical , Vol. 26, pp. 251–256.

Dario, P., Laschi, C., Carrozza, M. C., Guglielmelli, E., Teti, G., Massa, B., Zecca, M., Taddeucci, D. and Leoni, F. (2000), An integrated approach for the design and development of a grasping and manipulation system in humanoid robotics, in 'Proc IEEE/RSJ International Conference on Intelligent Robots and Systems', Vol. 1, pp. 1–7.

Dayan, P. and Abbott, L. (2001), Theoretical Neuroscience, MIT Press, Cambridge.

Dean, A. F. (1981), "The relationship between response amplitude and contrast for cat striate cortical neurones", J Physiology , Vol. 318, pp. 413–427.

Debrégeas, G., Prevost, A. and Scheibert, J. (2009), "Toucher digital humain: transduction mécanique de l'information tactile et rôle des empreintes digitales", Images de la Physique , pp. 11–17.

Decherchi, S., Gastaldo, P., Dahiya, R. S., Valle, M. and Zunino, R. (2011), "Tactile-data classification of contact materials using computational intelligence", IEEE Trans Robotics , Vol. 27, pp. 635–639.

Diamond, M. E., von Heimendahl, M., Knutsen, P. M., Kleinfeld, D. and Ahissar, E. (2008), "'where' and 'what' in the whisker sensorimotor system", Nature reviews. Neuroscience , Vol. 9, pp. 601–612.

DiCarlo, J. J. and Johnson, K. O. (1999), "Velocity invariance of receptive field structure in somatosensory cortical area 3b of the alert monkey", J Neurosci , Vol. 19, pp. 401–419.

Dirac, P. A. M. (1958), The Principles of Quantum Mechanics, International Series of Monographs on Physics, Clarendon Press.

Domingos, P. and Pazzani, M. (1996), Beyond independence: Conditions for the optimality of the simple bayesian classifier, in 'Proc 13th International Conference on Machine Learning', pp. 105–112.

Domingos, P. and Pazzani, M. (1997), "On the optimality of the simple bayesian classifier under zero-one loss", Mach Learn , Vol. 29, pp. 103–130.

Douglas, P. R., Ferrington, D. G. and Rowe, M. (1978), "Coding of information about tactile stimuli by neurones of the cuneate nucleus", J Physiol , Vol. 285, pp. 493–513.

Duda, R. O., Hart, P. E. and Stork, D. G. (2001), Pattern Classification, J. Wiley-Interscience.

Dykes, R. W., Rasmusson, D. D., Sretavan, D. and Rehman, N. B. (1982), "Submodality segregation and receptive-field sequences in cuneate, gracile, and external cuneate nuclei of the cat", J Neurophysiol , Vol. 47, pp. 389–416.

Eccles, J. C., Itō, M. and Szentágothai, J. (1967), The Cerebellum as a Neuronal Machine, Springer-Verlag.

Edin, B. B., Essick, G. K., Trulsson, M. and Olsson, K. A. (1995), "Receptor encoding of moving tactile stimuli in humans. i. temporal pattern of discharge of individual low-threshold mechanoreceptors", J Neurosci , Vol. 15, pp. 830–847.

Ego-Stengel, V., Le Cam, J. and Shulz, D. E. (2012), "Coding of apparent motion in the thalamic nucleus of the rat vibrissal somatosensory system", J Neurosci , Vol. 32, pp. 3339–3351.

Engel, J., Chen, N., Tucker, C., Liu, C., Kim, S.-H. and Jones, D. (2006), Flexible multimodal tactile sensing system for object identification, in 'Proc 5th IEEE Conference on Sensors', pp. 563–566.

Fanselow, E. E., Sameshima, K., Baccala, L. A. and Nicolelis, M. A. (2001), "Thalamic bursting in rats during different awake behavioral states", Proc Natl Acad Sci USA , Vol. 98, pp. 15330–15335.

Fishel, J. A. and Loeb, G. E. (2012), "Bayesian exploration for intelligent identification of textures", Front Neurorobot , Vol. 6.

Freeman, A. W. and Johnson, K. O. (1982), "Cutaneous mechanoreceptors in macaque monkey: temporal discharge patterns evoked by vibration, and a receptor model", J Physiol , Vol. 323, pp. 21–41.

Furukawa, S., Xu, L. and Middlebrooks, J. C. (2000), "Coding of sound-source location by ensembles of cortical neurons", J Neurosci , Vol. 20, pp. 1216–1228.

Fyffe, R. E., Cheema, S. S., Light, A. R. and Rustioni, A. (1986b), "Intracellular staining study of the feline cuneate nucleus. II. Thalamic projection neurons", J Neurophysiol , Vol. 56, pp. 1284–1296.

Fyffe, R. E., Cheema, S. S. and Rustioni, A. (1986a), "Intracellular staining study of the feline cuneate nucleus. I. Terminal patterns of primary afferent fibers", J Neurophysiol , Vol. 56, pp. 1268–1283.

Gardner, E. P. and Palmer, C. I. (1990), "Simulation of motion on the skin. iii. mechanisms used by rapidly adapting cutaneous mechanoreceptors in the primate hand for spatiotemporal resolution and two-point discrimination", J Neurophysiol , Vol. 63, pp. 841–859.

Garrido, J. A., Carrillo, R. R., Luque, N. R. and Ros, E. (2011), Event and time driven hybrid simulation of spiking neural networks, in J. Cabestany, I. Rojas and G. Joya, eds, 'Advances in Computational Intelligence', Vol. 6691 of Lecture Notes in Computer Science, Springer Berlin Heidelberg, pp. 554–561.

Gartner, L. P. and Patestas, M. A. (2009), A textbook of neuroanatomy, John Wiley & Sons.

Gates, B. (2007), "A robot in every home", Scientific American , Vol. 296, pp. 58–65.

Gautrais, J. and Thorpe, S. (1998), "Rate coding versus temporal order coding: a theoretical approach", Biosystems , Vol. 48, pp. 57–65.

Gawne, T. J., Kjaer, T. W. and Richmond, B. J. (1996), "Latency: another potential code for feature binding in striate cortex", J Neurophysiol , Vol. 76, pp. 1356–1360.

Georgopoulos, A. P., Kettner, R. E. and Schwartz, A. B. (1988), "Primate motor cortex and free arm movements to visual targets in three-dimensional space. II. coding of the direction of movement by a neuronal population", J Neurosci , Vol. 8, pp. 2928–2937.

Gerling, G. J., Scanlon, J. R., Wan, L., Rivest, I. I. and Lesniak, D. R. (2013), "Validating a population model of tactile mechanotransduction of slowly adapting type i afferents at levels of skin mechanics, single-unit response and psychophysics", IEEE Trans Haptics , IEEE, p. 1.

Gerling, G. J. and Thomas, G. W. (2008), "Fingerprint lines may not directly affect SA-I mechanoreceptor response", Somatosens Motor Res , Vol. 25, pp. 61–76.

Germagnoli, F. and Magenes, G. (1996), A neural network-based system for tactile exploratory tasks, in 'Proc IEEE International Workshop on Neural Networks for Identification, Control, Robotics, and Signal/Image Processing', pp. 458–466.

Gerstner, W. and Kistler, W. M. (2002), Spiking Neuron Models: Single Neurons, Populations, Plasticity, Cambridge University Press.

Ghazanfar, A. A. and Nicolelis, M. A. (1997), "Nonlinear processing of tactile information in the thalamocortical loop", J Neurophysiol , Vol. 78, pp. 506–510.

Giguere, P. and Dudek, G. (2011), "A simple tactile probe for surface identification by mobile robots", IEEE Trans Robotics , Vol. 27, pp. 534–544.

Gollisch, T. and Meister, M. (2008), "Rapid neural coding in the retina with relative spike latencies", Science , Vol. 319, pp. 1108–1111.

Goodwin, A. W. and Wheat, H. E. (1999), "Effects of nonuniform fiber sensitivity, innervation geometry, and noise on information relayed by a population of slowly adapting type i primary afferents from the fingerpad", J Neurosci , Vol. 19, pp. 8057–8070.

Gordon, G. and Jukes, M. G. (1964), "Descending influences on the exteroceptive organizations of the cat's gracile nucleus", J Physiol , Vol. 173, pp. 291–319.

Grant, R., Mitchinson, B., Fox, C. W. and Prescott, T. J. (2009), "Active touch sensing in the rat: anticipatory and regulatory control of whisker movements during surface exploration", Journal of neurophysiology , Vol. 101, Am Physiological Soc, pp. 862–874.

Güçlü, B. and Bolanowski, S. J. (2003), "Correlation of spatial event plots with simulated population responses of mechanoreceptive fibers", Somatosens Mot Res , Vol. 20, pp. 199–208.

Güçlü, B. and Bolanowski, S. J. (2004), "Tristate markov model for the firing statistics of rapidly-adapting mechanoreceptive fibers", J Comput Neurosci , Vol. 17, pp. 107–126.

Guyonneau, R., VanRullen, R. and Thorpe, S. J. (2011), "Neurons tune to the earliest spikes through STDP", Neural Comput. , Vol. 17, pp. 859–879.

Haddad, R., Lanjuin, A., Madisen, L., Zeng, H., Murthy, V. N. and Uchida, N. (2013), "Olfactory cortical neurons read out a relative time code in the olfactory bulb", Nat Neurosci , Vol. 16, pp. 949–957.

Hagbarth, K. E. and Vallbo, A. B. (1968), "Discharge characteristics of human muscle afferents during muscle stretch and contraction", Experimental Neurology , Vol. 22, pp. 674–694.

Harvey, M. A., Saal, H. P., Dammann, III, J. F. and Bensmaia, S. J. (2013), "Multiplexing stimulus information through rate and temporal codes in primate somatosensory cortex", PLoS Biol , Vol. 11, Public Library of Science, p. e1001558.

Hebb, D. O. (1949), Organization of behavior, John Wiley and Sons.

Heil, P. (2004), "First-spike latency of auditory neurons revisited", Curr Opin in Neurobiol , Vol. 14, pp. 461–467.

Hochberg, L. R., Bacher, D., Jarosiewicz, B., Masse, N. Y., Simeral, J. D., Vogel, J., Haddadin, S., Liu, J., Cash, S. S., van der Smagt, P. and Donoghue, J. P. (2012), "Reach and grasp by people with tetraplegia using a neurally controlled robotic arm", Nature , Vol. 485, pp. 372–375.

Hodgkin, A. L. and Huxley, A. F. (1952), "A quantitative description of membrane current and its application to conduction and excitation in nerve", J Physiol , Vol. 117, pp. 500–544.

Hollins, M., Faldowski, R., Rao, S. and Young, F. (1993), "Perceptual dimensions of tactile surface texture: a multidimensional scaling analysis", Percept Psychophys , Vol. 54, pp. 697–705.

Hollins, M. and Risner, S. R. (2000), "Evidence for the duplex theory of tactile texture perception", Percept Psychophys , Vol. 62, pp. 695–705.

Hopfield, J. J. (1995), "Pattern recognition computation using action potential timing for stimulus representation", Nature , Vol. 376, pp. 33–36.

Horner, D. T. (1991), "The effects of complexity on the perception of vibrotactile patterns", Percept Psychophys , Vol. 49, p. 551–562.

Houghton, C. and Sen, K. (2008), "A new multineuron spike train metric", Neural Comput , Vol. 20, pp. 1495–1511.

Howe, R. D. (1993), "Tactile sensing and control of robotic manipulation", Adv Robot , Vol. 8, pp. 245–261.

Howe, R. D. and Cutkosky, M. R. (1993), "Dynamic tactile sensing: Perception of fine surface features with stress rate sensing", IEEE Trans Robotics and Automation , Vol. 9, pp. 140–151.

Hsiao, S. S., Lane, J. and Fitzgerald, P. (2002), "Representation of orientation in the somatosensory system", Behav Brain Res , Vol. 135, pp. 93–103.

Hsiao, S. and Yau, J. (2008), Neural basis of haptic perception, Birkhäuser, Basel, pp. 103–112.

Hubel, D. H. and Wiesel, T. N. (1959), "Receptive fields of single neurones in the cat's striate cortex", J Physiol , Vol. 148, pp. 574–591.

Hughes, B. (2011), "Movement kinematics of the braille-reading finger", J Visual Impair Blind , Vol. 105, pp. 370–381.

Hughes, B., Van Gemmert, A. W. A. and Stelmach, G. E. (2011), "Linguistic and perceptual-motor contributions to the kinematic properties of the braille reading finger", Hum Mov Sci , Vol. 30, pp. 711–730.

Hulliger, M., Nordh, E., Thelin, A. E. and Vallbo, A. B. (1979), "The responses of afferent fibres from the glabrous skin of the hand during voluntary finger movements in man", J Physiol , Vol. 291, pp. 233–49.

Hyvärinen, J. and Poranen, A. (1978), "Movement-sensitive and direction and orientation-selective cutaneous receptive fields in the hand area of the post-central gyrus in monkeys.", J Physiol , Vol. 283, pp. 523–537.

Ichikawa, S. (1985), "Quantitative and structural factors in the judgment of pattern complexity", Attention, Perception, & Psychophysics , Vol. 38, pp. 101–109.

Ito, M. (1974), Control mechanisms of cerebellar motor system, MIT Press, pp. 293–303.

Ito, M. (1984), The Cerebellum and Neural Control, Raven Press.

Ito, M. and Kano, M. (1982), "Long-lasting depression of parallel fiber-purkinje cell transmission induced by conjunctive stimulation of parallel fibers and climbing fibers in the cerebellar cortex", Neurosci Lett , Vol. 33, pp. 253–258.

Izhikevich, E. M. (2003), "Simple model of spiking neurons.", IEEE Trans. Neural Netw. , Vol. 14, pp. 1569–1572.

Jakab, R. L. and Hamori, J. (1988), "Quantitative morphology and synaptology of cerebellar glomeruli in the rat", Anat Embryol (Berl) , Vol. 179, pp. 81–88.

Jamali, N. and Sammut, C. (2011), "Majority voting: material classification by tactile sensing using surface texture", IEEE Trans Robotics , Vol. 27, pp. 508–521.

Johansson, R. S. (1978), "Tactile sensibility in the human hand: receptive field characteristics of mechanoreceptive units in the glabrous skin area", J Physiol , Vol. 281, pp. 101–25.

Johansson, R. S. and Birznieks, I. (2004), "First spikes in ensembles of human tactile afferents code complex spatial fingertip events", Nat Neurosci , Vol. 7, pp. 170–177.

Johansson, R. S. and Flanagan, J. R. (2009), "Coding and use of tactile signals from the fingertips in object manipulation tasks", Nat Rev Neurosci , Vol. 10, pp. 345–359.

Johansson, R. S., Landström, U. and Lundström, R. (1982), "Responses of mechanoreceptive afferent units in the glabrous skin of the human hand to sinusoidal skin displacements", Brain Res , Vol. 244, pp. 17–25.

Johansson, R. S. and Vallbo, A. B. (1979), "Tactile sensibility in the human hand: relative and absolute densities of four types of mechanoreceptive units in glabrous skin", J Physiol , Vol. 286, pp. 283–300.

Johansson, R. S. and Vallbo, A. B. (1983), "Tactile sensory coding in the glabrous skin of the human hand", Trends Neurosci. , Vol. 6(1), pp. 27–32.

Johnson, K. (2004), Neural Basis of Haptic Perception, Vol. 1, John Wiley & Sons, New York, pp. 537–583.

Johnson, K. O. (2001), "The roles and functions of cutaneous mechanoreceptors", Curr Opin Neurobiol , Vol. 11, pp. 455–461.

Johnson, K. O. and Hsiao, S. S. (1992), "Neural mechanisms of tactual form and texture perception", Annu Rev Neurosci , Vol. 15, pp. 227–250.

Johnson, K. O. and Lamb, G. D. (1981), "Neural mechanisms of spatial tactile discrimination: neural patterns evoked by braille-like dot patterns in the monkey", J Physiol , Vol. 310, pp. 117–144.

Johnson, K. O. and Phillips, J. R. (1988), "A rotating drum stimulator for scanning embossed patterns and textures across the skin", J Neurosci Methods , Vol. 22, pp. 221–231.

Johnson, K. O., Yoshioka, T. and Vega-Bermudez, F. (2000), "Tactile functions of mechanoreceptive afferents innervating the hand", J Clin Neurophysiol , Vol. 17, pp. 539–558.

Jones, E. G. (2000), "Cortical and subcortical contributions to activity-dependent plasticity in primate somatosensory cortex", Annu Rev Neurosci , Vol. 23, pp. 1–37.

Joris, P. X., Schreiner, C. E. and Rees, A. (2004), "Neural processing of amplitude-modulated sounds", Physiol Rev , Vol. 84, pp. 541–577.

Kakuda, N. (1992), "Conduction velocity of low-threshold mechanoreceptive afferent fibers in the glabrous and hairy skin of human hands measured with microneurography and spike-triggered averaging", Neurosci Res , Vol. 15, pp. 179–88.

Kandel, E. R., Schwartz, J. H. and Jessel, T. M. (2000), Principles of Neural Science (4th edition), McGraw-Hill.

Katz, D. (2013), The world of touch, Psychology Press.

Kayser, C., Montemurro, M. A., Logothetis, N. K. and Panzeri, S. (2009), "Spike-phase coding boosts and stabilizes information carried by spatial and temporal spike patterns", Neuron , Vol. 61, pp. 597–608.

Kim, S. S., Sripati, A. P. and Bensmaia, S. J. (2010), "Predicting the timing of spikes evoked by tactile stimulation of the hand", J Neurophysiol , Vol. 104, pp. 1484–1496.

Knibestöl, M. (1975), "Stimulus-response functions of slowly adapting mechanoreceptors in the human glabrous skin area", J Physiol , Vol. 245, pp. 63–80.

König, P., Engel, A. K. and Singer, W. (1996), "Integrator or coincidence detector? the role of the cortical neuron revisited", Trends Neurosci , Vol. 19, pp. 130–137.

Kreuz, T., Haas, J. S., Morelli, A., Abarbanel, H. D. and Politi, A. (2007), "Measuring spike train synchrony", J Neurosci Methods , Vol. 165, pp. 151–161.

Kuffler, S. W. (1953), "Discharge patterns and functional organization of mammalian retina", J Neurophysiol , Vol. 16, pp. 37–68.

LaMotte, R. H. and Srinivasan, M. A. (1987), "Tactile discrimination of shape: responses of slowly adapting mechanoreceptor afferents to a step stroked across the monkey fingerpad", J Neurosci , Vol. 7, pp. 1655–1671.

Lapicque, L. (1907), "Recherches quantitatives sur l'excitation électrique des nerfs traitée comme une polarisation", Journal de Physiologie et Pathologie Général , Vol. 9, pp. 620–635.

Lederman, S. J. and Klatzky, R. L. (1987), "Hand movements: a window into haptic object recognition", Cogn Psychol , Vol. 19, pp. 342–368.

Lederman, S. J. and Klatzky, R. L. (1993), "Extracting object properties through haptic exploration", Acta psychologica , Vol. 84, pp. 29–40.

Lederman, S. J. and Klatzky, R. L. (2009), "Haptic perception: a tutorial", Atten. Percept. Psychophys. , Vol. 71, pp. 1439–1459.

Lederman, S. J. and Pawluk, D. (1992), "Lessons from the study of biological touch for robotic tactile sensing", Advanced Tactile Sensing for Robots Ed. HR Nicholls , pp. 151–192.

Lee, S., Carvell, G. E. and Simons, D. J. (2008), "Motor modulation of afferent somatosensory circuits", Nature Neurosci , Vol. 11, pp. 1430–1438.

Leiras, R., Velo, P., Martin-Cora, F. and Canedo, A. (2010), "Processing afferent proprioceptive information at the main cuneate nucleus of anesthetized cats", J Neurosci , Vol. 30, pp. 15383–15399.

Lennie, P. (2003), "The cost of cortical computation", Curr Biol , Vol. 13, pp. 493–497.

Lesniak, D. R. and Gerling, G. J. (2009), "Predicting SA-I mechanoreceptor spike times with a skin-neuron model", Mathematical biosciences , Vol. 220, pp. 15–23.

Lev-Ram, V., Wong, S. T., Storm, D. R. and Tsien, R. Y. (2002), "A new form of cerebellar long-term potentiation is postsynaptic and depends on nitric oxide but not camp", Proc Natl Acad Sci USA , Vol. 99, pp. 8389–8393.

Libouton, X., Barbier, O., Berger, Y., Plaghki, L. and Thonnard, J. L. (2012), "Tactile roughness discrimination of the finger pad relies primarily on vibration sensitive afferents not necessarily located in the hand", Behav Brain Res , Vol. 229, pp. 273–279.

Lin, C. H., Erickson, T. W., Fishel, J. A., Wettels, N. and Loeb, G. E. (2009), Signal processing and fabrication of a biomimetic tactile sensor array with thermal, force and microvibration modalities, in 'Proc IEEE International Conference on Robotics and Biomimetics', pp. 129–134.

Liu, H., Wu, K., Meusel, P., Seitz, N., Hirzinger, G., Jin, M., Liu, Y. W., Fan, S. W., Lan, T. and Chen, Z. P. (2008), Multisensory five-finger dexterous hand: The dlr/hit hand ii, in 'Proc IEEE/RSJ International Conference on Intelligent Robots and Systems', pp. 3692–3697.

Loeb, G. E., Tsianos, G. A., Fishel, J. A., Wettels, N. and Schaal, S. (2011a), "Understanding haptics by evolving mechatronic systems", Progress Brain Res , Vol. 192, p. 129.

Loeb, G. E., Tsianos, G. A., Fishel, J. A., Wettels, N. and Schaal, S. (2011b), "Understanding haptics by evolving mechatronic systems", Prog Brain Res , Vol. 192, pp. 129–144.

Looft, F. J. (1996), "Response of monkey glabrous skin mechanoreceptors to random noise sequences: Ii. dynamic stimulus state analysis", Somatosens Motor Res , Vol. 13, pp. 11–28.

Loomis, J. M. (1981), "On the tangibility of letters and braille", Percep Psychophys , Vol. 29, pp. 37–46.

Loomis, J. M. (1985), "Tactile recognition of raised characters: A parametric study.", Bulletin of the Psychonomic Society , Psychonomic Society.

Loomis, J. M. and Lederman, S. J. (1986), Tactual perception, Vol. 2, Wiley, New York.

Lumpkin, E. A. and Caterina, M. J. (2007), "Mechanisms of sensory transduction in the skin", Nature , Vol. 445, pp. 858–865.

Lumpkin, E. A., Marshall, K. L. and Nelson, A. M. (2010), "The cell biology of touch", J Cell Biol , Vol. 191, pp. 237–248.

MacKay, D. M. and McCulloch, W. S. (1952), "The limiting information capacity of a neuronal link", Bull Math Biophys , Vol. 14, pp. 127–135.

Mackevicius, E. L., Best, M. D., Saal, H. P. and Bensmaia, S. J. (2012), "Millisecond precision spike timing shapes tactile perception", J Neurosci , Vol. 32, pp. 15309–15317.

Maheshwari, V. and Saraf, R. (2008), "Tactile devices to sense touch on a par with a human finger", Angew Chem Int Ed Engl , Vol. 47, pp. 7808–7826.

Mainen, Z. F. and Sejnowski, T. J. (1995), "Reliability of spike timing in neocortical neurons", Science , Vol. 268, pp. 1503–1506.

Maricich, S. M., Wellnitz, S. A., Nelson, A. M., Lesniak, D., Gerling, G. J., Lumpkin, E. A. and Zoghbi, H. Y. (2009), "Merkel cells are essential for light-touch responses", Science , Vol. 324, pp. 1580–1582.

Marino, J., Aguilar, J., Soto, C. and Canedo, A. (2001), "The cerebral cortex modulates the cutaneous transmission through the dorsal column nuclei", Rev Neurol , Vol. 33, pp. 448–454.

Marino, J., Canedo, A. and Aguilar, J. (999), "Sensorimotor cortical influences on cuneate nucleus rhythmic activity in the anesthetized cat", Neurosci , Vol. 95, pp. 657 – 673.

Marr, D. (1969), "A theory of cerebellar cortex", J Physiol , Vol. 202, pp. 437–470.

Masquelier, T., Guyonneau, R. and Thorpe, S. J. (2008), "Spike timing dependent plasticity finds the start of repeating patterns in continuous spike trains", PLoS ONE , Vol. 3, p. e1377.

Masquelier, T., Guyonneau, R. and Thorpe, S. J. (2009), "Competitive STDP-based spike pattern learning.", Neural Comput. , Vol. 21, pp. 1259–1276.

Masquelier, T., Hugues, E., Deco, G. and Thorpe, S. J. (2009), "Oscillations, phase-of-firing coding, and spike timing-dependent plasticity: an efficient learning scheme.", J. Neurosci. , Vol. 29, pp. 13484–13493.

Masquelier, T. and Thorpe, S. J. (2007), "Unsupervised learning of visual features through spike timing dependent plasticity", PLoS Comput Biol , Vol. 3, p. e31.

McCallum, A. and Nigam, K. (1998), A comparison of event models for naive bayes text classification, in 'Proc AAAI-98 Workshop on Learning for Text Categorization', AAAI Press, pp. 41–48.

Medina, J. F., Repa, J. C., Mauk, M. D. and LeDoux, J. E. (2002), "Parallels between cerebellum- and amygdala-dependent conditioning", Nat Rev Neurosci , Vol. 3, pp. 122–31.

Miall, R. C., Reckess, G. Z. and Imamizu, H. (2001), "The cerebellum coordinates eye and hand tracking movements", Nat Neurosci , Vol. 4, pp. 638–644.

Miall, R. C., Weir, D. J., Wolpert, D. M. and Stein, J. F. (1993), "Is the cerebellum a smith predictor?", J Mot Behav , Vol. 25, pp. 203–216.

Millar, J., Basbaum, A. I. and Wall, P. D. (1976), "Restructuring of the somatotopic map and appearance of abnormal neuronal activity in the gracile nucleus after partial deafferentation", Exp Neurol , Vol. 50, pp. 658–672.

Mountcastle, V. B. (1957), "Modality and topographic properties of single neurons of cat's somatic sensory cortex", J Neurophysiology , Vol. 20, pp. 408–434.

Mountcastle, V. B. (1974), Medical Physiology, Mosby, St. Louis.

Mountcastle, V. B. (1997), "The columnar organization of the neocortex.", Brain , Vol. 120, pp. 701–722.

Navarro, J., Sanchez, E. and Canedo, A. (2005), Coding strategies in early stages of the somatosensory system, in 'Mechanisms, Symbols, and Models Underlying Cognition', pp. 213–222.

Navarro, J., Sánchez, E. and Canedo, A. (2006), "Spatio-temporal information coding in the cuneate nucleus", Neurocomputing , Vol. 69, pp. 1946–1953.

Navarro, J., Sanchez, E. and Canedo, A. (2007), "Information coding in early stages of the somatosensory system", Natural Computing , Vol. 6, pp. 253–267.

Newman, S. E., Hall, A. D., Foster, D. J. and Gupta, V. (1984), "Learning as a function of haptic discriminability among items", Am J Psychol , Vol. 97, pp. 359–372.

Nicolelis, M. A. (2005), "Computing with thalamocortical ensembles during different behavioural states", J Physiol , Vol. 566, pp. 37–47.

Nicolelis, M. A. L. and Lebedev, M. A. (2009), "Principles of neural ensemble physiology underlying the operation of brain-machine interfaces", Nat Rev Neurosci , Vol. 10, pp. 530–540.

Nolan, C. Y. and Kederis, C. J. (1969), Perceptual factors in braille word recognition, American Foundation for the Blind.

O'Connor, D. H., Hires, S. A., Guo, Z. V., Li, N., Yu, J., Sun, Q. Q., Huber, D. and Svoboda, K. (2013), "Neural coding during active somatosensation revealed using illusory touch", Nat Neurosci , Vol. 16, pp. 958–965.

Oddo, C. M., Controzzi, M., Beccai, L., Cipriani, C. and Carrozza, M. C. (2011), "Roughness encoding for discrimination of surfaces in artificial active-touch", IEEE Trans Robot , Vol. 27, IEEE, pp. 522–533.

O'Doherty, J. E., Lebedev, M. A., Ifft, P. J., Zhuang, K. Z., Shokur, S., Bleuler, H. and Nicolelis, M. A. (2011), "Active tactile exploration using a brain-machine-brain interface", Nature , Vol. 479, pp. 228–231.

Pais-Vieira, M., Lebedev, M. A., Wiest, M. C. and Nicolelis, M. A. (2013), "Simultaneous top-down modulation of the primary somatosensory cortex and thalamic nuclei during active tactile discrimination", J Neurosci , Vol. 33, pp. 4076–4093.

Pantoja, J., Ribeiro, S., Wiest, M., Soares, E., Gervasoni, D., Lemos, N. A. and Nicolelis, M. A. (2007), "Neuronal activity in the primary somatosensory thalamocortical loop is modulated by reward contingency during tactile discrimination", J Neurosci , Vol. 27, pp. 10608–10620.

Panzeri, S., Petersen, R. S., Schultz, S. R., Lebedev, M. and Diamond, M. E. (2001), "The role of spike timing in the coding of stimulus location in rat somatosensory cortex", Neuron , Vol. 29, pp. 769–777.

Passot, J.-B., Luque, N. R. and Arleo, A. (2013), "Coupling internal cerebellar models enhances online adaptation and supports offline consolidation in sensorimotor tasks", Vol. 7.

Passot, J.-B., Sheynikhovich, D., Duvelle, E. and Arleo, A. (2012), "Contribution of cerebellar sensorimotor adaptation to hippocampal spatial memory", PLoS ONE , Vol. 7, p. e32560.

Paul, R. L., Merzenich, M. and Goodman, H. (1972), "Representation of slowly and rapidly adapting cutaneous mechanoreceptors of the hand in brodmann's areas 3 and 1 of macaca mulatta", Brain Res , Vol. 36, pp. 229–249.

Perkel, D. H. and Bullock, T. H. (1968), "Neural coding", Neurosci Res Program Bull , Vol. 63, pp. 221–348.

Petersen, R. S., Panzeri, S. and Diamond, M. E. (2002), "Population coding in somatosensory cortex", Curr Opin Neurobiol , Vol. 12, pp. 441–447.

Petrovskaya, A. and Khatib, O. (2011), "Global localization of objects via touch", IEEE Trans Robot , Vol. 27, pp. 569–585.

Pettit, M. J. and Schwark, H. D. (1993), "Receptive field reorganization in dorsal column nuclei during temporary denervation", Science , Vol. 262, pp. 2054–2056.

Pfeifer, R., Lungarella, M. and Iida, F. (2007), "Self-organization, embodiment, and biologically inspired robotics", Science , Vol. 318, pp. 1088–1093.

Phillips, J., Johansson, R. and Johnson, K. (1990), "Representation of braille characters in human nerve fibres", Exp Brain Res , Vol. 81, pp. 589–592.

Phillips, J. R., Johansson, R. S. and Johnson, K. O. (1992), "Responses of human mechanoreceptive afferents to embossed dot arrays scanned across fingerpad skin", J Neurosci , Vol. 12, pp. 827–839.

Phillips, J. R. and Johnson, K. O. (1981a), "Tactile spatial resolution. ii. neural representation of bars, edges, and gratings in monkey primary afferents", J Neurophysiol , Vol. 46, pp. 1192–1203.

Phillips, J. R. and Johnson, K. O. (1981b), "Tactile spatial resolution. iii. a continuum mechanics model of skin predicting mechanoreceptor responses to bars, edges, and gratings", J Neurophysiol , Vol. 46, pp. 1204–1225.

Phillips, J. R., Johnson, K. O. and Browne, H. M. (1983), "A comparison of visual and two modes of tactual letter resolution", Percep Psychophys , Vol. 34, pp. 243–249.

Phillips, J. R., Johnson, K. O. and Hsiao, S. S. (1988a), "Spatial pattern representation and transformation in monkey somatosensory cortex", Proceedings of the National Academy of Sciences of the United States of America , Vol. 85, pp. 1317–1321.

Phillips, J. R., Johnson, K. O. and Hsiao, S. S. (1988b), "Spatial pattern representation and transformation in monkey somatosensory cortex", Proc Natl Acad Sci USA , Vol. 85, pp. 1317–1321.

Pinoteau, J., Bologna, L. L., Garrido, J. A. and Arleo, A. (2012), A closed-loop neurorobotic system for investigating braille-reading finger kinematics, in 'Haptics: Perception, Devices, Mobility, and Communication', pp. 407–418.

Pouget, A., Beck, J. M., Ma, W. J. and Latham, P. E. (2013), "Probabilistic brains: knowns and unknowns", Nature neuroscience , Vol. 16, pp. 1170–1178.

Powell, T. P. and Mountcastle, V. B. (1959), "Some aspects of the functional organization of the cortex of the postcentral gyrus of the monkey: a correlation of findings obtained in a single unit analysis with cytoarchitecture", Bull Johns Hopkins Hosp , Vol. 105, pp. 133–162.

Pruszynski, A., Jenmalm, P. and Johansson, R. S. (2011), Information processing in human tactile afferent neurons, in 'Society for Neuroscience Abstracts, No. 750.07, Washington DC, USA'.

Pubols, B. H., Haring, J. H. and Rowinski, M. J. (1989), "Patterns of resting discharge in neurons of the raccoon main cuneate nucleus", J Neurophysiol , Vol. 61, pp. 1131–1141.

Purves, D., Augustine, G. J., Fitzpatrick, D., Hall, W. C., LaMantia, A.-S., McNamara, J. O. and White, L. E. (2008), Neuroscience, 4th edn, Sinauer, Sunderland.

Quian Quiroga, R., Kreuz, T. and Grassberger, P. (2002), "Event synchronization: a simple and fast method to measure synchronicity and time delay patterns", Phys Rev E Stat Nonlin Soft Matter Phys , Vol. 66, p. 041904.

Quiroga, R. Q. and Panzeri, S. (2009), "Extracting information from neuronal populations: information theory and decoding approaches.", Nat. Rev. Neurosci. , Vol. 10, pp. 173–185.

Randolph, M. and Semmes, J. (1974), "Behavioral consequences of selective subtotal ablations in the postcentral gyrus of macaca mulatta", Brain Res , Vol. 70, pp. 55–70.

Raspopovic, S., Capogrosso, M., Badia, J., Navarro, X. and Micera, S. (2012), "Experimental validation of a hybrid computational model for selective

stimulation using transverse intrafascicular multichannel electrodes", IEEE Trans Neural Syst Rehabil Eng , Vol. 20, pp. 395–404.

Ratnasingam, S. and McGinnity, T. M. (2011a), A comparison of encoding schemes for haptic object recognition using a biologically plausible spiking neural network, in 'Proc IEEE/RSJ International Conference on Intelligent Robots and Systems', pp. 3446–3453.

Ratnasingam, S. and McGinnity, T. M. (2011b), A spiking neural network for tactile form based object recognition, in 'Proc IEEE International Joint Conference on Neural Networks (IJCNN)', pp. 880–885.

Reich, D. S., Mechler, F. and Victor, J. D. (2001), "Temporal coding of contrast in primary visual cortex: when, what, and why", J Neurophysiol , Vol. 85, pp. 1039–1050.

Rieke, F., Warland, D., De Ruyter van Stevenick, R. and Bialek, W., eds (1999), Spikes: Exploring the neural code., MIT Press, Cambridge.

Romano, J. M., Hsiao, K., Niemeyer, G., Chitta, S. and Kuchenbecker, K. J. (2011), "Human-inspired robotic grasp control with tactile sensing", IEEE Trans Robot , Vol. 27, pp. 1067–1079.

Ros, E., Carrillo, R., Ortigosa, E. M., Barbour, B. and Agís, R. (2006), "Event-driven simulation scheme for spiking neural networks using lookup tables to characterize neuronal dynamics", Neural Comput , Vol. 18, pp. 2959–2993.

Saal, H. P., Ting, J.-A. and Vijayakumar, S. (2010), Active estimation of object dynamics parameters with tactile sensors, in 'Proc IEEE/RSJ International Conference on Intelligent Robots and Systems'.

Saal, H. P., Vijayakumar, S. and Johansson, R. S. (2009), "Information about complex fingertip parameters in individual human tactile afferent neurons", J Neurosci , Vol. 29, pp. 8022–8031.

Safo, P. and Regehr, W. G. (2008), "Timing dependence of the induction of cerebellar LTD", Neuropharmacology , Vol. 54, pp. 213–218.

Sallet, J., Quilodran, R., Rothé, M., Vezoli, J., Joseph, J. P. and Procyk, E. (2007), "Expectations, gains, and losses in the anterior cingulate cortex", Cogn Affect Behav Neurosci , Vol. 7, pp. 327–336.

Sanchez, E., Barro, S. and Canedo, A. (2002), Edge detection and motion discrimination in the cuneate nucleus, in 'Artificial Neural Networks — ICANN', pp. 198–203.

Sánchez, E., Barro, S., Marino, J. and Canedo, A. (2001), A realistic computational model of the local circuitry of the cuneate nucleus, in 'Proceedings of the 6th International Work-Conference on Artificial and Natural Neural Networks: Connectionist Models of Neurons, Learning Processes and Artificial Intelligence-Part I', IWANN '01, Springer-Verlag, pp. 21–29.

Sánchez, E., Barro, S., no, J. M. and Canedo, A. (2003), "A computational model of cuneothalamic projection neurons", Network , Vol. 14, pp. 211–231.

Sanchez, E., Mucientes, M. and Barro, S. (2001), A cuneate-based network and its application as a spatio-temporal filter in mobile robotics, in 'Bio-Inspired Applications of Connectionism', pp. 418–425.

Sanchez, E., Reboreda, A., Romero, M. and Lamas, J. A. (2006), "Spontaneous bursting and rhythmic activity in the cuneate nucleus of anaesthetized rats", Neuroscience , Vol. 141, pp. 487–500.

Scheibert, J., Leurent, S., Prevost, A. and Debrégeas, G. (2009), "The role of fingerprints in the coding of tactile information probed with a biomimetic sensor.", Science , Vol. 323, pp. 1503–1506.

Schreiber, S., Fellous, J. M., Whitmer, D., Tiesinga, P. and Sejnowski, T. J. (2003), "A new correlation-based measure of spike timing reliability", Neurocomputing , Vol. 52-54, pp. 925–931.

Sellers, P. H. (1974), "An algorithm for the distance between two finite sequences", Journal of Combinatorial Theory, Series A , Vol. 16, pp. 253–258.

Semmes, J. and Turner, B. (1977), "Effects of cortical lesions on somatosensory tasks", J Invest Dermatol , Vol. 69, pp. 181–189.

Serrano-Gotarredona, T., Masquelier, T., Prodromakis, T., Indiveri, G. and Linares-Barranco, B. (2013), "Stdp and stdp variations with memristors for spiking neuromorphic learning systems", Front Neurosci , Vol. 7.

Shadlen, M. N. and Newsome, W. T. (1994), "Noise, neural codes and cortical organization", Curr Opin Neurobiol , Vol. 4, pp. 569–579.

Shannon, E. (1948), "A mathematical theory of communication", The Bell System Technical Journal , Vol. 27, pp. 379–423, 623–656.

Shimojo, M. and Ishikawa, M. (1993), An active touch sensing method using a spatial filtering tactile sensor, in 'Proc IEEE International Conference on Robotics and Automation', Vol. 1, pp. 948–954.

Sinapov, J., Sukhoy, V., Sahai, R. and Stoytchev, A. (2011a), "Vibrotactile recognition and categorization of surfaces by a humanoid robot", IEEE Trans Robotics , Vol. 27, pp. 488–497.

Sinapov, J., Sukhoy, V., Sahai, R. and Stoytchev, A. (2011b), "Vibrotactile recognition and categorization of surfaces by a humanoid robot", IEEE Trans Robotics , Vol. 27, pp. 488–497.

Sjöström, P. J., Rancz, E. A., Roth, A. and Häusser, M. (2008), "Dendritic excitability and synaptic plasticity", Physiol Rev , Vol. 88, pp. 769–840.

Slavik, P. and Bell, J. (1995), "A mechanoreceptor model for rapidly and slowly adapting afferents subjected to periodic vibratory stimuli", Math Biosci , Vol. 130, Elsevier, pp. 1–23.

Snowden, R. J., Treue, S. and Andersen, R. A. (1992), "The response of neurons in areas v1 and mt of the alert rhesus monkey to moving random dot patterns", Exp Brain Res , Vol. 88, pp. 389–400.

Softky, W. R. (1995), "Simple codes versus efficient codes", Curr Opin Neurobiol , Vol. 5, pp. 239–247.

Softky, W. R. and Koch, C. (1993), "The highly irregular firing of cortical cells is inconsistent with temporal integration of random EPSPs", J Neurosci , Vol. 13, pp. 334–350.

Spigler, G., Oddo, C. M. and Carrozza, M. C. (2012), Soft-neuromorphic artificial touch for applications in neuro-robotics, in 'Proc IEEE/RAS/EMBS International Conference on Biomedical Robotics and Biomechatronics', pp. 1913–1918.

Srinivasan, M. A. and LaMotte, R. H. (1987), "Tactile discrimination of shape: responses of slowly and rapidly adapting mechanoreceptive afferents to a step indented into the monkey fingerpad", J Neurosci , Vol. 7, pp. 1682–1697.

Sripati, A. P. (2006), "A continuum mechanical model of mechanoreceptive afferent responses to indented spatial patterns", Journal of Neurophysiology , Vol. 95, pp. 3852–3864.

Sur, M., Garraghty, P. E. and Bruce, C. J. (1985), "Somatosensory cortex in macaque monkeys: laminar differences in receptive field size in areas 3b and 1", Brain Res , Vol. 342, pp. 391–395.

Sur, M., Wall, J. T. and Kaas, J. H. (1984), "Modular distribution of neurons with slowly adapting and rapidly adapting responses in area 3b of somatosensory cortex in monkeys", J Neurophysiol , Vol. 51, pp. 724–744.

Thach, W. T., Goodkin, H. P. and Keating, J. G. (1992), "The cerebellum and the adaptive coordination of movement", Annu Rev Neurosci , Vol. 15, pp. 403–442.

Theunissen, F. and Miller, J. P. (1995), "Temporal encoding in nervous systems: a rigorous definition", J Comput Neurosci , Vol. 2, pp. 149–162.

Thorpe, S., Delorme, A. and Van Rullen, R. (2001), "Spike-based strategies for rapid processing", Neural Netw , Vol. 14, pp. 715–725.

Thorpe, S., Fize, D. and Marlot, C. (1996), "Speed of processing in the human visual system", Nature , Vol. 381, pp. 520–522.

Thorpe, S. and Gautrais, J. (1998), Rank order coding, Plenum Press, New York, pp. 113–118.

Thorpe, S. and Imbert, M. (1989), "Biological constraints on connectionist modelling", Conn Persp , pp. 63–92.

Tolhurst, D. J., Movshon, J. A. and Dean, A. F. (1983), "The statistical reliability of signals in single neurons in cat and monkey visual cortex", Vision research , Vol. 23, pp. 775–785.

Truccolo, W., Friehs, G. M., Donoghue, J. P. and Hochberg, L. R. (2008), "Primary motor cortex tuning to intended movement kinematics in humans with tetraplegia", J Neurosci , Vol. 28, pp. 1163 –1178.

Vallbo, A. B. (1995), Single-afferent neurons and somatic sensation in humans, MIT Press, Cambridge, MA, pp. 237—252.

Vallbo, A. B. and Johansson, R. S. (1984), "Properties of cutaneous mechanoreceptors in the human hand related to touch sensation", Hum Neurobiol , Vol. 3, pp. 3–14.

Van Doren, C. L. (1989), "A model of spatiotemporal tactile sensitivity linking psychophysics to tissue mechanics", J Acoust Soc Am , Vol. 85, pp. 2065–2080.

van Rossum, M. C. (2001), "A novel spike distance", Neural Comput , Vol. 13, pp. 751–763.

Vega-Bermudez, F. and Johnson, K. O. (1999), "Surround suppression in the responses of primate sa1 and ra mechanoreceptive afferents mapped with a probe array", J Neurophysiol , Vol. 81, pp. 2711–2719.

Vega-Bermudez, F., Johnson, K. O. and Hsiao, S. S. (1991), "Human tactile pattern recognition: active versus passive touch, velocity effects, and patterns of confusion", J Neurophysiol , Vol. 65, pp. 531–546.

Victor, J. D. and Purpura, K. P. (1996), "Nature and precision of temporal coding in visual cortex: a metric-space analysis", J Neurophysiol , Vol. 76, pp. 1310–1326.

Wang, X., Merzenich, M. M., Sameshima, K. and Jenkins, W. M. (1995), "Remodelling of hand representation in adult cortex determined by timing of tactile stimulation", Nature , Vol. 378, pp. 71–75.

Wang, Y. T. and Linden, D. J. (2000), "Expression of cerebellar long-term depression requires postsynaptic clathrin-mediated endocytosis", Neuron , Vol. 25, pp. 635–647.

Werner, G. and Mountcastle, V. B. (1965), "Neural activity in mechanoreceptive cutaneous afferents: stimulus-response relations, weber funtions, and information transmission", J Neurophysiol , Vol. 28, pp. 359–397.

Westling, G. and Johansson, R. S. (1984), "Factors influencing the force control during precision grip", Exp Brain Res , Vol. 53, pp. 277–284.

Wheat, H. E., Goodwin, A. W. and Browning, A. S. (1995), "Tactile resolution: peripheral neural mechanisms underlying the human capacity to determine positions of objects contacting the fingerpad", J Neurosci , Vol. 15, pp. 5582–5595.

Whitsel, B. L., Petrucelli, L. M. and Sapiro, G. (1969), "Modality representation in the lumbar and cervical fasciculus gracilis of squirrel monkeys", Brain Res , Vol. 15, pp. 67–78.

Wiesel, T. N. and Hubel, D. H. (1966), "Spatial and chromatic interactions in the lateral geniculate body of the rhesus monkey", J Neurophysiol , Vol. 29, pp. 1115–1156.

Wolpert, D. M. and Miall, R. C. (1996), "Forward models for physiological motor control", Neural Netw , Vol. 9, pp. 1265–1279.

Wolpert, D. M., Miall, R. C. and Kawato, M. (1998), "Internal models in the cerebellum", Trends Cogn Sci , Vol. 2, pp. 338–347.

Wu, W. and Srivastava, A. (2011), "An information-geometric framework for statistical inferences in the neural spike train space", J Comput Neurosci , Vol. 31, pp. 725–748.

Xu, D., Loeb, G. E. and Fishel, J. A. (2013), "Tactile identification of objects using bayesian exploration", Proc. ICRA, Karlsruhe .

Yodogawa, E. (1982), "Symmetropy, an entropy-like measure of visual symmetry", Percept Psychophys , Vol. 32, pp. 230–240.

Yousef, H., Boukallel, M. and Althoefer, K. (2011), "Tactile sensing for dexterous in-hand manipulation in robotics — A review", Sens Actuators A Phys , Vol. 167, pp. 171–187.

Yu, C., Derdikman, D., Haidarliu, S. and Ahissar, E. (2006), "Parallel thalamic pathways for whisking and touch signals in the rat", PLoS Biol , Vol. 4, p. e124.

Zhang, H. (2004), The optimality of naive bayes, in 'Proc FLAIRS Conference'.

Appendix

List of Publications

Journals

Pinoteau, J.*; Bologna, L. L.*; Passot, J-B.; Garrido, J. A.; Vogel, J.; Ros Vidal, E. and Arleo, A. A closed-loop neurobotic system for fine touch sensing. *Journal of Neural Engineering*, 10 (4): 046019, 2013. *(* equal contribution)*

Bologna, L. L.; **Pinoteau, J.**; Brasselet, R.; Maggiali, M. and Arleo, A. Encoding/decoding of first and second order tactile afferents in a neurorobotic application. *Journal of Physiology P*, 105 (1-3): 25-35, 2011.

Peer reviewed proceedings

Pinoteau, J.*; Bologna, L.L.*; Garrido, J. and Arleo, A. A Closed-loop neurorobotic system for investigating Braille-reading finger kinematics. In Isokoski, P. and Springare, J., editors, *LNCS - Haptics: Perception, Devices, Mobility, and Communication*, vol. 7282, pages 407-418, Springer, 2012. *(* equal contribution)*

Pinoteau, J.*; Bologna, L.L.*; Garrido, J. and Arleo, A. Active tactile sensing in a neurorobotic Braille-reading system. *In Proceedings of the 4th IEEE RAS/EMBS International Conference on Biomedical Robotics and Biomechatronics (BioRob 2012)*, pages 1925-1930, Rome, Italy, 2012. *(* equal contribution)*

Arleo, A.; Brasselet, R.; Bologna, L. L.; **Pinoteau, J.**; Jörntell, H. and Johansson, R. S. Neural coding in the early stages of the somatosensory pathway: a metrical information theory analysis of human microneurography data. *In Proceedings of the 10th French Society for Neuroscience Meeting*, Marseille, France, 2011.